8-2023

Novel insights into oligodendrocyte biology from developmental myelination studies in autophagy deficient mice and analysis of oligodendrocyte translatome response to contusive spinal cord injury.

Michael David Forston
University of Louisville

NOVEL INSIGHTS INTO OLIGODENDROCYTE BIOLOGY FROM DEVELOPMENTAL MYELINATION STUDIES IN AUTOPHAGY DEFICIENT MICE AND ANALYSIS OF OLIGODENDROCYTE TRANSLATOME RESPONSE TO CONTUSIVE SPINAL CORD INJURY

By

Michael David Forston
B.A., Concordia College, 2014
M.S., University of Louisville, 2019

A Dissertation
Submitted to the Faculty of the
School of Medicine of the University of Louisville
in Partial Fulfillment of the Requirements
for the Degree of

Doctor of Philosophy
in Anatomical Sciences and Neurobiology

Department of Anatomical Sciences and Neurobiology
University of Louisville
Louisville, Kentucky

August 2023

NOVEL INSIGHTS INTO OLIGODENDROCYTE BIOLOGY FROM DEVELOPMENTAL MYELINATION STUDIES IN AUTOPHAGY DEFICIENT MICE AND ANALYSIS OF OLIGODENDROCYTE TRANSLATOME RESPONSE TO CONTUSIVE SPINAL CORD INJURY

By

Michael David Forston
B.A., Concordia College, 2014
M.S., University of Louisville, 2019

A Dissertation Approved on

May 26, 2023

By the following Dissertation Committee:

_____
Dissertation Co-Director: Dr. Scott R. Whittemore

_____
Dissertation Co-Director: Dr. Michal Hetman

_____
Dr. Martha Bickford

_____
Dr. Chad Samuelsen

_____
Dr. Aaron W. McGee

_____
Dr. Eric C. Rouchka

DEDICATION

This dissertation is dedicated to my wife,

Morgan Forston,

And to my parents,

David and Marcia Forston.

Your love and support made this work possible.

I am forever grateful.

ACKNOWLEDGEMENTS

First, I would like to thank my committee members, Drs. Martha Bickford, Chad Samuelsen, Aaron McGee and Eric Rouchka for their support and guidance throughout my time as a graduate student. I would like to thank the Core personnel at the Kentucky Spinal Cord Research Center; Christine Armstrong for her surgical expertise, Darlene Burke for her statistical analyses, and Jason Beare for his helping hand in microscopy. I would like to thank Allison Smith, Margaret Bates, and Dr. Mary Bunge for their contributions to the work in chapter II. I would also like to thank the Whittemore and Hetman lab members, both at present and those I've seen move on to their next adventures in their careers. A special thanks to Kariena Andres for generating our animals and always being available to help with any animal needs. I also want to thank Russ Howard for his teaching and assistance in cell culture, plasmid generation and other molecular biological procedures. A very special thanks to a past post-doctoral fellow Dr. Andrew Bankston. His guidance and wisdom he shared during my first few years in the lab are deeply cherished. I also want to give a special thanks Dr. George Wei who helped optimize the RiboTag procedure used in Chapter III.

I cannot begin to express my thanks to my mentors Dr. Scott Whittemore and Dr. Michal Hetman. Thank you beyond words for your support, guidance and above all, patience.

Finally, I want to thank my wife, Morgan Forston. Your confidence and positive attitude are contagious. Thank you for your love, patience, kindness, and support during this last leg of my degree.

ABSTRACT

NOVEL INSIGHTS INTO OLIGODENDROCYTE BIOLOGY FROM DEVELOPMENTAL MYELINATION STUDIES IN AUTOPHAGY DEFICIENT MICE AND ANALYSIS OF OLIGODENDROCYTE TRANSLATOME RESPONSE TO CONTUSIVE SPINAL CORD INJURY

Michael David Forston

May 26, 2023

Loss of myelin causes severe neurological disorders and functional deficits in white matter injuries (WMI) such as traumatic spinal cord injury (SCI). This dissertation is focused on autophagy in OL development and the OL translatome after SCI.

Chapter I describes the history of myelin, OL development, and their involvement in neurodegenerative diseases and SCI. The proteostasis network, in particular autophagy, and its contributions to white matter pathology is discussed. It concludes examining advantages and disadvantages of unbiased omics tools, like RiboTag, to study transcriptional/translational landscapes after SCI.

Chapter II focuses on autophagy in OPC/OL differentiation, survival, and proper myelination in the mouse brain during development. Conditional deletion of *Atg5,* an essential autophagy gene, in neonatal mice develop a tremor and is lethal. Further investigation revealed OPC apoptosis, reduced differentiation, and

reduced myelination. *Atg5*$^{-/-}$ OPCs capable of differentiating failed to properly myelinate. Lastly, pharmacologically inhibiting or activating autophagy in OPC/dorsal root ganglion(DRG) co-cultures blocked and enhanced myelination, respectively. It is proposed autophagy is an important regulator in OPC survival, maturation, and myelination.

Chapter III is focused on the OL translatome before and after SCI. Using RiboTag, the OL translatome was determined in the intact mouse spinal cord and 2, 10 and 42 days post contusive thoracic SCI. Biphasic upregulation of mitochondrial-respiration mRNAs at days 2 and 42 suggest OLs shift metabolism to oxidative phosphorylation. Pro-survival and cell death regulators peaked at day 2. Acute OL upregulation of the iron oxidoreductase *Steap3*, was confirmed at the protein level and further tested *in vitro*. It is proposed metabolic shift to oxidative phosphorylation may contribute to oxidative stress and exacerbated by proteins such as STEAP3.

Collectively, autophagy is a critical regulator in OPC development and myelination and may facilitate myelin compaction. Such critical roles magnifies the importance of maintaining proteostasis, and its potential as a therapeutic target in white matter injuries. OL translatomic data suggests OLs response to SCI is dynamic, and metabolic shifts may indicate biphasic waves of oxidative stress. It also identifies new targets like *Steap3* that have not previously been explored, proving a valuable dataset to explore OL response to SCI.

TABLE OF CONTENTS

LIST OF FIGURES

CHAPTER I INTRODUCTION

Myelin in the central nervous system: historical perspective

Scientific investigation of the central nervous system (CNS) has historically been challenging. The earliest recorded evidence of myelin, the white, protein and lipid rich substance coating neuron axons, originates during the Renaissance (16th century, ~1543), when Andreas Vesalius (1514-1564), the father of anatomy, described the nervous system composed of grey matter and white matter[1]. In 1717, using his own crafted lens Antoni van Leeuwenhoek (1632-1723) first described nerves in the peripheral nervous system (PNS) as "composed of very slender vessels of an indescribable fineness, running lengthwise to form the nerve"[2]. It wasn't until the 19th century that others such as CG Ehrenberg discovered that nerves in the PNS were composed of "brain tubes" ensheathed with "nerve marrow"[3]. Ehrenberg's work paved the way for future discoveries such as Remak's primitive band in 1837[4], and von Kolliker's description of the primitive band as the "axon" in 1896[4,5].

The first description of the Schwann cell, the myelinating glia of the PNS and named after its discoverer Theodor Schwann in 1847, was originally accepted as a supporting cell to the axon and did not produce the "nerve marrow" which Schwann renamed "white substance"[5,6]. The word "myelin" to

describe “nerve marrow” or “white substance” was first introduced by Rudolf Ludwig Virchow[7]. However, like others before him, Virchow did not believe myelin was secreted by a supporting cell, but from the “axis-cylinder” (axon) itself. Through his observations Virchow formulated the first insulation theory in 1858[8].

The advent of staining techniques, in particular the osmium stain by Max Schultze still influential to this day, allowed for further investigation into the composition of the nervous system[5]. Quite a few investigators were using the osmium stain to understand the nervous system, and like many stains at the time the staining was not always consistent. Oftentimes breaks in the stain were observed and attributed to artifacts of the staining. However, Louis-Antoine Ranvier recognized that these breaks were not artifacts but evenly spaced throughout the axon. He also observed nuclei evenly spaced between segments of myelin. Ranvier’s observations established what we know today as the nodes of Ranvier, the spacing in between myelin segments that allow for saltatory conduction[5,9]. He also put forth a convergent hypothesis with Virchow, that the myelin sheath played an insulation role, and famously compared axon electrical conductance to the transatlantic telegraph cables, operational in 1866. He states,

“Myelin has perhaps another role; it is probably an insulating envelope. We know that electrical connections which are immersed in a conductive medium must be isolated by a non-conductive sleeve; construction of submarine cables rest on this principle. It is conceivable that transmission of the sensitive or motor impulses may have some analogy with the transmission of electricity, so perhaps

each nervous tube [axon] must be isolated for this transmission to be more efficient"[5,9].

Ranvier went further with this hypothesis and was one of the first to suggest that myelin confers an evolutionary advantage. At the time it was believed invertebrates do not have "nerve tubes with myelin", and thus myelin is not essential for nervous system development and function[5,9]. Ranvier was incorrect, but his work further pushed the field to recognize that myelin had a unique functional role in the nervous system and essential for vertebrate evolution.

Despite the advances in PNS myelination by Schwann cells, very little was known about CNS myelination and the cells that produce it. It was mostly due to technical staining limitations available at the time. It was not until Pio del Rio-Hortega (1882-1945), a student of Santiago Ramon y Cajal and father of neuroscience, perfected the silver carbonate stain that oligodendroglia (OLs), the myelinating glia of the CNS, were discovered. In fact, Pio del Rio-Hortega's staining revealed the cells attributed to Cajal's "third element", which were microglia and interfascicular glia (OLs)[10,11]. Rio-Hortega formally introduced these interfascicular glia as OLs in 1921, whose drawings elegantly showed OL cytoplasmic processes spiraling around unstained myelin (Figure 1A). Rio-Hortega was also one of the first to compare OLs to Schwann cells as having "identical functions of support, isolation and nutrition connected with nerve conduction"[5,10,11]. During this period of neuroscience there was no evidence of a physical link between OLs or Schwann cells to myelin. In fact, most of the field

believed the axon produced myelin itself[5]. Rio-Hortega's identification of OLs was not easily accepted by skeptics, including Ramon y Cajal. It was not until 1924 when Wilder Graves Penfield (1891-1976), an American surgeon and visiting scholar in Rio-Hortega's laboratory, published a landmark article in *Brain* that convinced neuroscientists to accept OLs as the myelinating glia of the CNS[12].

In 1928, Rio-Hortega wrote a memoir classifying 4 types of OLs: Type I – named Robertson cells after William Ford Robertson who used an inconsistent platinum impregnation stain that took several months and revealed small branched cells that wrapped multiple small axons. Type II - cells that contacted parallel axons. Type III – cells that contacted few large axons (Figure 1A). And Type IV – cells that had a one-to-one relationship with the largest axons similarly to Schwann cells[5,10,12,13].

As more sophisticated techniques were introduced, myelin ultrastructure became the next stone to turn. Originally, the consensus was that the axon secreted myelin, and formed concentric rings around the axon as the secreted lipid-protein droplets crystallized. However, in 1953, Betty Ben Geren (1922-2020) observed by electron microscope the addition of myelin layers inside Schwann cell cytoplasm of chick embryos during consecutive days of development. She observed that myelin in the PNS did not form concentric rings, but instead spiralized around the axon[5,14]. She also speculated on possible compaction mechanisms, suggesting that there was a drive by the inner "mesaxon" which extruded cytoplasm from myelin[5,14]. Her work was groundbreaking in how we understand the development of myelin today. Still, this

work was all done in the PNS, and lack of evidence for OLs producing spiral-wrapping myelin around the CNS axons was subject for debate.

Fixation protocols did not work well in the CNS compared to the PNS until the introduction of osmium tetraoxide, a strong lipid fixative ideal for staining lipid rich myelin. The work of Richard Paul Bunge (1932-1996) and his wife Mary Bartlett Bunge (1941-) finally filled the blanks in unanswered questions regarding CNS myelination. Their work was first built on a sophisticated model proposed in 1961 (Figure 1C), which suggested OLs produced myelin for the CNS axon, and unlike Schwann cells, a single OL can have several branches capable of myelinating multiple axons at once[15,16]. In 1962, they produced electron micrographs that convincingly showed myelinating OLs spirally wrapping around CNS axons[17,18] (Figure 1B).

As internationally known basic scientists, the Bunge's were recruited to join the Miami Project to Cure Paralysis to continue their work investigating myelination in the intact CNS as well as after spinal cord injury (SCI) in which white matter damage contributes to functional deficits. The Miami Project to Cure Paralysis continues to be a leading center in the SCI field today.

OL biology is rich in history, but in a way is also surprising. It took over 400 years (1547-1962) to firmly establish OLs as the myelinating glia of the CNS. It wasn't until more sophisticated techniques were developed that scientists were able to confirm such benchmarks. Even so, OLs were still not studied to the degree of other neural cells. It was thought that OLs mainly contributed to CNS architecture and action potential propagation, and little more.

Oligodendrocyte lineage

During development, oligodendrocyte progenitor cells (OPCs) undergo tightly regulated processes of proliferation, migration, differentiation and maturation into myelinating OLs. OPCs arise from neuroepithelial cells and populate the CNS in three temporal waves from ventricular zones of the brain and spinal cord. The first wave in the mouse brain occurs at the embryonic stage (~E12.5) and arises from the medial ganglionic eminence (MGE) and anterior entopeduncular area in the ventral forebrain[19–21]. This is followed by a smaller wave (~E15.5) from the lateral and caudal ganglionic eminences (LGE and CGE). Lastly, a third wave occurs in the postnatal cortex[20,22–25]. In the mouse spinal cord, OPCs arise from the same motor neuron progenitor domain (pMN) as motor neurons and migrate during the embryonic stage of development[26]. The first wave of OPCs arise from the ventral ventricular zones of the central canal of the spinal cord, followed by a dorsally derived OPC wave[19,22–25,27]. There is an overproduction of OPCs, leading to competition for space, axons to myelinate, and molecular factors provided by other CNS cells involved in OPC differentiation and survival[23,28,29]. Thus, OPCs go through a pruning stage, where many of the first cortical wave die[23,25,28].

Maturation of OPCs into myelinating OLs can be tracked by stage-specific markers. Neuroepithelial cells expressing the transcription factor (TF) *Olig2* give rise to OPCs and remains expressed throughout the OL lineage[30–33]. Early stages of OPCs display bipolar morphology and express platelet derived growth factor receptor alpha (PDGFRα), whose ligand, PDGF, acts as a survival and

proliferation factor[34,35]. Early stage OPCs with multipolar morphology express the chondroitin sulfate proteoglycan neuron-glial antigen 2 (NG2)[36]. Later, premyelinating OLs can be identified by monoclonal antibodies O4, followed by O1 and 2',3'-cyclic nucleotide 3' phosphodiesterase (CNP), as the cell fully commits to becoming a mature OL[37,38]. Once OPCs no longer divide and differentiate into myelinating OLs, they express major myelin proteins such as proteolipid protein 1 (PLP1) and myelin basic protein (MBP), that myelinate axons in a region-specific manner[39,40]. However, the exact mechanisms for such selectivity remain incompletely understood.

In order to populate the CNS, OPCs migrate throughout grey and white matter by "hitching rides" on developed blood vessels[41]. This migratory action is regulated by factors that provide both guidance and motility, as well as temporal and mechanical control to detach from blood vessels[41–45]. OPCs tile throughout the CNS parenchyma through self-repulsion and remain tiled throughout adulthood[46]. Adult OPCs are thought to act as "pools" of cells on standby, ready to respond to cases of demyelination, OL cell death, myelin maintenance and adaptive myelination; a process poorly understood but thought to be controlled by activity dependent firing of axons[47–49]. Thus, OPCs can differentiate into mature, myelinating OLs throughout adulthood[50,51].

OLs and white matter damage

The first recorded attribution of myelin to a disease is credited to Jean-Martin Charcot, who diagnosed multiple sclerosis (MS) as a demyelinating disease in 1868.

"…These myelin drops and fatty granules can infiltrate the mesh of the reticulum and spread wide; they never occupy the center of the sclerotic plaque, since there, the fibrillary metamorphosis and the destruction of the nervous tubes are completed; but, on the contrary, one finds them at the plaque edges, where the medullated cylinder disappears progressively…"[52].

MS is the most common demyelinating disease of the brain and spinal cord and can cause physical, cognitive, and sometimes psychiatric deficits[53,54]. MS is considered a chronic neuroinflammatory and autoimmune disorder in which immune cells infiltrate an area within the brain or spinal cord and repeatedly attack myelin causing myelin degeneration or demyelination of local axons, axonal damage and loss of neuronal synapses[53–56]. Spared axons within the demyelinated lesions are remyelinated by differentiated OPCs, although usually not as efficiently as the original myelin sheath[57–62]. MS lesions often endure repeated demyelination and remyelination, which can exhaust the available OPC pool and limit remyelination capacity[62–65]. Additionally, OLs not only produce myelin, but also provide neurotrophic and metabolic support to axons[55,66–70]. It is likely repeated and prolonged demyelination eventually leads to axon degeneration due not only to disruption in axon firing potential, but also removal of an important source of trophic and bioenergetic factors that maintain axon integrity and health[25,71].

OLs within and around the lesion area, as well as the OPCs that continuously attempt to remyelinate, are not only vulnerable to direct autoimmune attack and inflammatory cytokines. For example, reactive oxygen species (ROS) contribute to the lesion microenvironment which has shown to cause mitochondrial damage and prolonged oxidative stress in OPCs and OLs. OLs, and even more so OPCs, are particularly vulnerable to alterations in metabolic processes and cellular stresses[62,72–76]. Similar vulnerabilities to the OL lineage have been shown in other demyelinating diseases.

Pelizeus-Merzbacher Disease (PMD) is a fatal, X-linked recessive neurological disorder caused by mutations in *Plp1*, a gene that transcribes a major myelin protein involved in compaction and myelin maintenance[77–79]. The PLP1 mutations lead to OLs inability to properly myelinate around axons (dysmyelination), reducing neurons' ability to propagate an action potential. PMD-associated PLP mutations can result in protein accumulation within the endoplasmic reticulum (ER) lumen[77–79]. In order to combat the accumulated protein, OLs activate the ER stress response (ERSR) and unfold protein response (UPR) to help mitigate damage. However, prolonged activation due to an inability to rescue the PLP protein accumulation often leads to apoptosis or other forms of cell death. Interestingly, in a mouse model of PMD, OLs can also undergo ferroptosis, a form of cell death dependent on intracellular iron and accumulation of lethal lipid ROS due to iron-dependent lipid peroxidation[80]. Treatment with iron chelators increases OL survival and myelination[79]. This is not

all too surprising as OLs contain the highest amounts of iron in the CNS, and iron is directly required for myelination[81,82].

Other neurodegenerative diseases such as schizophrenia or Major Depression, Alzheimer's Disease (AD), Parkinson's Disease (PD), Huntington's disease (HD) and multiple system atrophy (MSA) display changes in white matter structure even before clinical symptoms have manifested[83–88]. In MSA, OLs display accumulation of α-synuclein and cytoplasmic inclusions, which impairs their function likely due to ER stress and leading to axon degeneration[89]. Similarly, accumulation of protein aggregates in AD, PD and HD, as well as mitochondrial damage in MS suggest protein homeostasis plays a major role in contributing to disease outcomes[76,90–93].

Proteostasis Network

The proteostasis, or protein homeostasis, network is an intracellular network orchestrating the protein synthesis, their folding, disaggregation, or degradation[94]. It comprises all components required for proper protein synthesis and function, including translational machinery, chaperone proteins that assist in proper protein folding of larger proteins, and degradation pathways such as the ubiquitin proteasome system (UPS) and autophagy. While both degradation pathways assist in removing damaged or dysfunctional proteins and organelles, the UPS is suspected to degrade 90% of all cellular proteins[95]. Many of these proteins, usually those larger than 100 amino acids or roughly 90% of all cellular proteins, do not spontaneously form their final conformational state, but require

chaperones to assist in proper folding. Despite this, under normal physiological conditions as much as 30% of nascent proteins are degraded.

The cell has adapted to protein overload and imbalances in proteostasis through activation of several stress response pathways. These include the heat shock response (HSR), the ERSR, the integrated stress response (ISR), and the UPR[96]. These stress response pathways often overlap and determine whether proteostasis can be restored or cell death mechanisms such as apoptosis must be initiated[96,97]. Cellular stress due to disruption of proteostasis can also activate autophagy or the UPS[98–100].

Autophagy has been implicated in numerous neurodegenerative diseases including MS, AD, HD, PD, and aging[76,90–93]. Autophagy is an evolutionary conserved lysosomal degradation pathway required for cellular homeostasis through the sequestration and breakdown of damage or dysfunctional proteins and organelles[100–102]. Although the number of autophagy degradation modalities has increased dramatically over the years, there are classically three main forms: macroautophagy, microautophagy, and chaperone-mediated autophagy. Macroautophagy (herein referred as autophagy) is the most well documented form of autophagy. Upon induction, dysfunctional or accumulated proteins and organelles are sequestered and packaged into an autophagosome, a double-membraned vesicle. A lysosome, which contains high pH, proteases and hydrolases, fuses with the autophagosome to form an autolysosome. Acidic conditions of the autolysosome cause degradation of the sequestered cargo as well as the inner membrane of the double membrane autophagosome. The

broken-down contents are then released into the cytosol and recycled by the cell[100–102].

Multiple selective forms of autophagy such as mitophagy (degradation of mitochondria), reticulophagy (degradation of ER), ribophagy (degradation of ribosomes), and aggrephagy (degradation of protein aggregates) have been described[100]. Under physiological conditions, evidence for specialized autophagy argues the degradation can be highly selective based on the needs of the cell and contributes to cellular homeostasis beyond general means. However, dysfunction or disruption of autophagy can have serious adverse implications: the result often being programmed cell death. Due to its vital role in proteostasis and cell health in other cell types of the CNS, we explore the role of autophagy in OPCs during development in Chapter II.

Traumatic SCI

Traumatic SCI often results in severe neurological deficits in motor and sensation, as well as persistent health problems throughout life. In 2022, the estimated population living with SCI in the United States was ~334 million people[103]. Since 2015, roughly 18,000 people in the U.S. suffer from traumatic SCI, with most cases occurring in the male population (79%)[103,104]. The level of injury contributes to the degree of functional deficits. The most common injury is cervical (~55%), followed by thoracic (~35%), lumbar (~10%) and sacral (~0.5%)[105].

The pathophysiology of SCI can be separated into two phases. The primary injury is caused by mechanical impact to the spinal cord damaging the

vertebral columns and leading to spinal cord tissue compression or transection. Such an insult results in disruption of the spinal cord blood barrier and damage to spinal cord vasculature, as well as necrosis of neurons and glia within the lesion area[106–108]. The primary phase is followed by a secondary phase of prolonged damage that can occur minutes to months after the injury. The secondary phase involves a cascade of events including, but not limited to, ischemia, inflammation, glutamate excitotoxicity, and cell death[108–111]. Such secondary events are not immediately contained to the lesion area but spread rostral and caudal from the lesion epicenter[106]. Like other neurodegenerative insults such as MS, OLs are particularly susceptible to acute secondary damage cascades such as oxidative stress from ROS, excitotoxicity, extracellular ATP release from dying cells, as well as pro-inflammatory cytokine release from microglia and infiltrating macrophages[107–109,112].

In the rodent model, SCI secondary injury can be loosely categorized into 3 stages; acute (~0-3 days), subacute (~4-14) and subchronic (6-10 weeks)[107]. CNS cells respond to each of these stages quite differently. During the acute stage, microglia become “activated” releasing cytokines such as TNFα and IL-1β. Neuron, astrocyte and OL cell death is also highly prevalent during this period. However, OPCs respond quickly and begin proliferating and differentiating into OLs by 3 days post-SCI. By the subacute stage, cytokine release by microglia begins to drop, and growth factors such as CNTF and FGF-2 are elevated. Astrocyte and neuron cell death is no longer seen, whereas OLs within and around the lesion area continue to undergo apoptosis within degenerating axon

tracts. Early stages of remyelination by newly formed OLs is also observed. Lastly, monocyte and microglia-derived macrophage activation begins to peak at the subacute timepoint[107]. At the subchronic stage, newly formed OLs are present and limited remyelination continues, the tissue milieu stabilizes, and growth factors remain elevated compared to the uninjured cord[107].

Proper function of the proteostastic network is unsurprisingly critical for nervous system function. Dysregulation of any of many steps within the network have been tied to several neurodegenerative diseases and injuries[93]. SCI is no exception, and dysfunction to the proteostasis network is believed to be a mediator of secondary damage cascades[76]. All cells capable of protein translation utilize the proteostasis network, which means understanding each component of the intricate network and their contributions to cellular survival and death in CNS pathology is critical for therapeutic intervention. However, interventions targeting the proteostasis network can act as a scale tipping towards therapeutic or detrimental. For example, manipulating the ISR can lead to enhanced inflammasome activation, which could cause more damage through sustained inflammation[113,114]. Regardless, therapeutic strategies that target such a ubiquitous and essential network to cellular health may be more effective than those targeting single effector systems such as specific ion channels, ROS or oxidative stress, or individual signaling pathways. Many of these strategies also focus on targeting a single cell type, thus limiting therapeutic potential.

Omics contributions to SCI pathology

Traumatic SCI is associated with ER stress and apoptosis in OPCs and OLs[109,115,116]. OL cell death and white matter loss is particularly critical in functional recovery outcomes in contusive thoracic injuries, where white matter is most prevalent compared to cervical and lumbar enlargements[117]. Therefore, it is critical to identify drivers of OPC and OL response to SCI. The dynamic response to secondary damage merits a need to systematically determine such responses across the recovery process.

Activation of the ERSR/UPR/ISR regulates major translation and transcription events to restore proteostasis. Furthermore, autophagy can act to restore proteostasis through selective degradation of damaged organelles including parts of the ER, mitochondria and translational machinery such as ribosomes[100,118]. Activation of the ERSR/ISR leads to increased phosphorylation of eIF2α, which acts as a switch turning off general protein translation[76,119,120]. At the same time master TFs are activated that turn on protein translation of ER chaperones and machinery involved in protein degradation, including autophagy and the UPS[119,121]. Such protein degradation systems are in place to restore ER integrity and remove protein aggregates causing ER stress. Furthermore, upregulated proteins of autophagy and UPS are turned on by TFs activating transcription factor 4 (ATF4) and C/EBP (CCAAT enhancer binding protein) homologous protein (CHOP)[76,119,121]. Recent studies have identified critical roles not only for the ERSR/ISR in OL survival, but also greater functional recovery when preventing dephosphorylation of eIF2α, thereby continuously inhibiting general protein translation, with salubrinal in SCI mice[115,120]. Furthermore,

increases in white matter sparing, a measure of functional recovery after thoracic SCI, decreases in OL cell death and improvement in functional recovery was identified in *Chop*$^{-/-}$ mice[122]. The proteostasis network involves not only the ERSR and ISR, but also HSR, UPR, autophagy and UPS. Limited data is available for these pathways in OLs, however recent work by Saraswat and colleagues showed that deleting the essential autophagy gene *Atg5* in *Plp1* expressing OLs results in greater myelin loss, increased OL cell death and restricted hindlimb recovery after thoracic contusive SCI[123]. Such a critical role for the proteostasis network in OL survival after SCI argue a need to systematically investigate the transcriptional and translational landscapes that occur in these cells following white matter injury.

SCI has a complex pathology involving secondary damage cascades that are dynamic and time-dependent. Likewise, cellular diversity further adds to the complexity in identifying cell-specific responses that could be targeted for better therapeutic outcomes. The advent of “OMICS” sequencing and big data to identify RNA and protein has helped identify novel molecular components of many aspects of biology. Its power lies in its “unbiased” approach in identifying differentially expressed units (genes, proteins, lipids etc) that can both confirm previously known mechanisms, but also identify novel components and regulators of a disease phenotype.

Omics approaches have been applied extensively to SCI in hopes to provide insight into its pathology[124–126]. However standard omics strategies such as bulk RNA sequencing or whole tissue proteomics do not provide cell-specific

resolution and limit interpretation of observed changes. Additionally, identification of gene/protein expression changes in whole tissue without cell-specific control results in identifying general cellular responses, missing cell type-specific response mechanisms that only occur within that cell type compared to others. Another critical point to address is the assumption that differentially expressed genes identified by RNA sequencing directly represents the protein pool within the tissue or cell being investigated. For example, after SCI thousands of mRNAs are differentially expressed in the contused spinal cord, however only a fraction of differentially expressed mRNAs showed similar results at the protein level[125–127]. Such a difference in RNA to protein may be due to sensitivity of instruments used to measure each. However, it is more likely that mRNAs are selectively translated based on the needs of the cell arguing. Indeed, a recent study systematically showed as great as 97.5% of genes have differences in mRNAs and the proteins, they encode in the Drosphila nervous system[128]. Clearly, an unbiased approach addressing these issues of post-transcriptional regulation is required to better understand cellular response to a disease or injury.

Strategies such as RiboTag have been developed to address such issues through methods of immunoprecipitation in combination with transgenic gene expression of a hemagglutinin (HA) tag onto ribosomes. This technology allows one to isolate “actively translating” mRNAs, termed the translatome, from HA-tagged ribosomes. Additionally, one can cross the RiboTag mouse to a cell-specific promoter mouse line expressing Cre or Flp recombinase to target cells of interest in complex tissues[129]. In Chapter III we use *Plp1:Cre^{ERT2}:Rpl22^{HA}*

RiboTag mice to describe the OL translatome in response to progressive stages of SCI.

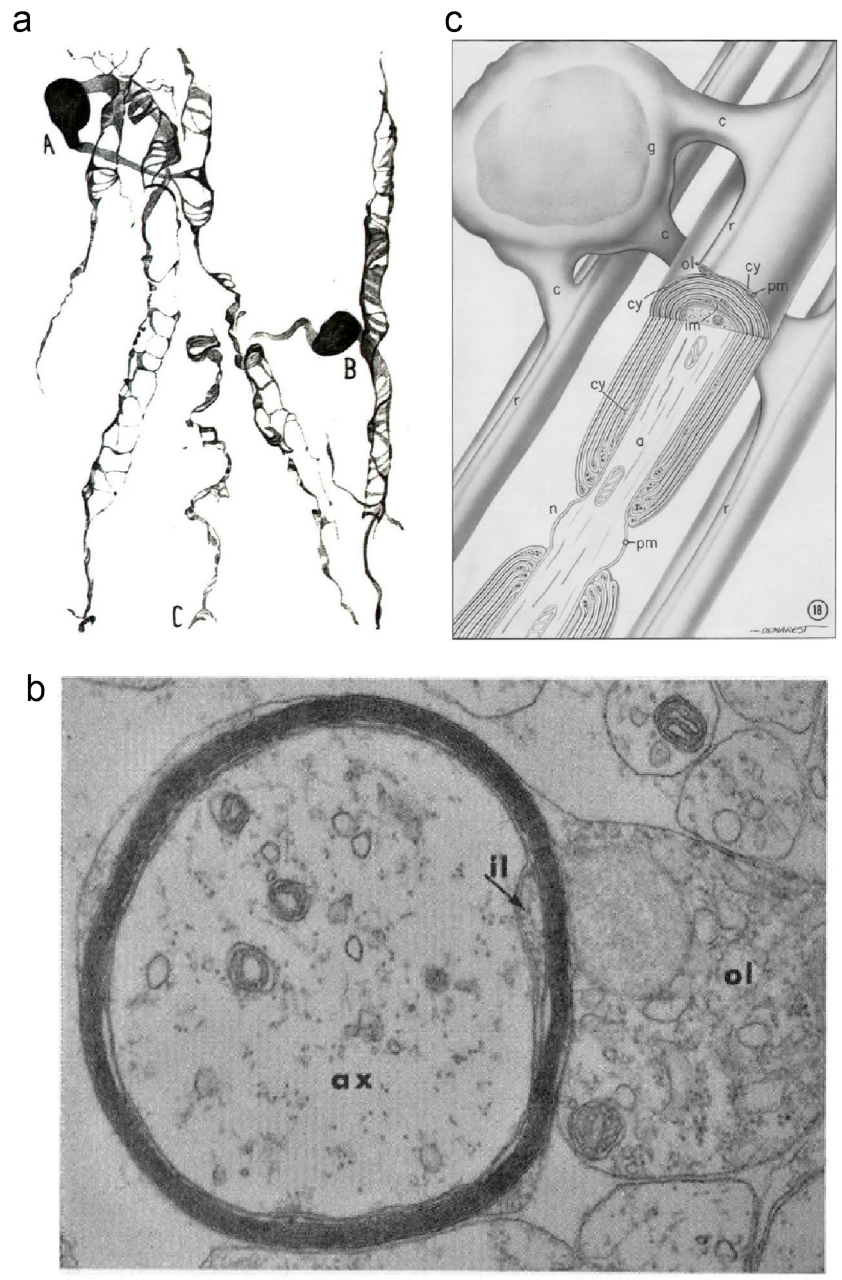

<u>Figure 1.</u> Early evidence of oligodendrocytes: the myelinating glia of the central nervous system.

(a) Drawing by Pío del Rio-Hortega (1928) of the third type oligodendrocytes stained by silver carbonate in the cat. A. depicts an OL with expansions forming reticular casings with three axons. B. OL with widened process around an axon,

and C. depicts a spiral ring-ending expansion[13]. **(b)** Electron micrograph (X 39,000) by Mary Bunge showing evidence of oligodendrocyte (ol) process plasma membrane in direct continuity with the myelin sheath in 5 day old kitten spinal cord. The leading edge (inner loop: (il)) is present between the axon and compact myelin[18]. **(c)** Diagram illustrating the known and hypothetical aspects of the oligodendrocyte, myelin sheath, and relationship to the axon in the 1960s[15]. The diagram is strikingly accurate to what is understood about axo-myelinic relationships today.

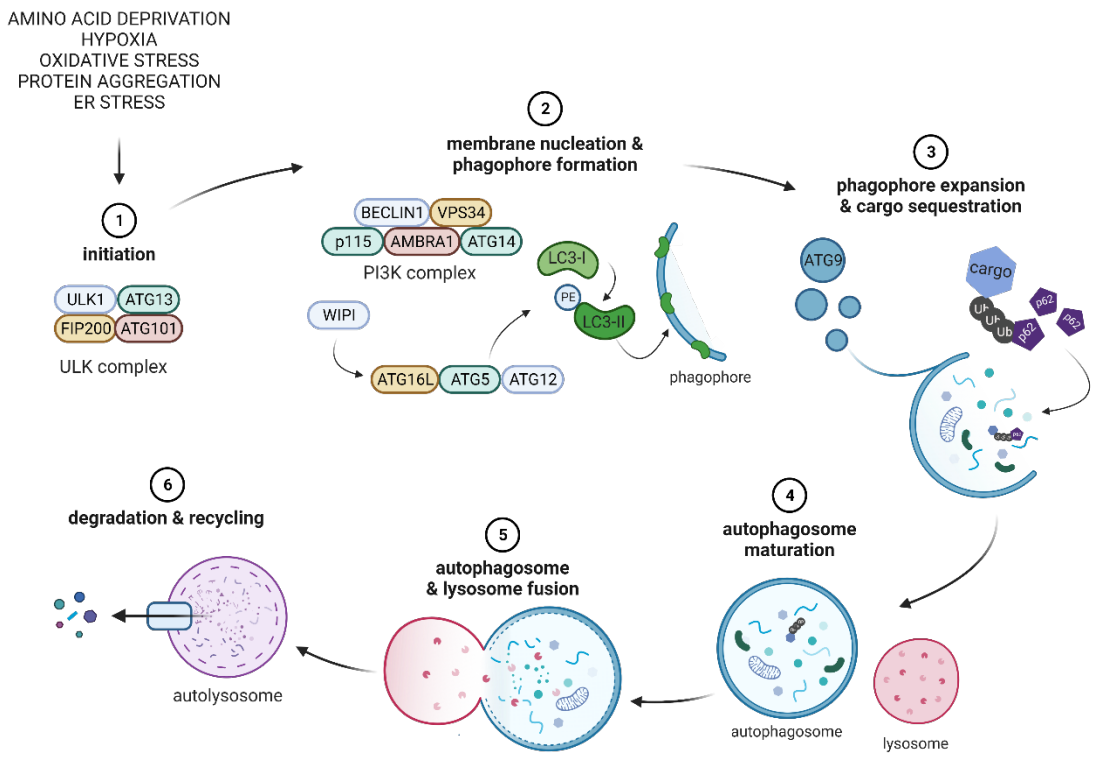

<u>Figure 2.</u> The macroautophagy pathway.

1. Initiation begins with the formation of the ULK complex, which is inhibited by mTORC1, and consists of ULK1, ATG13, FIP200, and ATG101[99,100,102,130,131]. 2. The PI3K complex, which comprises of Beclin-1, VPS34, AMBRA1, ATG14, and p115, together with the ULK complex, controls membrane nucleation and phagophore formation. WIPIs are recruited by phosphorylated lipids (PI3P), which in turn results in covalent conjugation of the ATG12-ATG5-ATG16L complex using ubiquitin-conjugation machinery. The ATG12-ATG5-ATG16L enhances the lipidation of LC3-I to form LC3-II conjugated to phosphatidylethanolamine (PE) and acts as a scaffold to continue phagophore formation [99,100,102,130,131]. 3. ATG9-containing vesicles contribute to phagophore expansion. Cytoplasmic cargo such as aggregated proteins and proteins bound

to p62 or LIR sites of LC3 is sequestered into the maturing autophagosome. 4. Autophagosome is sealed, and SNARE proteins are recruited to form a mature autophagosome [99,100,102,130,131]. 5. Fusion with the lysosome releases protein-degrading hydrolases into the autophagosome. 6. Complete fusion results in the autolysosome. The inner membrane of the autophagosome and its cargo are degraded, and byproducts are released into the cytoplasm to be recycled by the cell [99,100,102,130,131]. Created with Biorender.com

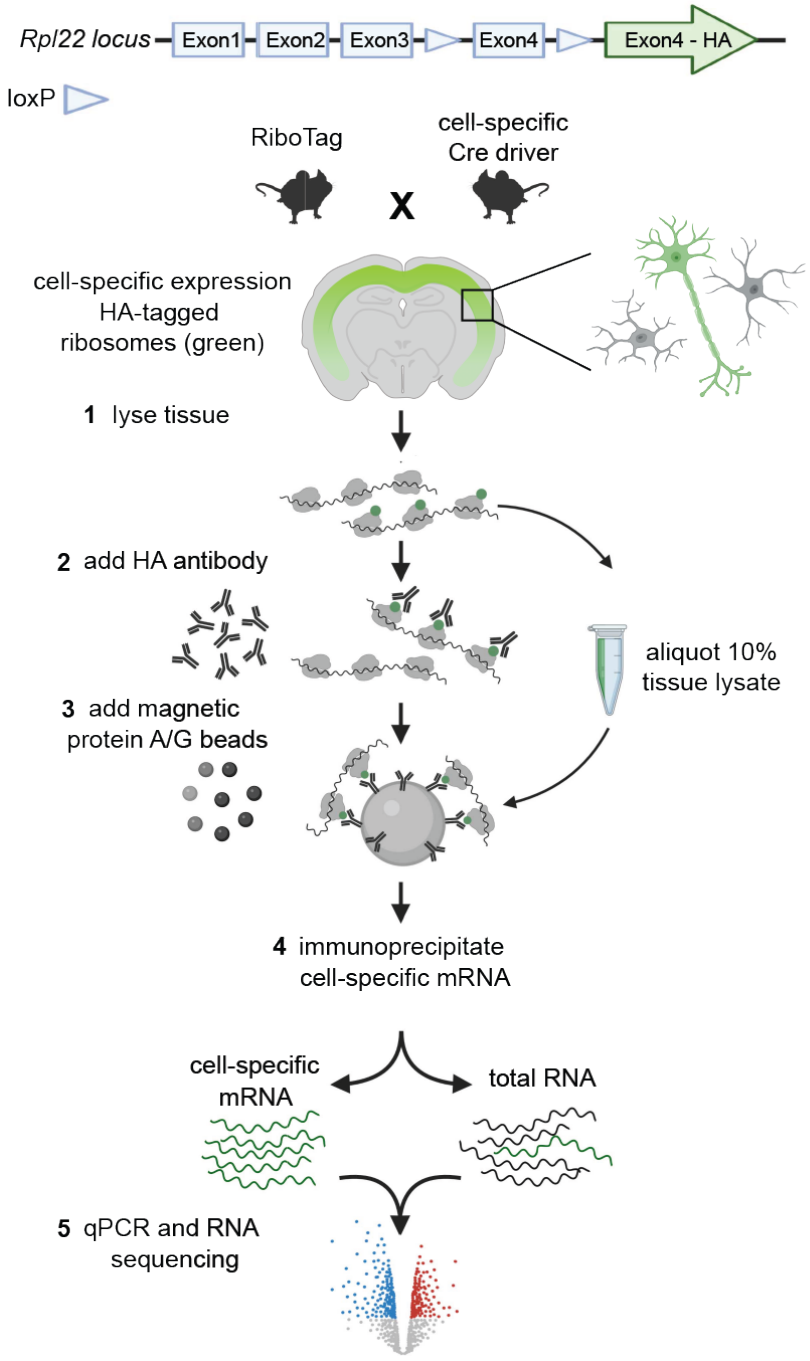

Figure 3. Schematic of the RiboTag mouse model and workflow.

In RiboTag transgenic mice, the 60S ribosomal gene *Rpl22* is modified with LoxP site insertions on either ends of the last exon, exon 4, followed by an identical exon 4 that is tagged with three copies of the hemagglutinin (HA) epitope[129].

Crossing RiboTag mice with *Cre*-expressing mice will result in offspring that have the floxed exon 4 deleted through Cre recombinase activity and replaced with the exon 4 HA tag as its terminal exon. The Cre expressing tissue or cell type of interest now incorporates the HA-tagged ribosomal protein into “actively translating” polyribosomes. Polyribosomes can then be isolated using high salt buffers to maintain polyribosome arrangement and immunoprecipitation via HA antibodies and magnetic beads to isolate HA-tagged ribosomes bound to actively translating mRNAs. The tissue or cell-specific mRNAs, along with total mRNA if isolated from the total lysate (input), can be analyzed via qPCR or RNA sequencing.

CHAPTER II

AUTOPHAGY IS ESSENTIAL FOR OLIGODENDROCYTE DIFFERENTIATION, SURVIVAL, AND PROPER MYELINATION[132]

Introduction

Proper myelination is critical for normal function of the CNS and is provided exclusively by OLs[133]. Myelination is the culmination of a process involving OPC proliferation, migration, and differentiation. Differentiating OLs extend increasingly complex branched processes, express myelin proteins, and produce highly specialized myelin membrane[134,135]. The myelin membrane is then spirally wrapped around neuronal axons and compacted through extrusion of nearly all cytoplasm and organelles[133]. While the control of gene expression during OL development is well understood[136], the requirement of other cellular programs is less studied. The specific mechanisms regulating myelin wrapping and compaction are not well characterized[137]. These same mechanisms are important during myelin repair in demyelinating injuries, such as autoimmune insult in multiple sclerosis or after traumatic injury[55,138–142]. However, the maturation and myelination processes in myelin repair often fail or are incomplete[143]. Further study of the pathways regulating maturation and myelination are needed to identify potential targets for development of therapies to promote myelin repair.

Autophagy was recently implicated in the development of CNS neurons and astrocytes[144,145]. Autophagy is a highly regulated lysosome-dependent degradation pathway that maintains cell homeostasis through clearance and recycling of damaged or unneeded proteins and organelles[146]. Autophagy is induced in response to starvation, endoplasmic reticulum (ER) stress, and apoptosis, and in development of various cell lineages[147]. Autophagosome formation requires the action of the PI3K Vps34/Beclin-1 complex, covalent conjugation of ATG12 to ATG5 and oligomerization with ATG16L, and cleavage and lipidation of LC3B (ATG8) with phosphatidyl ethanolamine, converting LC3B-I to LC3B-II[146]. The cargo adapters, such as p62, bind targets and LC3B-II and are degraded upon autophagosome fusion with the lysosome[148]. Global knockouts of essential autophagy genes, *Beclin-1* and *Atg5* are embryonic lethal[149,150]. Tissue-specific deletion of *Atg5*$^{fl/fl}$ results in impaired function in skeletal and cardiac muscle, pancreas, small intestine, immune cells, podocytes, and neural cells[151]. Moreover, autophagy regulates cell spreading in macrophages, neurite outgrowth, and neuron and astrocyte differentiation[144,145,152]. Deletion of *Atg7* in Schwann cells does not disrupt myelination but causes swelling of the Schwann cell soma[153]. Dysmyelinated Long-Evans shaker (*les*) rats, with mutant myelin basic protein (MBP)[154], accumulate autophagosome vesicles and proteins[155]. Intermittent fasting, with effects including autophagy induction and cleared autophagosomes improved myelination. We therefore sought to directly test the role of autophagy in CNS myelin development.

Pharmacological manipulation of autophagy has classically targeted proteins upstream of the autophagy pathway, such as mammalian target of rapamycin (mTOR) or 5' AMP-activated protein kinase (AMPK), which have pleiotropic effects on many cell signaling pathways besides autophagy[147]. Recently developed compounds allow more specific targeting of the autophagy pathway. The Tat-beclin1 peptide (HIV-1 Tat protein and amino acids 267-824 of Beclin1) induces autophagy by disrupting the binding of autophagy inhibitor GAPR-1 to Beclin1[156]. Verteporfin inhibits autophagy by stimulating oligomerization of p62, preventing autophagosome closure[157,158]. Here, we present evidence that autophagy regulates OL and myelin development and implicate autophagy as a key regulator of OPC survival, differentiation, and proper myelination during neurodevelopment.

Materials and Methods

Animals

All animal procedures were performed in strict accordance with the Public Health Service Policy on Humane Care and Use of Laboratory Animals, *Guide for the Care and Use of Laboratory Animals*[159], and with the approval of the University of Louisville Institutional Animal Care and Use Committee and the Institutional Biosafety Committee. Timed-pregnant Sprague-Dawley rats and wild type C57Bl/6 mice (6-8 weeks) were obtained from Envigo (Indianapolis, IN). *Pdgfrα-Cre*^{ERT2} mice were acquired from Jackson laboratories (B6N.Cg-Tg (Pdgfra-cre/ERT) 467Dbe/J, Cat# 018280, RRID: IMSR_JAX:018280). *Atg5*$^{fl/fl}$ mice were from the Riken BioResource Center (B6.129S-*Atg5*<tm1Myok>, Cat#

RBRC02975, RRID: MGI:3713121) and were rederived by Taconic Biosciences (Rensselaer, NY). Mice from the two lines were bred to produce litters in which all pups were homozygous for *Atg5*$^{fl/fl}$ and had at least one copy of *Pdgfrα-Cre*^{ERT2}. All *Pdgfrα-Cre*^{ERT2}*:Atg5*$^{fl/fl}$ pups were administered vehicle or 100 µg tamoxifen (2 mg/mL in sunflower oil, 50 µL) intraperitoneally once per day from postnatal day 5-9 (P5-9). *Pdgfrα-Cre*^{ERT2}*:Atg5*$^{fl/fl}$ mice were perfused at P9 or P15 as indicated.

Tissue processing

Mice were euthanized with an overdose of 2.0% avertin (2,2,2-tribromoethanol) in sterile NaCl solution administered intraperitoneally (i.p.) before slow transcardial perfusion with ice cold phosphate buffered saline (PBS) (10-12 mL over 3-5 minutes) until the liver was clear and subsequent fixation with perfusion of 20 ml ice cold 4% paraformaldehyde (PFA). Following fixation, brains were removed and post-fixed for 1 h in 4% PFA at 4°C. Cryoprotection was performed by immersion into a 30% sucrose solution for at least 72 h at 4°C. Brains were blocked in tissue freezing medium (Triangle Biomedical Sciences, Durham, NC, Cat# TFM-5) and frozen at -20°C before coronal sectioning with a Leica Model cryostat at 20 µm. Tissue sections were transferred to gelatin-coated slides and stored at -20°C.

For immunoblots, mice were anesthetized with 2.0% avertin in sterile NaCl administered i.p. prior to transcardial perfusion with ice cold PBS. Following perfusion, brains were removed and the corpora callosa (CC) from bregma to -2.5 mm bregma were dissected away from surrounding cortical and striatal tissue in cold Hanks buffered saline solution (HBSS) lacking calcium and magnesium

(Life Technologies, Carlsbad, CA, Cat# 14185-052). Following dissection, CC were diced by hand using a razor blade and incubated in lysis buffer [50 mM Tris, pH 7.4, 150 mM NaCl, 1% Triton X-100, and protease inhibitors (Sigma-Aldrich, St. Louis, MO, Cat# 4693159001)] for 10 minutes at 4°C.

Neonatal rat OPC isolation and differentiation assays

Rat OPC (rOPC) were immuno-isolated with O4-magnetic beads (Miltenyi Biotec, San Diego, CA, Cat# 130-094-543) from the cortices of both male and female P5 Sprague-Dawley rat pups with magnetic activated cell sorting[120,160]. Briefly, cortices were dissected and digested in enzyme mix 1 of the Neural Dissociation Kit (Miltenyi Biotec, Cat# 130-092-628). Samples were further digested with enzyme mix 2 and mechanically dissociated with three progressively smaller bore-size fire polished Pasteur pipettes and strained. The single cell suspension was incubated with a mouse O4 hybridoma supernatant and rat anti-mouse IgM magnetic beads. $O4^+$ cells were finally eluted and seeded at a density of 8,000–12,000 rOPC/cm^2 into a pre-equilibrated 10 cm tissue culture dish coated with poly-D-lysine (PDL) (5 µg/ml) and laminin (20 µg/ml) (both from Sigma-Aldrich, Cat# P6407 and Cat# L2020) containing rOPC proliferation medium. Cells were incubated at 37°C in 5% CO_2. Differentiation was induced by replacing the cell culture medium with rOPC differentiation medium, which lacks growth factors and contains 40 ng/mL triiodothyronine (T3), for 72 hours. Following experimental condition assignment and the 72-hour differentiation or proliferation period, total protein was collected from each plate in lysis solution and processed as described above. Each differentiation assay

was replicated with independent rOPC isolates to achieve n=4 for immunoblot based experiments and n=3 for immunocytochemistry (ICC) assessment of OL differentiation markers.

To measure autophagy flux during differentiation, rOPC were infected with a retrovirus expressing mCherry-EGFP-LC3B or mCherry-LC3B for 48 hours. pBABE-puro mCherry-EGFP-LC3B was a gift from Jayanta Debnath (Addgene plasmid # 22418, Cambridge, MA). Virus-containing media was then replaced with either rOPC proliferation media or rOPC differentiation media for 2, 4, or 7 days. OPCs/OLs expressing pBABE-puro mCherry-LC3B were visualized live using a Zeiss Observer.Z1 fluorescent microscope while in an incubation chamber equilibrated to 37°C and 5% CO_2. Cultures were fixed in 4% PFA at room temperature for 10 minutes before photomicrographs were captured using a Nikon TiE 300 inverted microscope with a DXM-1200C coded digital camera and NIS Elements software (Nikon, Melville, NY). Images were randomized and counts were performed by a lab member blinded to experimental groups. To calculate the puncta per area, counts of cell body and processes from proliferation and differentiation day 4 groups were measured using the “Object Count” feature of NIS-Elements software. The Intensity option of the Object Count feature was manually set to segmentally outline the cell. The Smooth and Clear options were set to x14 and the Separate option x2. Total area was quantified by summation of all segments that outlined the cell. Using the “Auto Detect ROI” feature, the area of only the cell body was determined. The cell body

area was subtracted from the total cell area to determine the area of cell processes.

To assess the effect of ATG5 inhibition during differentiation, rOPC were infected with empty vector, wildtype (WT) *Atg5* (*wtAtg5*), or dominant-negative *Atg5* (*dnAtg5*) pRevTRE (Clontech, Mountain View, CA) retrovirus overnight. Cultures were then transfected with pRetroOn (Clontech) encoding doxycycline-inducible reverse tetracyclin-controlled transactivator (rTTA) using lipofectamine 2000 (Invitrogen) according to the manufacturer's instructions. rOPC culture medium was changed to rOPC differentiation medium containing 5 μg/mL doxycycline 24 hours after transfection. Cultures were differentiated for 3 days prior to immunostaining.

Immunoblot

The BCA kit (Pierce, Rockford, IL, Cat# 23225) was used to quantify the protein lysates. Equal concentration of proteins was separated on SDS-PAGE gels and transferred to nitrocellulose membrane (Schleicher & Schuell, Keene, NH) and processed as described previously[115]. Primary antibodies against ATG5 (rabbit, 1:500, Novus Biologicals, Littleton, CO, Cat# NB110-53818, RRID: AB_828587), Beclin1 (rabbit, 1:1000, Cell Signaling, Danvers, MA, Cat# 3495S, RRID: AB_1903911), LC3B (mouse, 1:500, Medical and Biological Laboratories, Nagoya, Japan, Cat# M186-3, RRID: AB_10897859), p62 (mouse, 1:500, Novus, Cat# H00008878-M01), Olig2 (rabbit, 1:500, Millipore, Billerica, MA, Cat# AB9610, RRID: AB_10141047), myelin basic protein (MBP) (rabbit, 1:5000, Millipore, Cat# AB980, RRID: AB_92396), cleaved caspase-3 (CC3) (rabbit, 1:50,

Cell Signaling, Cat# 9661S, RRID: AB_2341188), and GAPDH (mouse, 1:1000, Millipore, Cat# MAB374, RRID: AB_2107445) were incubated overnight at 4°C.

Immunohistochemistry and Immunocytochemistry

Coronal brain sections were blocked with 5% BSA, 10% normal donkey serum (NDS), and 0.2% Triton-X-100 in PBS for 1 h at room temperature. Primary polyclonal antibodies against ~160 kDa neurofilament protein M (NF-M) (guinea pig, 1:500, Synaptic Systems; Goettingen, Germany, Cat# 171204, RRID: AB_2619872), glial fibrillary acidic protein (GFAP) (sheep, 1:500, R&D Systems, Minneapolis, MN, Cat# BAF2594, RRID: AB_2109655), Olig2 (rabbit, 1:100, Millipore, Cat# AB9610, RRID: AB_10141047), platelet-derived growth factor receptor α (PDGFRα) (rat, 1:50, Millipore, Cat# CBL1366, RRID: AB_11211998), APC (mouse, 1:200, Abcam, Cambridge, United Kingdom, Cat# ab16794, RRID: AB_443473), MBP (rabbit, 1:100, Millipore, Cat# AB980, RRID: AB_92396), ATG5 (chicken, 1:50, Novus, Cat# NB110-53818, RRID: AB_828587), LC3B (rabbit, 1:50, Novus, Cat# NB100-2220SS, RRID: AB_791015), p62 (mouse, 1:50, BD Biosciences, San Jose, CA, Cat# 610832, RRID: AB_398151), and CC3 (rabbit, 1:50, Cell Signaling, Cat# 9661S, RRID: AB_2341188) were incubated for 24 h at 4 °C with 5% BSA, 1% NDS, and 0.1% Triton-X-100 in PBS. Sections were next washed at room temperature (x3) with PBS and incubated with species-specific Alexa405-, Alexa488-, Alexa594-, or Alexa647-conjugated F(ab′)2 secondary antibodies (donkey, 1:200, Jackson ImmunoResearch; West Grove, PA) for 1 h at room temperature. Species-specific IgG isotype controls were used to account for any non-specific binding or

other cellular protein interactions. Hoechst™ was used to identify nuclei. Fluorescent imaging was done on a Nikon Eclipse TE 300 inverted microscope with a spot CCD camera. Exposure times remained identical across all images. Myelinated axon cross-sections were captured at 60x by confocal microscopy using an Olympus FV1000 Confocal and FluoView software (Shinjuku, Japan). Orthogonal slices were generated using the Nikon NIS-Elements software.

For rOPC differentiation experiments, immunostaining against the surface marker O1 was used to mark differentiated OLs. The immunostaining protocol was as follows: Cells were washed with the appropriate culture medium and incubated with O1 hybridoma supernatant diluted to 40% v/v in 50% culture medium and 10% NDS for 1 hour at 4°C. Following washes (x3) with culture medium, cells were fixed with 4% PFA at room temperature for 10 minutes and washed (x3) with DPBS prior to incubation with Alexa594-conjugated F(ab′)2 secondary antibodies (donkey, 1:200, Jackson ImmunoResearch) for 1 hour at room temperature. Hoechst™ was used to identify nuclei. Photomicrographs were captured using a Nikon TiE 300 inverted microscope with a DXM-1200C coded digital camera and NIS Elements software. Images were randomized and counts were performed by a lab member blinded to experimental groups. The percentages of $O1^+$/$Hoechst^+$ cells per total $Hoechst^+$ nuclei were used for quantification.

Myelinating co-culture

For OPC/DRG (dorsal root ganglion (neuron)) co-cultures, DRGs were isolated from E15 Sprague-Dawley rat embryos as previously described[161,162].

Following isolation, DRGs were plated (7,500 cells/cm^2) and maintained on PDL/collagen-coated coverslips in NB1 neurobasal medium to permit neurite outgrowth for at least two weeks and no more than four weeks prior to seeding with rOPC (10,000 cells/cm^2). Once seeded, OPC/DRG co-cultures were maintained 7 days in differentiation media without penicillin/streptomycin to permit OPC maturation with half media change every other day using pre-equilibrated media.

For co-cultures overexpressing gain or loss of ATG5 function, rOPC were first infected, as above, with *wtAtg5* or *dnAtg5* pRevTRE retrovirus overnight, respectively. Cultures were then transfected with pRetroOn encoding doxycycline-inducible rTTA. rOPC were then seeded onto DRG cultures and maintained 7 days in differentiation media containing 5 µg/mL doxycycline. For pharmacological induction and inhibition of autophagy, rOPC were seeded onto DRG cultures and maintained 7 days in differentiation media containing 500 nM Tat-beclin1 (Millipore, Cat# 5.06416.0001) or 1 µM KU55933 (Tocris, Bristol, United Kingdom, Cat# 3544) or 150 nM Verteporfin (Sigma-Aldrich, Cat# SML0534).

Cultures were fixed with 4% PFA at room temperature for 10 minutes and washed (x3) with DPBS. Each myelination assay was replicated with independent rOPC isolates to achieve n=3 for ICC assessment of myelin segments by MBP and NFM immunostaining.

Transmission Electron Microscopy (TEM)

Mice were euthanized with an overdose of 2.0% avertin (2,2,2-tribromoethanol) in sterile NaCl solution administered intraperitoneally (i.p.) before slow transcardial perfusion (10-12 mL over 3-5 minutes) with ice cold PBS until the liver was clear and subsequent fixation with perfusion of cold 2% PFA/2% glutaraldehyde. Following fixation, brains were removed and 1 mm sagittal sections cut through the CC. Sections were post-fixed overnight in 2% glutaraldehyde and 100 mM sucrose in 0.05 M Sorensen's phosphate buffer and rinsed in 0.15 M phosphate buffer (x3) before post-fixing overnight with 1% OsO_4 at 4°C. Subsequently, sections were rinsed, dehydrated in graded ethanol solutions and embedded in Embed (Electron Microscopy Sciences, Hatfield, PA). Thin sections obtained with a Leica Ultracut E microtome were stained with uranylacetate/lead citrate for examination in a Philips CM-10 transmission electron microscope[163]. Axons and myelin were analyzed using Nikon Elements software. Using Nikon Elements software, 5800X and 6000X field images were used to determine density of myelinated and unmyelinated axons, myelin thickness, axon diameter, and frequency of myelin abnormalities. The sum of the axon diameter and myelin thickness was used to calculate myelinated axon diameter. G-ratios were calculated by taking the ratio of axon diameter to the myelinated axon diameter.

MTT Assay

DRGs were isolated from E15 Sprague-Dawley rat embryos as previously described[161,162,164]. Following isolation, DRGs were plated (7,500 cells/cm^2) and maintained on PDL/collagen-coated coverslips in NB1 neurobasal medium to

permit neurite outgrowth for at least two weeks and no more than four weeks. Monocultures were maintained for 3 days in OPC differentiation medium without OPCs containing 500 nM Tat-beclin1 (Millipore, Cat# 5.06416.0001) or 1 μM KU55933 (Tocris, Bristol, United Kingdom, Cat# 3544) or 150 nM Verteporfin (Sigma-Aldrich, Cat# SML0534). DRG survival was assayed by measuring tetrazolium, MTT (Sigma-Aldrich) to formazan at 570 nm wavelength as previously described[165].

Statistical Analysis

All data are presented as mean ± SD. Student's or one-sample *t* tests were used for two or one sample comparisons, respectively. For multiple comparisons, one-way ANOVA or two-way ANOVA analysis was performed followed by an appropriate post test as indicated in the figure legends.

Results

Maturing oligodendrocytes express elevated levels of autophagy markers

Immunohistochemistry (IHC) and confocal imaging confirmed that within the OL lineage, all cells express the autophagy markers ATG5 and LC3B (Figure 4). To more specifically assess changes in autophagy during OL differentiation, we performed immunoblot of lysates from proliferating OPCs and OLs differentiated for three days (Figure 5A). Conjugated ATG5 and LC3B-II were significantly increased in differentiated OLs compared to OPCs, and p62 levels were significantly decreased in differentiated OLs (Figure 5B). These changes are consistent with increased autophagosome formation and fusion with lysosomes during OL differentiation. The ratio of LC3B-II to LC3B-I was also

significantly increased, indicating autophagosome formation was increased (Figure 5C). We confirmed the increased autophagy activity in differentiating OPCs by infecting them with a retrovirus expressing mCherry-EGFP-LC3B, a well-established method for quantitatively measuring autophagic activity[166–168]. In these cells, as autophagosomes form, LC3B is incorporated which is N-terminally tagged with the two fluorescent proteins in tandem. Autophagosomes appear as yellow puncta due to the co-localization of red and green puncta. Upon fusion with the lysosome, the resulting acidification quenches the EGFP signal but not the mCherry signal, marking autolysosomes as red puncta. OPCs have few puncta of either type, whereas OLs display a marked increase in autophagosomes and autolysosomes compared to OPCs (Figure 5D). The overall numbers of autophagic vesicles were significantly increased in the processes of OLs compared to OPCs (Figure 5E). However, because OL processes grow larger as they differentiate, it is possible that the increase in autophagy vesicles is secondary to the increased space available in the processes. To address this issue, we compared the density of autophagy vesicles in the processes between proliferating OPCs (P) and OLs at day 4 of differentiation (D4). We detected a significant increase in the number of autophagy puncta per area in the processes of D4 differentiated OLs compared to OPCs (Figure 5F). The ratio of autolysosomes to autophagosomes, an indicator of autophagic flux, in the processes did not change (Figure 5G), although an increasing trend was seen during differentiation. Together, these

data suggest an increased functional requirement of autophagy during initial OL differentiation.

ATG5-dependent autophagy is required during myelin formation

The increasing autophagy activity during OL differentiation suggests a role for autophagy during OL maturation and/or myelination, which led us to investigate whether autophagy markers are present in developing myelin sheaths. Immunostaining revealed that these markers are present throughout the soma and processes of many OLs throughout the CC at P21 (Figure 6A). In myelinating co-culture, we see ATG5 puncta within the myelin around axons, suggesting that autophagosome biogenesis may be occurring there (arrows, Figure 6B). Furthermore, analysis of spinal cord cross sections at P12 demonstrates that ATG5 and LC3B are indeed detected in the myelin sheath (arrows, Figure 6C). Live-imaging of mCherry-LC3B tagged autophagosomes trafficking from the myelin/OL processes to OL soma in myelinating co-culture supports the possibility of distal autophagosome formation in OLs (arrows, Figure 6D). These data suggest that the requirement for autophagy could extend into the myelination process.

The increased autophagy activity and presence of autophagosomes in distal OL processes and myelin suggests that autophagy may regulate and be necessary for OL and myelin development. We tested this hypothesis by genetic ablation of *Atg5* specifically in OPCs. *Pdgfrα-Cre*^{ERT2}*:Atg5*$^{fl/fl}$ mice were analyzed after tamoxifen-induced deletion of *Atg5* in OPCs at P5-P9. The tamoxifen-injected mice developed a prolonged tremor by P12 (data not shown), showed

decreased weight gain (Figure 7A,B), and did not survive past P15. The reduction of ATG5 in OPCs of tamoxifen-treated mice can be detected as early as P9 (Figure 7C). Immunohistochemistry detected a 75% reduction in MBP immunostaining in the CC of tamoxifen-injected mice compared to vehicle-injected mice at P15 (Figure 7D,E). Ultrastructural analysis at P15 revealed a severe reduction in myelinated axon density in the CC in the tamoxifen-injected animals (Figure 7F,G). The CC from tamoxifen-injected mice contained a 4-fold reduction in the percent of myelinated axons compared to vehicle-injected mice (Figure 7G). Of those myelinated axons, 90% appeared abnormal in tamoxifen-injected mice (Figure 7H,I). Myelin abnormalities found in tamoxifen-injected mice include cytoplasm retention within uncompact myelin wraps (arrows), swelling of the inner tongue (asterisks), and myelin outfolding (arrowheads). Lastly, g-ratios of tamoxifen-treated increased compared to vehicle-treated mice, despite showing similar trends in axon caliber (Figure 7J-L). The severe effects on MBP immunofluorescence intensity as well as both the amount and quality of myelin strongly implicate autophagy as a critical regulator of myelin formation and structural integrity.

Loss of Atg5 severely impairs OPC survival and abates differentiation

To further investigate the underlying mechanism of the severe myelin deficiency in tamoxifen-treated mice, we analyzed the number of OL lineage cells in the CC of *Pdgfrα-Cre^{ERT2}:Atg5$^{fl/fl}$* mice after vehicle or tamoxifen administration at P5-P9. Immunostaining detected a loss of Olig2^{+} cells in the CC of tamoxifen-treated mice at P15 (Figure 8A,B). Further analysis at P15 found that the loss of

Olig2^{+} cells is likely mediated by reduced OPC numbers, marked by PDGFRα (Figure 8C,D). The loss of OPCs could be mediated either by reduced proliferation or increased cell death. *Pdgfrα-Cre^{ERT2}:Atg5$^{fl/fl}$* mice were injected with vehicle or tamoxifen, but sacrificed on the day of the last injection (P9) to visualize the OPC reaction to loss of *Atg5* before the cells themselves are lost. Tamoxifen-injected mice harbored elevated levels of CC3^{+}/APC^{+}(not significant) and CC3^{+}/PDGFRα^{+} double-positive cells compared to vehicle-injected mice (Figure 8E,F). These data indicate that apoptotic death of *Atg5$^{-/-}$* OPCs is one underlying cause of the severe myelin deficiency seen in tamoxifen-treated *Pdgfrα-Cre^{ERT2}:Atg5$^{fl/fl}$* mice.

While loss of *Atg5* leads to a drastic reduction in OPCs, some remain and produce myelin in the CC. Surviving OLs deficient in autophagy produce abnormal myelin that retains increased cytoplasm in the inner tongue and myelin wraps, as well as myelin outfoldings. We determined whether autophagy is necessary for OPC differentiation. Immunostaining for PDGFRα and APC of brain slices from vehicle- and tamoxifen-treated *Pdgfrα-Cre^{ERT2}:Atg5$^{fl/fl}$* mice was performed at P9, a time point before cells are lost for markers of the OL lineage (Figure 8G). Quantification revealed a significant decrease in APC^{+} cells in tamoxifen-treated animals compared to vehicle-treated (Figure 8H). However, it remained unclear whether the reduced OPC differentiation was due to OPC apoptosis or inhibited differentiation.

To distinguish these possibilities, neonatal OPC cultures were infected with a retrovirus containing no insert (empty vector, EV), *wtAtg5*, or *dnAtg5*

controlled by a Tet-responsive element (TRE). The transduced cultures were then transfected with pRetro-ON plasmid, which provides doxycycline-inducible expression rTTA that will then activate *wtAtg5* or *dnAtg5* expression and treated with doxycycline. EV, *wtAtg5*, and *dnAtg5* cells were immunostained for the mature OL marker, $O1^+$, after 3 days of differentiation (Figure 9A). Quantification revealed a significant reduction in the percentage of cells which were $O1^+$ in *dnAtg5*-expressing cells, compared to EV- or *wtAtg5*-expressing cultures. Importantly, a significant increase in the percentage of $O1^+$ cells was also detected in *wtAtg5*-expressing cultures compared to EV (Figure 9B). Immunoblots of OPC lysates showed an increase or decrease in LC3B-II in *wtAtg5*- or *dnAtg5*-expressing cells respectively, confirming changes in autophagic flux (Figure 9C,D). Furthermore, immunoblots indicated no significant increase in CC3, an indicator of apoptosis, of *dnAtg5*-expressing cells as was seen with loss of autophagy *in vivo* (Figure 9E,F). Together, these data suggest that autophagy directly regulates the developmental progression of the OL lineage, and even small changes in autophagic activity can have a drastic effect on OL differentiation.

Autophagy induction and suppression promotes and inhibits myelination, respectively

Data thus far demonstrate a role for autophagy in OPC survival, differentiation, and myelination. However, whether the autophagy pathway represents a viable target to modulate myelination is unknown. We compared the ability of *wtAtg5*- or *dnAtg5*-expressing OPCs to myelinate DRG neurons in co-

cultures. Myelin segments were visualized by immunostaining for MBP and NFM (Figure 10A). Cultures expressing wtATG5 produced significantly more myelin segments than dnATG5-expressing cultures (Figure 10B).

Control of myelination through pharmacological modulation of autophagy would indicate that autophagy is a promising target for further development of therapies for diseases involving myelin deficiency. We tested whether pharmacological induction and inhibition of autophagy, using drugs that directly target the autophagy pathway, altered myelination in the DRG/OPC co-cultures. KU55933 targets the Vps34 complex, preventing autophagosome formation and causing accumulation of p62[169]. Verteporfin inhibits autophagy through p62 oligomerization, resulting in disrupted autophagosome closure and exhausted single protein p62 levels[157,158]. Immunoblots on lysates of proliferating OPCs using autophagy inhibitors KU55933 and verteporfin confirmed the efficacy of these drugs, indicated by the increase and decrease of p62, respectively (Figure 10C,D). Autophagy inhibition with either KU55933 or verteporfin resulted in reduced number of myelin segments (Figure 10E,F). These cells display a symmetrical network of processes that often extended across axons without making myelin. When autophagy was enhanced using Tat-beclin1, increased numbers of myelin segments were observed, despite only a trend towards significance observed by immunoblot (Figure 10D).

Given the documented role of autophagy in neuronal maintenance, it is possible that these drugs may affect neuronal health in the DRG co-cultures. To address this possibility, we treated DRG monocultures with each drug for 3 days

before analyzing cell viability using an MTT assay. There was no significant difference in neuronal health between vehicle and experimental groups (Figure G,H).

Discussion

Differentiating OPCs display a clear induction of autophagy that persists through myelin formation. Homeostatic autophagy activity is found in all cell types[101]. This makes immunoblot studies of whole tissues lysates to detect changes in autophagy markers within a specific lineage difficult. Mature OLs appeared to display more robust immunostaining for autophagy markers than OPCs, especially in later stages of myelin development (Figure 4). The developmental progression of OPCs to OLs includes many potential stresses, such as the long distance migration, robust upregulation of transcription/translation, drastic changes in morphology, and an eventual culling of many OLs that have not associated with axons[135–137,139,140,170,171]. Autophagy serves as a pro-survival homeostatic pathway in many cell types and could provide a balance to prevent accumulation of errors in these processes during OL development[91,155,172].

Increased expression alone does not indicate increased autophagic activity. The increase of conjugated ATG5 and cleaved LC3B demonstrate activation of autophagy during OL differentiation, and the decrease of p62 levels suggests fusion with the lysosomes (Figure 5A-C). This was confirmed using mCherry-EGFP-LC3B, which labels autophagosomes with a fluorescent tag and indicates acidification. More fluorescent puncta overall and an increasing trend of

mCherry^{+}/EGFP^{-} puncta demonstrate both increased autophagosome formation and fusion with lysosomes during OL differentiation (Figure 5D-G). This increased autophagy during OL differentiation in culture suggests that the role of autophagy may extend beyond a pro-survival role during the demands of brain development. Moreover, the enrichment of autolysosomes in OL processes (Figure 5D-G) suggests that autophagy may have a specialized role specific to these processes. In neurons, autophagosomes form in the distal axon, migrate retrograde, and often fuse with lysosomes in the axon[173]. Multiple lines of evidence demonstrate the presence of autophagy proteins and autophagosomes in myelin in the brain and in culture (Figure 6). These data suggest an active role for autophagy in myelination, requiring induction of autophagy above basal levels.

Deletion of the essential autophagy gene *Atg5* during myelin development allowed direct assessment of the role of autophagy in myelination. The drastic reduction in MBP immunostaining and myelinated axons seen ultrastructurally indicate that autophagy is absolutely critical for myelination (Figure 7). Deletion of *Atg7*, another essential autophagy gene, in Schwann cells caused abaxonal accumulation of excess cytoplasm and organelles, as well as small fiber hypermyelination, suggesting autophagy regulates the structural formation of myelin in these cells[153]. However, in contrast to the CNS, the number of myelinated axons was not affected with *Atg7*$^{-/-}$ Schwann cells. Autophagy seems to play a broader role in myelinating OLs. Mice harboring OPC-specific deletion of *Atg5* display severely reduced numbers of myelinated axons (Figure 7F,G).

Furthermore, very few of the myelinated axons have normal appearing myelin. Most myelinated axons had myelin with expanded inner tongues, poor compaction of myelin wraps, and/or outfoldings of myelin (Figure 7H,I). Myelinated axons also possessed larger g-ratios despite similar trends in axon caliber (Figure 7J-L), suggesting a reduction in myelin thickness and myelin progression. To understand the mechanism(s) underlying the severe reduction in the overall amount of myelin in mice with OPC-specific *Atg5* deletion, multiple stages of OL development were assessed for the impacts of autophagy deficiency.

Studies in the Long-Evans shaker (*les*) rats showed that a mutation in MBP causes severe CNS dysmyelination and eventual demyelination[155]. Interestingly, *les* OLs also accumulate early and late autophagosomes as well as autophagy markers, including p62. Glucose and serum starvation enhanced *les* OL survival and membrane synthesis *in vitro*. Myelination in *les* rats undergoing intermittent fasting was also increased. In both cases, increased autophagy was observed. However, these results did not directly implicate autophagy in regulating normal OL development. We observed that OPC-specific loss of *Atg5* led to >2-fold reduction in Olig2^{+} cells (Figure 8). Furthermore, many more *Atg5*$^{-/-}$ OPCs were CC3^{+} prior to the dramatic loss of Olig2^{+} cells, which was beyond typical OL cell death observed during development and within vehicle-treated mice[28,170]. These data confirmed that the loss of OL lineage cells resulted in part from reduced OPC survival.

Although we sought to inhibit autophagy in OPCs alone, a subset of CNS pericytes, cells responsible for capillary blood flow and microcirculation, also express Pdgfrα. There is a possibility inhibition of *Atg5* in this subpopulation of pericytes may contribute to OL survival as well as the animal's overall health[174]. However, as in neurons and astrocytes[118,144,145,153,175,176], autophagy deficiency inhibits OL differentiation *in vitro* and *in vivo* (Figure 9), suggesting *Atg5*$^{-/-}$ pericytes are not the main contributors to OPC loss and irregular myelin development. This may also explain the much greater reduction in myelination compared to the decreased number of Olig2^{+} cells seen in *Pdgfrα-Cre*^{ERT2}*:Atg5*$^{-/-}$ mice.

Autophagy has been implicated in the control of cytoskeletal dynamics and signaling cascade regulation in other cell types. In macrophages and cortical neurons, autophagy regulates cell spreading and neurite extension by modulating Rho-family GTPase activity and actin dynamics[152,177]. During OL differentiation, the cytoskeleton undergoes extensive regulation to drive the changes in morphology[134]. Moreover, Nawaz et al. (2015) and Zuchero et al. (2015) demonstrated that actin disassembly and likely removal is required for myelination[178,179]. Whether autophagy regulates the precise signaling pathway transition or cytoskeleton component status in OL requires further investigation.

Many of the factors driving OL differentiation induce autophagy in other cell types. The sphingolipid network, MAPK pathway, and mTOR are all critical regulators of OL differentiation, and all have known roles in the regulation of autophagy[180–186]. Many of the drugs commonly used to control autophagy target

signaling proteins upstream of the autophagy pathway. Myelination by neuropathic Schwann cells was promoted by the mTOR inhibitor rapamycin, which enhances autophagy[187]. However, mTOR signaling is a master switch that also regulates protein synthesis, lipid synthesis, lysosomal biogenesis, energy metabolism, cell survival/metabolism, and cytoskeletal organization[188]. Thus, delineating its role solely as an autophagy activator is problematic. In current studies using myelinating co-cultures, we used drugs that target the autophagy pathway directly. Intriguingly, enhancing autophagy using the Tat-beclin1 peptide, which activates the Beclin-1/Vps34 complex, promoted myelination (Figure 10C,D). Conversely, blocking autophagy with KU55933 targeting the Beclin-1/Vps34 complex or Verteporfin targeting p62 inhibits myelination. Importantly, similar myelination results were obtained by genetically enhancing and inhibiting autophagy through overexpression of wtATG5 and dnATG5, respectively (Figure 10A,B). Taken together, these data suggest autophagy has a key regulatory role in multiple stages of myelin development.

The induction of autophagy during OL differentiation, as well as the loss of OPCs, inhibition of differentiation, and lack of proper myelin formation in mice with OPC-specific autophagy deficiency provide strong evidence that autophagy is critical in many aspects of OL development and myelination. It remains unclear what initiates autophagy, but it is likely that multiple stage-specific triggers exist. Whether particular targets of autophagy exist that mediate the bulk of the myelin regulation requires further exploration. Determining the factor(s) that signal autophagosome formation and key functional targets of autophagy is essential to

delineating the entirety of the role of autophagy in myelination. However, the tremor phenotype and perinatal death of mice with OPC-specific autophagy deficiency makes autophagy an attractive target for development of myelin repair therapies. Until more specific pharmacological agents, with limited effects beyond autophagy, can be developed, therapeutic translation will be difficult. It is therefore critical that further work be performed to understand the role and regulation of autophagy in normal and pathological conditions, as well as its utility as a potential therapeutic target in dysmyelinating and demyelinating disease.

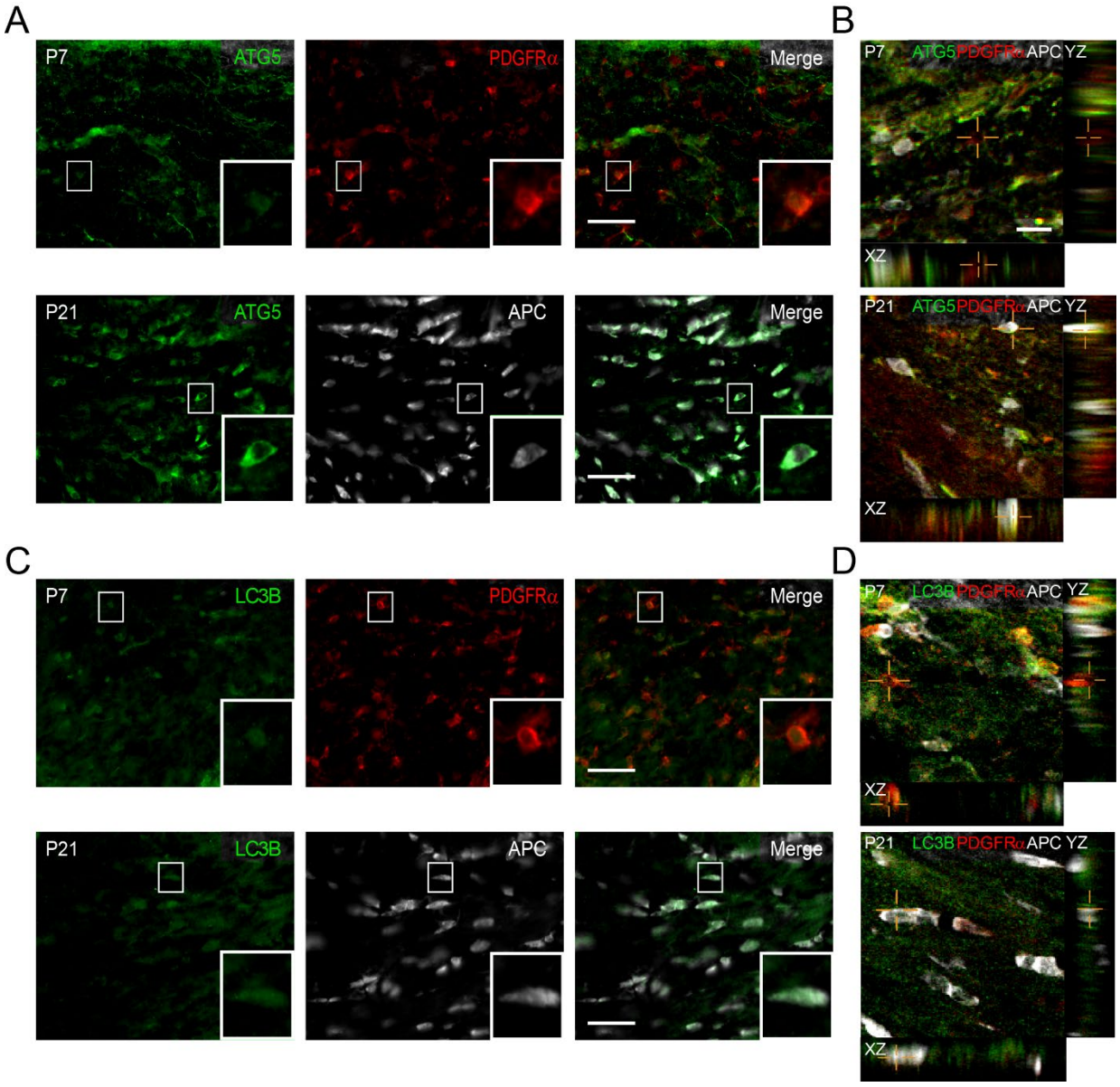

<u>Figure 4.</u> Autophagy markers are expressed throughout the OL lineage.

(**A**) ATG5 expression during OL lineage development in PDGFRα^{+} and APC^{+} cells in the CC at P7, and P21. Enlarged insets of a single cell are shown. Scale bar = 50 μm. (**B**) Confocal microscopy confirms the co-expression (crosshairs indicate representative cells) of ATG5 in APC^{+} cells at P7 and P21, as XZ and YZ focal planes are shown. Scale bar = 25 μm. (**C**) LC3B expression during OL

lineage development in PDGFRα$^+$ and APC$^+$ cells in the CC at P7 and P21. (**D**) Confocal microscopy confirms the co-expression (crosshairs indicate representative cells) of LC3B in PDGFRα$^+$ and APC$^+$ cells at P7 and P21, as XZ and YZ focal planes are shown.

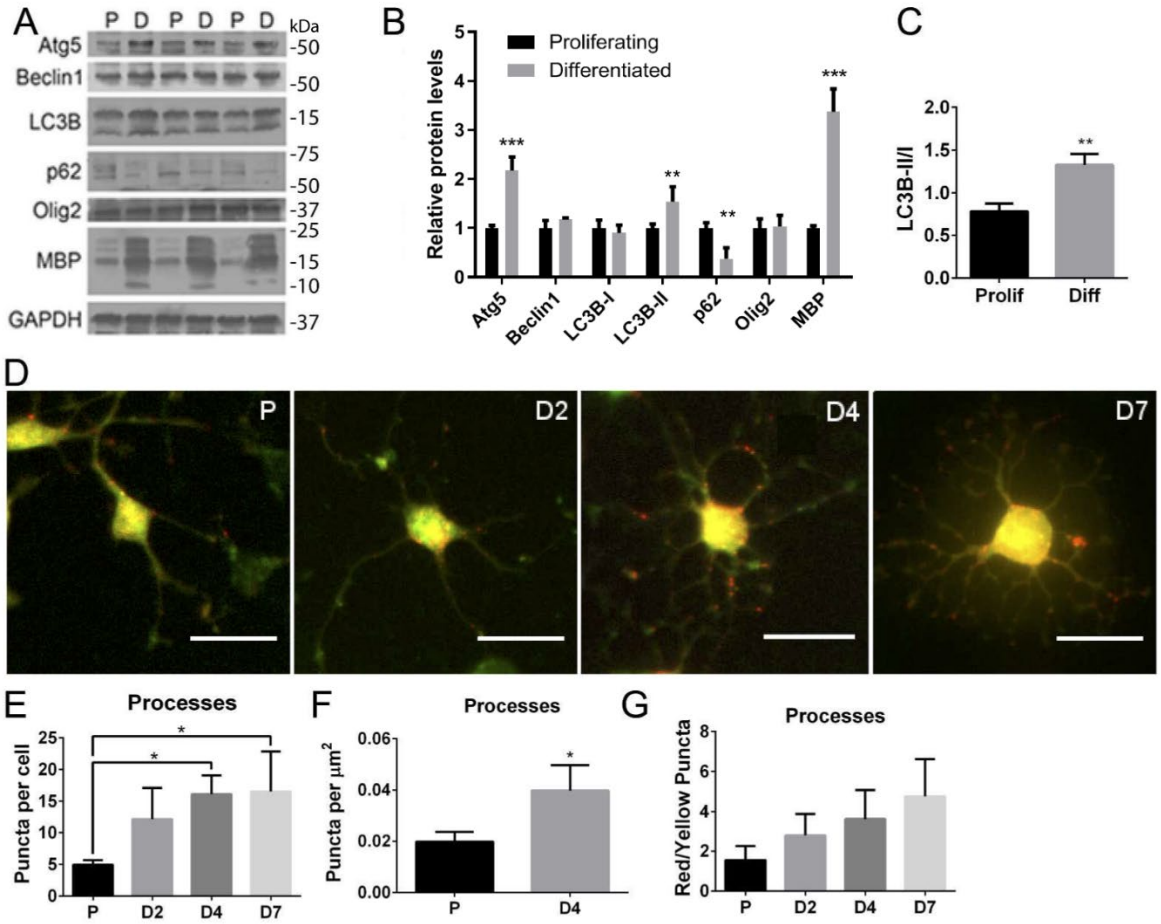

<u>Figure 5.</u> Autophagy activity increases during OL differentiation.

(**A**) Immunoblot of autophagy markers in proliferating OPCs (P) and OPCs differentiated for 3 days (D). In (**B**) data are quantified (± SD, n = 3; ***p<0.001, two-way ANOVA; **LC3B-II p<0.01, **p62 p<0.01, Bonferroni's post test). Increased ATG5 and LC3B-II and decreased p62 indicate upregulation of autophagic flux in OLs. (**C**) The ratio of LC3B-II to LC3B-I in immunoblots from proliferating and differentiating OPCs in (**A**) is quantified (± SD, n=3, **p<0.01, two-tailed *t* test). (**D**) OPCs were infected with a retroviral vector (pBABE-puro mCherry-GFP-LC3B) which marks autophagosomes yellow and autolysosomes

red. Scale bar = 20 μm. (**E**) The data in (**D**) are quantified showing the number of puncta (± SD, n = 3; **p<0.01, one-way ANOVA; **proliferating OPCs vs OLs differentiated 4 days (PvD4) p<0.01, **proliferating OPCs vs OLs differentiated 7 days (PvD7) p<0.01, Sidak's post test) in the processes relative to the total cell number. (**F**) The density of puncta in the processes (± SD, n=3, *p<0.05, two-tailed *t* test) on day 4. (**G**) The ratio of red to yellow puncta (± SD, n = 3) in the processes (ns).

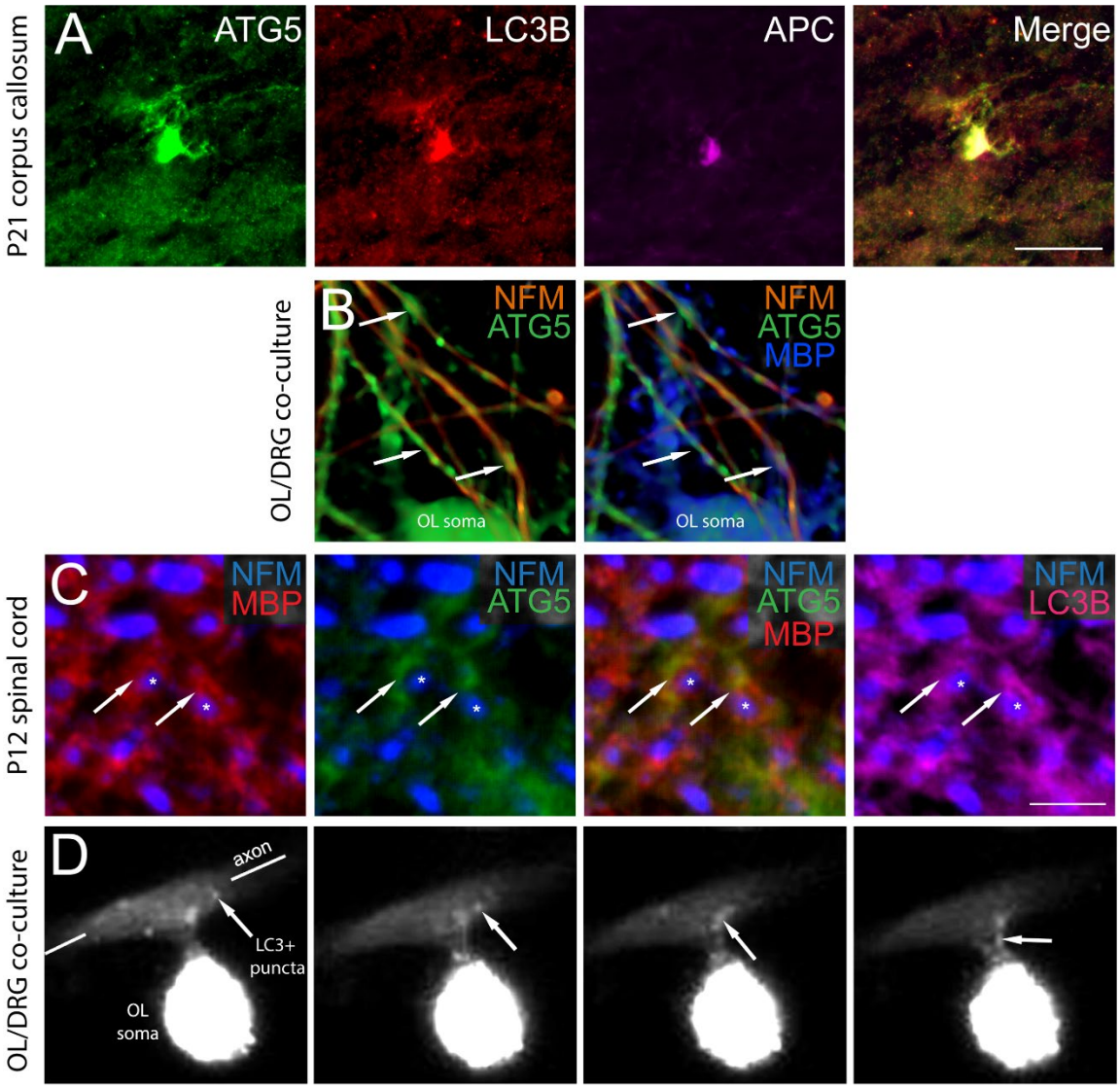

Figure 6. Autophagy is active in distal OL processes and myelin.

(**A**) Detection of ATG5 and LC3B in distal processes and soma of APC$^+$ mature OLs in CC from a 3 week old mouse. Scale bar = 50 μm. (**B**) OPCs were differentiated for 6 d in co-culture with DRG neurons and immunostained. In myelinating co-cultures, ATG5 co-stains with MBP; NFM marks axons. (**C**) Detection of ATG5 and LC3B in MBP$^+$ myelin wraps surrounding axons in spinal cord from a 2 week old mouse. Axons where exclusion of ATG5 from compact

myelin is most apparent are marked by *. Arrows indicate double immunostaining. Scale bar = 20 μm. (**D**) Live imaging frames of myelinating co-cultures where OLs express mCherry-LC3B. Arrow tracks mCherry-LC3B puncta from a presumably myelinated process to the OL soma.

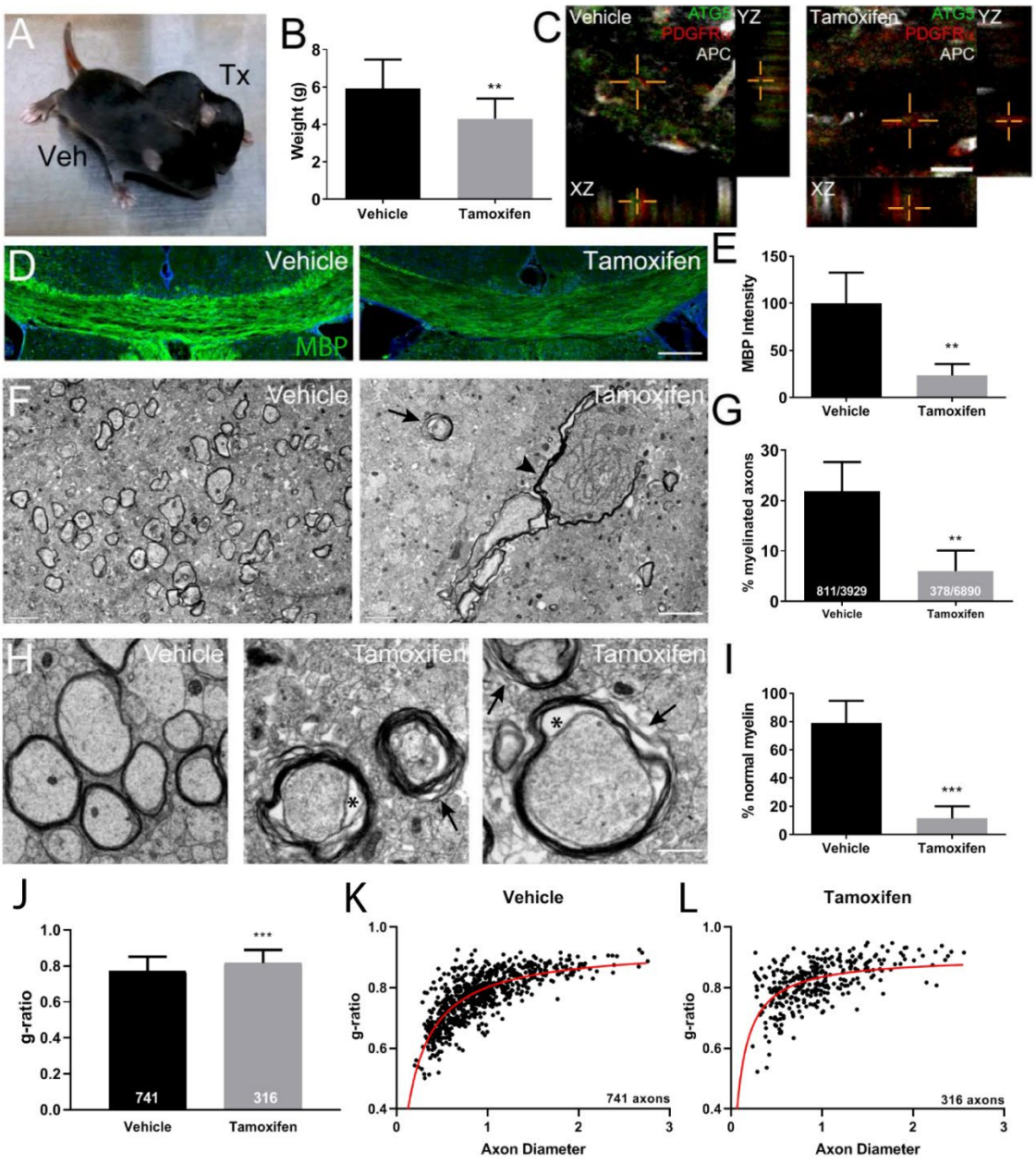

<u>Figure 7.</u> Reduced and defective myelination with OPC-specific deletion of Atg5.

(**A**) Image of vehicle- and tamoxifen-treated (beginning at P5) *Pdgfrα-Cre^{ERT2}:Atg5$^{fl/fl}$* mice at P10. (**B**) Average weight of vehicle- and tamoxifen-treated *Pdgfrα-Cre^{ERT2}:Atg5$^{fl/fl}$* mice at P10 (± SD, vehicle n=13, tamoxifen n=16;

p<0.01, two-tailed *t* test). (C**) Immunostaining to confirm *Atg5* deletion in OPCs in the CC of tamoxifen-treated mice at P9. Scale bar = 25 μm. Co-localization is seen in XZ and YZ planes, and is indicated by crosshairs. (**D**) *Pdgfrα-Cre^{ERT2}:Atg5$^{fl/fl}$* mice at P5 were administered daily i.p. injections of vehicle or tamoxifen for 6 days. MBP expression was reduced (± SD, n=4; **p<0.01, two-tailed *t* test) in tamoxifen-treated mice as quantified in (**E**). Scale bar = 200 μm. (**F**) Transmission electron micrographs showing reduced myelinated axons, impaired myelin compaction (arrows) and myelin outfoldings (arrowhead) in tamoxifen-treated *Pdgfrα-Cre^{ERT2}:Atg5$^{fl/fl}$* mice. Scale bar = 2 μm. (**G**) Percentage of axons which are myelinated in (**F**) (± SD, vehicle n=3, tamoxifen n=4; **p<0.01, two-tailed *t* test). The numbers of axons quantified are given. (**H**) High magnification TEM of axons in the CC showing disrupted myelin sheaths (arrows) and enlarged inner tongues (asterisks) in tamoxifen-treated *Pdgfrα-Cre^{ERT2}:Atg5$^{fl/fl}$* mice. Scale bar = 0.5 μm. (**I**) Percent of myelinated axons in vehicle- and tamoxifen-treated that have normal myelin with apparent abnormalities defined as swollen inner tongue, myelin decompaction, and/or myelin outfoldings (± SD, vehicle n=3, tamoxifen n=4; ***p<0.001, two-tailed *t* test). (**J**) g-ratios of myelinated axons in tamoxifen-treated and vehicle-treated *Pdgfrα-Cre^{ERT2}:Atg5$^{fl/fl}$* mice (± SD, vehicle n=3, tamoxifen n=4; ***p<0.001, two-tailed *t* test). The numbers of axons quantified are indicated. The relationship between axon diameter and g-ratio is shown for (**K**) vehicle-treated and (**L**) tamoxifen-treated *Pdgfrα-Cre^{ERT2}:Atg5$^{fl/fl}$* mice. The numbers of axons quantified are indicated.

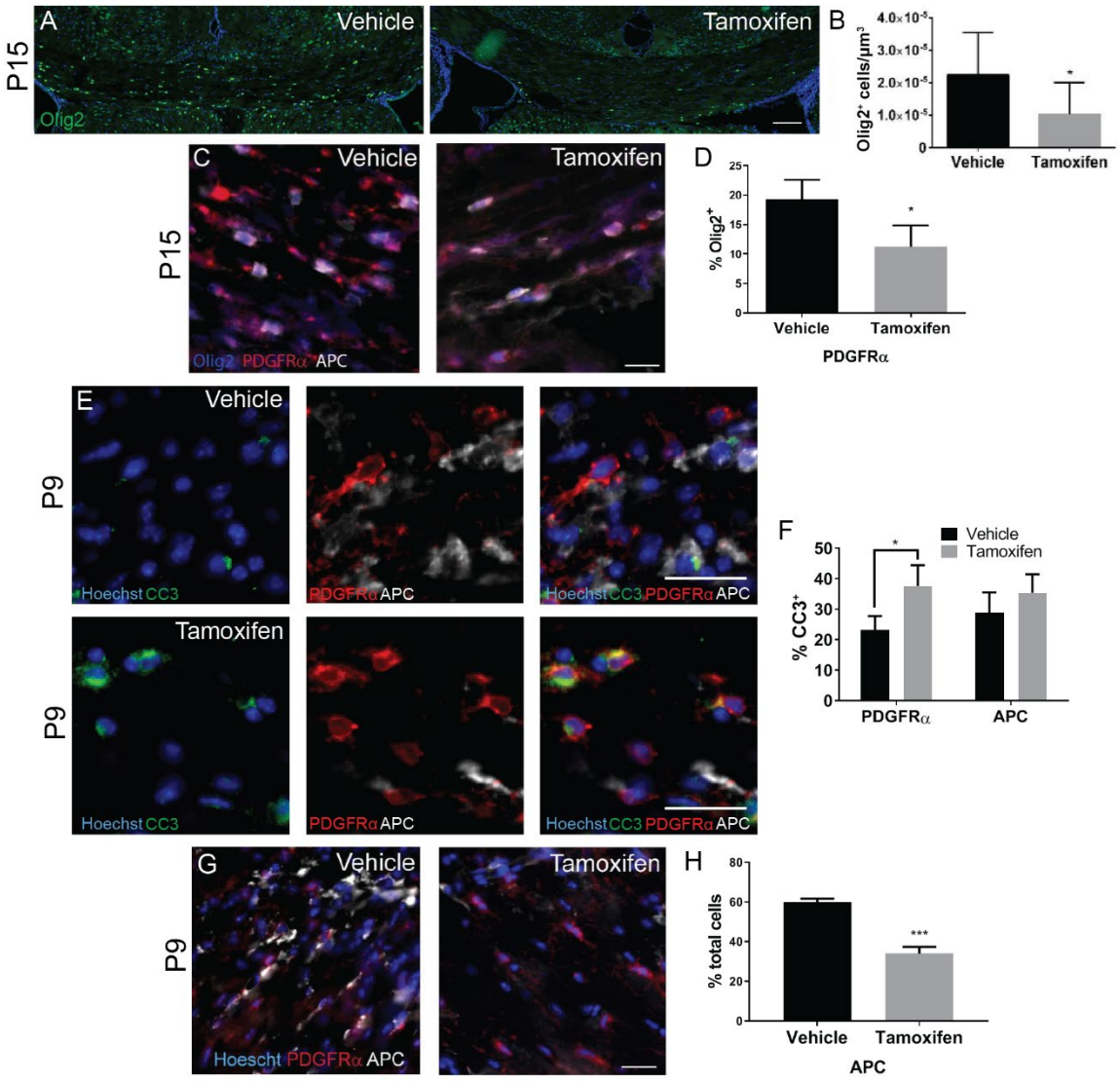

Figure 8. Apoptotic death and reduced differentiation of Atg5-/- OPCs.

(**A**) *Pdgfrα-Cre^{ERT2}:Atg5$^{fl/fl}$* mice at P5 were administered daily i.p. injections of vehicle or tamoxifen for 6 days. Olig2 expression in the CC was reduced in tamoxifen-treated mice. Scale bar = 200 μm. (**B**) The numbers of Olig2^{+} cells/μm^{3} in the CC were quantified (± SD, n=4; *p<0.05, two-tailed *t* test). (**C**) Reduced PDGFRα^{+} cells in the CC of tamoxifen-treated *Pdgfrα-Cre^{ERT2}:Atg5$^{fl/fl}$* mice. Scale bar = 25 μm. (**D**) The percent of Olig2 cells labeled by PDGFRα (OPC) was

reduced in tamoxifen-treated CC (± SD, n=4; *p<0.05, two-tailed *t* test). (**E**) Increased $CC3^+$/$PGDFR\alpha^+$ cells in the CC of tamoxifen-treated *Pdgfrα-Cre^{ERT2}:Atg5$^{fl/fl}$* mice; data are quantified in (**F**) (± SD, n=3; *p<0.05, two-way ANOVA; *p<0.05, Sidak's post test). Scale bar = 25 μm. (**G**) Prior to OPC loss, reduced numbers of APC^+ cells are detected in the CC from tamoxifen-treated *Pdgfrα-Cre^{ERT2}:Atg5$^{fl/fl}$* mice; data are quantified in (**H**) (± SD, n=3; ***p<0.001, two-tailed *t* test). Scale bar = 25 μm.

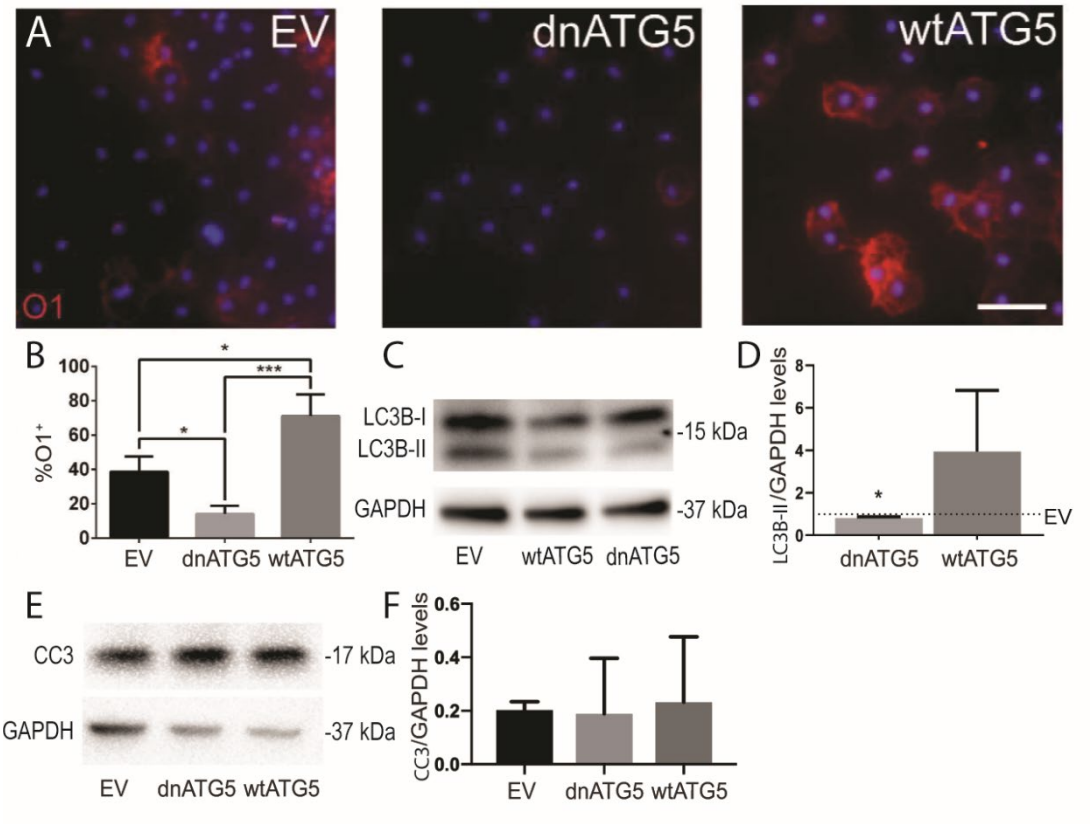

<u>Figure 9.</u> Autophagy is required for OL differentiation.

(**A**) Reduced and increased $O1^+$ cells in differentiated OL cultures overexpressing dnATG5 or wtATG5, respectively, compared to EV. Scale bar = 150 µm. (**B**) Data indicate the percentage of total cells which are $O1^+$ (± SD, n=3; ***p<0.001, one-way ANOVA; *dnATG5 p<0.05, *wtATG5 p<0.05, *** p<0.001, Tukey's post test). (**C**) Immunoblot of the autophagy marker LC3B in proliferating OPCs overexpressing wtATG5, dnATG5 or EV control; data are quantified in (**D**) relative to EV (dotted line) (± SD n=3; dnATG5* p<0.05, one-sample *t* test). (**E**) Immunoblot of CC3, an indicator of apoptosis, in differentiated OL cultures overexpressing wtATG5, dnATG5 or EV control; data are quantified in (**F**) (± SD n=3; n.s., one-way ANOVA).

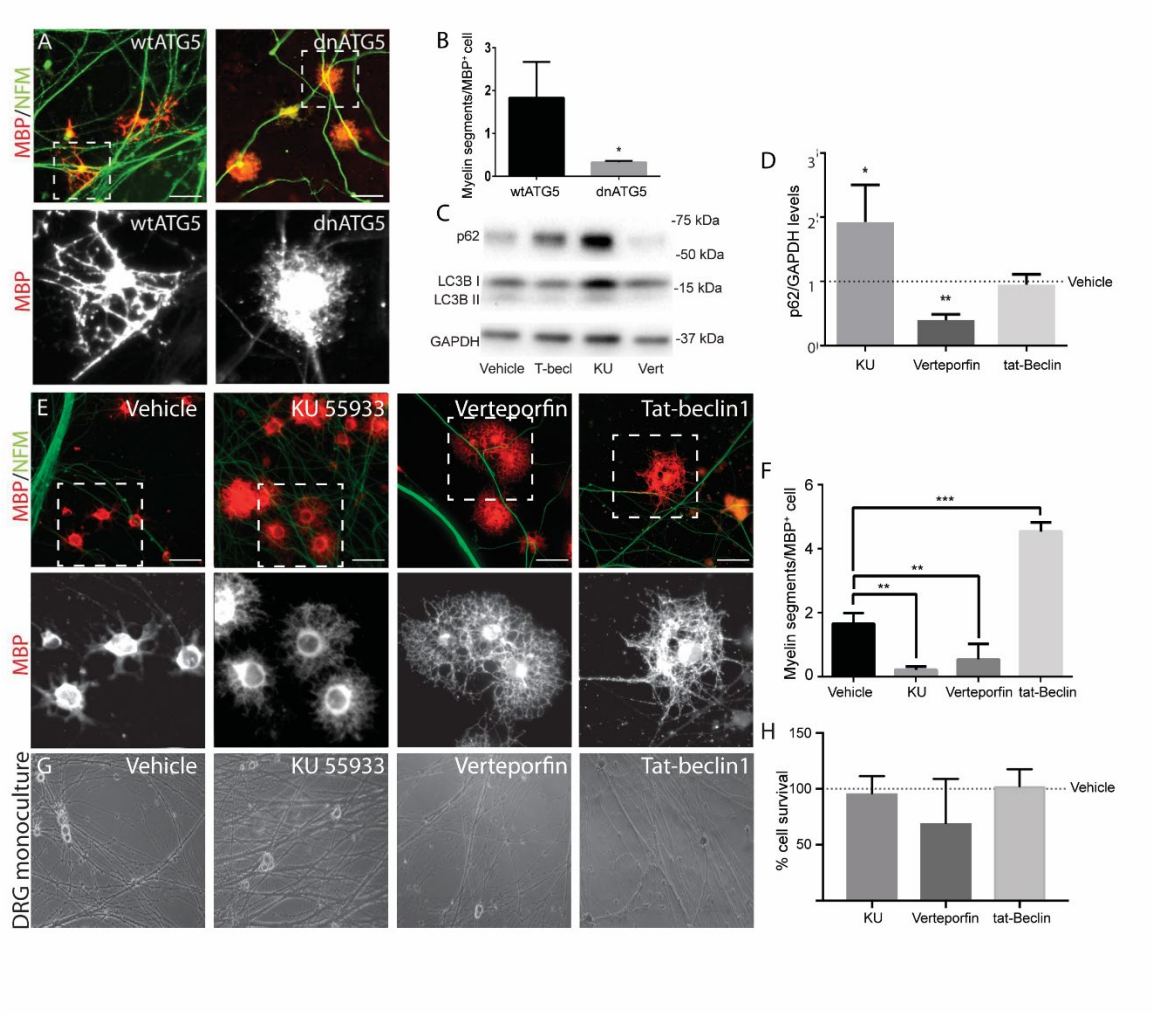

<u>Figure 10.</u> Myelination requires autophagy and can be enhanced by autophagy induction.

OPCs were differentiated for 6 d in co-culture with DRG neurons and then immunostained for MBP (red) and NFM (green): (**A**) *dnAtg5* overexpression in OPCs led to reduced number of myelin segments compared to *wtAtg5* overexpression. Scale bar = 50 μm. (**B**) Myelin segments (yellow co-localization) per cell in (A) are quantified (± SD, n=3; *p<0.05, two-tailed *t* test). (**C**) Immunoblot of the autophagy marker LC3B-I, LC3B-II, and p62 in proliferating OPCs treated with 1 μM KU55933, 100 nM Verteporfin, or 500 nM Tat-beclin1 for

24 hours; data are quantified in (**D**) (± SD, n=4, *p<0.05, one-way ANOVA; *KU p<0.05, **Verteporfin p<0.01, Dunnett's post test). (**E**) Reduced myelin segments after treatment with 1 μM KU55933 or 100 nM verteporfin, and increased myelin segments after treatment with 500 nM Tat-beclin1. Scale bar = 50 μm. Below each image, an enlarged inset of the MBP signal is shown. (**F**) The number of myelin segments (yellow co-localization) per cell in (**E**) is quantified (± SD, n=3; ***p<0.001, one-way ANOVA; **KU p<0.01, **Verteporfin (Vert) p<0.01, ***Tat-beclin1 (t-Becl) p<0.001, Tukey's post test). (**G**) phase-contrast images of DRG monocultures treated with autophagy drug for 3 days. (**H**) MTT assay showed no difference in cell viability of DRGs treated with autophagy drugs compared to vehicle control.

CHAPTER III

ENHANCED OXIDATIVE PHOSPHORYLATION, RE-ORGANIZATION OF INTRACELLULAR SIGNALING, AND EPIGENETIC DE-SILENCING AS REVEALED BY OLIGODENDROCYTE TRANSLATOME ANALYSIS AFTER CONTUSIVE SPINAL CORD INJURY

Introduction

Contusive SCI has a complex pathogenesis that involves time-dependent components including primary and secondary injuries as well as post-injury remodeling and plasticity[189]. SCI associated white matter damage including loss and / or demyelination of axons is a major driver of functional deficits below the level of injury[117,190]. Death of OLs contributes to white matter damage post-SCI[107,108]. However, few OL-expressed genes such as *p75 / Ngfr*[191]*, Bax*[192] or *Klk8*[193] have been implicated as mediators of SCI-induced OL death / white matter damage. This is at least partly due to limited insight into the OL gene expression programs after SCI.

Single cell (sc) RNASeq technology has been recently applied to study the SCI transcriptomic response at the cellular level[194,195]. Specifically, scRNASeq-enabled transcriptomic phenotyping revealed region-specific changes in OL subtype content at chronic timepoints after hemisection or contusion SCI[194]. However, few SCI-associated OL gene expression changes were detected[194].Importantly, the currently available scRNASeq technology has

significant limitations. Its reliance on successful sorting of suspensions of viable cells is a problem when dealing with cells that have complex morphologies, spatially-regulated transcriptomes and / or sustained significant damage due to injury[196]. Additional challenges include limited depths / low sensitivity, high level of stochastic variability of single cell transcriptomes, ambiguity in interpreting negative signals, and data set contamination with highly expressed mRNAs that were released from other cells that lysed during sample preparation and / or sorting[196,197]. Finally, scRNASeq is focused on overall cellular mRNA levels. Therefore, scRNASeq data lack information on gene expression regulation at the level of protein synthesis. Yet, such post-transcriptional regulation is present in neurons and OLs[198–200]. In addition, it plays a major role in response of those cells to pathologies[198–200].

Isolation of translating ribosomes and quantification of their associated mRNAs offers insight into the cell translatome and accounts for translation initiation, which is the critical regulatory step of protein synthesis[198–200]. RiboTag and translating ribosome affinity purification (TRAP) are two similar technologies to analyze cell type-specific translatomes in whole animal studies[129,201,202]. In RiboTag mice, cell type-specific expression of the Cre recombinase results in removal of a stop codon to produce the RPL22 protein with a hemagglutinin (HA) tag at the C-terminus[129,202]. The large ribosomal subunit that contains RPL22-HA associates with the small ribosomal subunit during successful translation initiation, which enables immunoaffinity isolation of translating ribosomes by targeting the HA tag. Then, cell type-specific translatomes are determined by

RNASeq[129,202]. RiboTag has been successfully applied to study gene expression changes in astrocytes and macrophages after contusive thoracic SCI[203,204].

The current study has been initiated to determine the translatome of mature OLs at various stages of recovery following moderate contusive SCI at the T9 level. RiboTag identified hundreds of differentially expressed genes in SCI-challenged OLs. These newly described gene expression landscapes implicate axonal disconnection and loss of myelin sheaths as major drivers of the acute OL gene expression response to SCI. Unexpectedly, similar factors may contribute to OL gene expression regulation in the subchronic phase of recovery.

Materials and Methods

Animals

All animal procedures were performed in strict accordance with the Public Health Service Policy on Humane Care and Use of Laboratory Animals, *Guide for the Care and Use of Laboratory Animals*[159]*,* and adhered to NIH guidelines on the use of experimental animals. Animal procedures were approved by the University of Louisville Institutional Animal Care and Use (IACUC) and Institutional Biosafety (IBC) Committees. Timed-pregnant Sprague-Dawley rats and wild-type (WT) C57Bl/6 mice (6-8 weeks) were obtained from Envigo (Indianapolis, IN). *Plp-cre*^{ERT2} (proteolipid protein) (B6.Cg-Tg (Plp1-Cre/ERT)3Pop/J; Stock No: 005975)[205] and RiboTag mice (*Rpl22*$^{fl(STOP)fl\text{-}HA/wt}$, B6J.129(Cg)-Rpl22 $^{tm1.1Psam2}$/SjJ); Stock No: 029977)[129,202], both on C57Bl/6 background, were acquired from the Jackson Laboratory (Bar Harbor, ME). These lines were crossed to produce OL-RiboTag mice (*Plp-*

Cre$^{ERT2+/wt}$*:Rpl22*$^{fl(STOP)fl-HA/wt}$). Genotypes of the crosses were confirmed using standard PCR genotyping as recommended by the Jackson Laboratory. To induce OL RiboTag expression, OL-RiboTag mice received 1 mg tamoxifen (20 mg / mL in sunflower oil) i.p. daily for 8 days as previously described[123]. Male and female mice were used for initial validation of RiboTag transgene induction.

Spinal cord injury

Female WT or OL-RiboTag mice were used for SCI at 8-10 weeks of age. In tamoxifen-induced mice, SCI was performed 3 weeks after completion of the induction treatment. Anesthetized animals (400 mg / kg body weight 2,2,2-tribromoethanol i.p.) were shaved around the surgical site and disinfected using 4% chlorohexidine solution. Lacri-Lube ophthalmic ointment (Allergen, Madison, NJ) was applied to prevent eye drying. Following dorsal laminectomy at the T9 vertebrae, moderate contusive SCI was performed using the IH impactor (50 kdyn force / 400-600 μm displacement, Infinite Horizons, Lexington, KY) as previously described[115]. Sham controls only received T9 laminectomy. Starting immediately after surgery, postoperative care included 0.1 ml saline (s.c. daily for 7 days), 5 mg / kg gentamycin (s.c. daily for 7 days), 0.1 mg/kg buprenorphine (s.c. every 12 h for 2 days), and manual expression of bladders twice a day for seven to ten days or until spontaneous voiding returned. All surgical and post-surgery procedures were completed according to NIH and IACUC guidelines. All surgeries were performed without knowledge of group assignment or genotype.

Tissue collection

Anesthetized mice were transcardially perfused with phosphate buffered saline (PBS, 4°C). For immunostaining, this was followed by 4% paraformaldehyde (PFA in PBS, 4°C) perfusion. Then, a 5 mm portion of the spinal cord spanning the injury epicenter was dissected and (i) post-fixed for 1 hr in 4% PFA at 4°C (immunostaining) or (ii) flash frozen in liquid nitrogen and stored at -80°C until further use (RiboTag polysome purification or RNA / protein isolation).

Immunostaining

Tissue processing, preparation of frozen 20 µm coronal (transverse) spinal cord sections, immunostaining and epifluorescent (RPL22-HA) or confocal (STEAP3, PCYOX1L) imaging followed standard protocols as previously described[115,132]. Primary antibodies used were as follows: anti-APC (mouse CC1 clone, 1:200, Abcam, Cambridge, UK, Cat# ab16794, RRID: AB_443473), anti-HA (mouse, 1:1000, HA.11 Clone 1612, Biolegend, San Diego, CA, Cat# 901516, RRID: AB_2820200), anti-STEAP3 (species: rabbit, dilution: 1:200, Thermo Fisher Scientific, Walthanm, MA, Cat# PA5-102321, RRID: AB_2851729), anti-PCYOX1L (species: rabbit, dilution: 1:200, Atlas Antibodies, Bromma, Sweden, Cat# HPA037463, RRID: AB_10673632), anti-CNP (species: mouse, dilution: 1:200, Biolegend Cat# 836404, RRID AB_2566639), anti-phospho-NFH (species: mouse, dilution: 1:500, Biolegend Cat# 801601, RRID: AB_2564641), anti-MBP (species: chicken, dilution: 1:500, Thermo Fisher Scientific Cat# PA1-10008, RRID: AB_1077024). Species- and isotype-specific Alexa488-, Alexa594-, or Alexa647- F(ab')2 secondary antibodies (donkey, 1:200, Life Technologies) were used. Counting RiboTag / HA^+ cells were

performed without knowledge of sample origin (genotype or tamoxifen treatment).

RiboTag RNA purification and RNASeq

Frozen spinal cord samples from 2 mice were pooled to produce one biological replicate (3 biological replicates/group representing 6 animals). Pooling was done to increase RNA yield of the RiboTag immunopurification as determined in pilot experiments. SCI and naïve mouse spinal cord samples were processed for input polysome-associated mRNAs (total spinal cord mRNA) or immune-purified OL polysome mRNAs using anti-HA antibody and magnetic beads as previously described[129,202]. RNA isolation, mRNA library preparation and RNA sequencing on the Illumina NextSeq 500 platform followed standard procedures. Before preparing RNASeq libraries, successful isolation of OL polysomes was verified by qPCR for OL- and non-OL cell marker transcripts.

Quantitative real-time PCR

To prepare cDNA, the SuperScript IV system was used following manufacturer's recommendations (Thermo Fisher, Cat# 18091050). qPCR was run using a microfluidic Custom TaqMan Gene Expression Array Card (Thermo Fisher, Cat# 43442249) containing primers for CNS cell-type specific marker mRNAs of oligodendrocytes (*Mbp, Plp1, Mog, Cldn11, Mobp, Opalin, Mag, Fa2h, Gjb1, Ermn, Gjc2, Klk6, Sox10*), astrocytes (*Aldh1l1, Hgf*), neurons (*Reln, Snap25, Lhx5*), and microglia/macrophages *(Osm, Cd68, Tmem19).* RNA levels were quantified using the ΔΔCT method with *Hprt, Ppia,* and 18S rRNA as reference transcripts. For each sample pair (OL translatome and total spinal cord

RNA from which OL translatome was isolated), OL mRNA levels were determined as a fold change of their total spinal cord expression.

RNASeq data analysis

Analysis of sequenced RNA was performed by the Kentucky IDeA Networks of Biomedical Research Excellence (KY INBRE) Bioinformatics Core. A quality control analysis was performed using FastQC (v.0.10.1) and indicated good sequencing quality. The reads were directly aligned to the *Mus musculus* reference genome (mm10.fa) using the STAR aligner (version 2.6). The average number of sequenced reads per sample was ~37,500,000 with an average alignment rate of 98.06%. Raw read counts were generated using HTSeq (v.0.10.0) and input to DESeq2 for differential expression analysis. The raw counts were normalized using Relative Log Expression (RLE) and filtered to exclude genes with fewer than 10 counts across samples. Principal component analysis (PCA) was performed on all 24 samples to measure variance of the overall mRNA expression pattern across all groups/sample sets. As part of the differential expression analysis, a DESeq2 interaction term was used to analyze differential OL enrichment after SCI and can be defined by delta $Log_2FC(OL/total)=Log_2FC(OL/total)\_SCI – Log_2FC(OL/total)\_naive$. In this analysis, OL translatome- and total spinal cord RNA samples from the same tissue were paired for determination of differential OL enrichment. To identify genes with an RNA origin-specific effect (OL vs. total) at one or more time points, the full regression model was compared to a reduced model using a likelihood ratio test. Group-specific effects were then identified at individual timepoints

using a Wald test for significance. All RNASeq data are available in GEO (Accession number: GSE225308). A searchable, public database is also available at http://scigenedatabase.com/.

Gene Ontology (GO) functional annotation analyses

GO analysis was performed using g:Profiler (version *e*108_eg55_p17_d098162)[206]. Mitochondrial respirasome genes (Respirasome_GO_0005746) were retrieved from g:Profiler, and cholesterol biosynthesis superpathway genes were retrieved from Kegg Pathway (mmu:00100 and mmu:00900) and BioCyc databases[207]. Mitochondrial respirasome (Respirasome_GO_0005746) and cholesterol biosynthesis superpathway gene lists were retrieved from Metascape or Kegg Pathway (mmu:00100 and mmu:00900) databases, respectively.

Gene list overlap analyses

Lists of top 500 neural cell type-enriched transcripts were obtained from the BrainRNASeq database (www.brainrnaseq.org)[208]. Their overlaps with the SCI-regulated OL mRNAs were analyzed using the hypergeometric test (http://nemates.org/MA/progs/overlap_stats.html). In those calculations, the maximal number of all identified transcripts across all analyzed samples (17,168) was used to define the size of the whole spinal cord transcriptome.

Immunoblotting

Immunoblotting followed standard methodology as previously described[115]. The primary antibodies included STEAP3 and GAPDH (loading control) (Chemicon, 1:1000, Temecula, CA). BioRad ChemiDoc MP Imaging

System was used. Immunoblot quantifications were performed using TIFF-formatted blot images and BioRad Image Lab software.

Cell culture

Isolation, culture, and OL differentiation of rat neonatal OPCs followed previously described methodology[132]. Cells were treated as follows: FCCP (50 uM working stock solution in 0.1% DMSO / cell culture medium that was diluted to final concentrations 500 nM or 100 nM in cell culture medium; the FCCP stock was always prepared fresh), Tunicamycin (10 mg / ml stock prepared in DMSO and diluted to the final concentration of 2 ug / ml in culture medium) or their vehicle (0.02% DMSO in culture medium). Each solution was made fresh on day of treatment.

Statistical analysis of immunostaining, qPCR and immunoblotting data

All ratiometric data including % RiboTag$^+$ cells, qPCR-determined total spinal cord-normalized OL mRNA levels and control treatment-normalized protein expression were performed using the two-tailed non-parametric Mann-Whitney *u*-test.

Results

Isolation and sequencing of the OL translatome from the spinal cord

OL-RiboTag mice (*Plp-Cre$^{ERT2+/wt}$:Rpl22$^{fl(STOP)fl-HA/wt}$*) were treated with tamoxifen to activate Cre-mediated recombination of the *Rpl22$^{fl(STOP)fl-HA}$* allele (Figure 11a). Four weeks later, HA immunostaining was observed in 75% or 5% of CC1$^+$ or CC1$^-$ cells throughout the thoracic spinal cord, respectively (Figure 11b-c). Double-positive cells were present in the white and grey matter, as

expected for mature, $CC1^+$ OLs (Figure 11b-c). Conversely, in vehicle-treated controls, HA^+ cells were rare (<2% or <0.5% CC1+ or CC1- cells, respectively, Figure 11b-c). Therefore, tamoxifen treatment resulted in efficient and OL-specific expression of the RPL22-HA in OL-RiboTag mice. Next, moderate contusive SCI (50 kdyn, T9) was performed in tamoxifen-induced OL-RiboTag mice and 5 mm spinal cord segments spanning the lesion site were collected at day post-injury (dpi) 2, 10, and 42. These time points were selected based on dynamics of spinal cord pathology after SCI including acute OL loss at the injury epicenter (dpi 2), peak of delayed OL apoptosis in the spared white matter (dpi 10) and limited remyelination (dpi 42)[107,108,209]. Uninjured, naïve OL-RiboTag mice were used as controls. After isolation of total spinal cord polysomes, OL polysomes were immunoprecipitated using anti-HA antibody. To ensure sufficient RNA yields, each biological sample combined spinal cord segments from two mice. Pilot studies revealed that polysome immunoprecipitation using a control IgG produced low RNA yields as compared to the anti-HA antibody confirming the specificity of the latter reagent (average of 48.4 or 285.34 ng RNA/sample with IgG or anti-HA, respectively; see Material and Methods for more details). Given such a disparity in RNA recovery between the control IgG and the anti-HA antibody, further analyses focused on anti-HA-purified OL translatomes. To verify their successful isolation, qPCR for neural cell marker transcripts was performed. As expected for translatomes from cells that are estimated to make about 20% of all spinal cord cells[210,211], the average enrichment of an OL marker mRNA reach 5.89 fold change (FC) total RNA control (Figure 11d). Conversely, several astrocytic,

neuronal or microglial marker transcripts were depleted from OL translatome samples (median FC 0.52, 0.36 or 0.1, respectively, Figure 11d). Such a differential enrichment pattern was observed across all samples regardless of SCI status. Therefore, OL-enriched translatomes were successfully isolated from spinal cord tissue of OL-RiboTag mice.

RNASeq was then performed on all samples. The principal component analysis (PCA) of the resulting mRNA expression data revealed robust separation of samples that represented OL-enriched translatome vs. total RNA input with the PC1 accounting for 70% variance (Figure 12a). Further separation was also evident including that between naïve and SCI samples (PC2, 19% variance, Figure 12a) or dpi 2 vs. other samples (PC3, 4% variance, Figure 12a).

Next, OL-enriched mRNAs were identified for each set of samples. As compared to total RNA inputs, OL enrichment of Log2FC(Total)>0.5 was observed for 3,511, 3,302, 3,262, or 3,313 mRNAs in naïve, dpi 2, dpi 10 or dpi 42 samples, respectively. While established mRNA markers of mature OLs were enriched, mRNA markers of neurons, astrocytes or microglia were depleted (Figure 12b). Gene ontology term enrichment analysis (GO) was performed for OL-enriched mRNAs (Figure 12c). The top enriched GO terms did not include OL-specific biological processes (BPs) or cellular components (CCs, Figure 12c). However, OL-specific GO-BPs/CCs such as axon ensheathment, myelination, or myelin sheath were highly overrepresented when the analysis focused on 520 mRNAs with highly selective OL expression as defined by $Log_2FC(Total)>2$, $q<0.05$ (Figure 12c). A similar pattern of GO term enrichment was observed when

analyzing OL-specific mRNAs from other samples sets including dpi 2, 10, or 42 (Figure 13). Therefore, OL translatomes were successfully isolated from both intact and injured spinal cords.

Identification of differentially expressed OL genes after SCI

To compare SCI-mediated changes in OL-enriched translatomes, differentially expressed mRNAs were identified between OL SCI vs. OL naive samples ($|Log_2FC/naïve/|>1$, $q<0.05$). However, several well-established markers of microglia/monocyte-derived macrophages were identified as OL-upregulated after SCI (Figure 14a). Those included such mRNAs as *Itgam/Cd11b*, *Cx3cr1*, and *Aif1/Iba1*, whose post-SCI protein expression has been confirmed in many studies to be microglia/macrophage-specific (as reviewed in David and Kroner[212] and Milich et al.[209]). In support of being expressed mainly by inflammatory cells, all those marker transcripts remained OL-depleted after SCI and their OL de-enrichment did not change significantly (Figure 14a). Moreover, extensive overlaps were observed between SCI-upregulated mRNAs from OL translatomes and the top 500-microglia-enriched mRNAs (Figure 14b). Such findings suggest that some mRNAs that are present in OL tranlsatome represent a contamination from non-OL cells, as recently shown in heterologous culture systems[213]. Importantly, such a non-specific co-purification with cell type-tagged ribosomes may be particularly relevant acutely after CNS injury when tissue cellularity changes and some mRNAs such as those expressed by the inflammatory cells become extremely abundant[195].

To reduce interference of those potential contaminating transcripts, a two-arm filtration procedure was applied to differentially expressed mRNAs from OL translatomes (Figure 14c). In arm 1, the identified transcripts were filtered using the DESeq2 interaction function to identify those that also showed differential OL enrichment of the same direction/magnitude (change of OL enrichment in SCI vs. naïve samples, $|Log_2FC/Total/_{SCI}-Log_2FC/Total/_{naïve}|>1$, $q<0.05$). This process eliminated mRNAs whose OL translatome changes are driven primarily by their parallel changes in the total RNA pool.

However, differential enrichment analysis may miss those mRNAs whose OL translatome levels change in the same direction/magnitude as in total spinal cord samples. In case of constantly OL-enriched mRNAs that also show preferential OL expression ($Log_2FC(Total)>1$, $q<0.05$), their exclusion is not justified as OLs are their major expressors and cross-contamination from other cell types is less likely. In total RNA samples, injury related changes of such OL-enriched transcripts are still a reflection of OL-specific response to SCI. Therefore, the second arm of the filtration procedure identified those highly regulated mRNAs that were also OL enriched regardless of passing the differential enrichment filtration. The resulting two-arm filtration process for differential or constantly high OL enrichment identified hundreds of mRNAs that represent high confidence components of OL gene expression response to SCI (Figure 14c). Importantly, OL upregulated genes that were identified in this manner did not show significant overlaps with the transcriptomic signature of microglia (Figure 14d).

Bioenergetic re-organization and reduced morphological complexity/connectivity as major components of OL-specific gene expression response to SCI

GO enrichment analysis was used to interpret the newly described changes of the OL-enriched translatome after SCI. Among 344 highly upregulated transcripts on dpi 2, the top-enriched GO-BP terms included several broad categories such as those related to development, nervous system development, regulation of biological quality or signaling (Figure 15a). More specificity emerged among top enriched GO-CC, GO-MF, and KEGG pathway terms. Those included such mitochondrial function-associated GOs as inner mitochondrial membrane, mitochondrion, proton-transporting ATP synthase activity, oxidative phosphorylation, or thermogenesis. Interestingly, eight components of the mitochondrial respirasome were highly upregulated ($Log_2FC(naïve)>1$, Figure 15b). Moreover, 30 additional respirasome genes were found when the OL upregulation threshold was lowered to $Log_2FC(naïve)>0.5$ ($q<0.05$, Figure 15b). Together, over 55% of 68 OL-expressed mitochondrial respirasome genes (GO:0005746) were upregulated with median $Log_2FC(naïve)=0.87$ ($q<0.05$) suggesting a coordinated response to increase oxidative phosphorylation.

On dpi 10, 155 highly upregulated mRNAs showed greatest overrepresentation of several broad GO-BP terms that were related to development (Figure 15c). In addition, enrichment of synapse-related GO-CCs was observed (Figure 15c). Upregulation of synapse-associated transcripts could

be interpreted as an attempt to re-establish OL-axonal synapses that were likely lost during the acute phase of SCI-associated axonal injury[43]. Development remained a top-enriched GO-BP theme among 294 highly upregulated mRNAs on dpi 42 (Figure 15d). In addition, high enrichment of mitochondria-associated GOs was found including the GO-CC or KEGG pathway terms mitochondrial inner membrane, mitochondrion, oxidative phosphorylation and thermogenesis (Figure 15d). On dpi 42, both the spectrum and scale of mitochondria-related mRNA upregulations appeared to be even greater than that on dpi 2. Specifically, 48 mitochondrial respirasome genes were upregulated in OLs on dpi 42 (Log_2FC(naïve)>0.5, q<0.05, Figure 15b) with median Log_2FC(naïve)=0.95). These data suggest that on dpi 42, OL metabolism is again reorganized to favor oxidative phosphorylation.

On dpi 2, 278 highly downregulated mRNAs from the OL-enriched translatome showed high level enrichment for several broadly defined GO-BP terms that are associated with development (Figure 17a). In addition, several top enriched GO-BP, GO-CC, and GO-MF terms were related to cytoskeleton organization, cell projection organization, cell periphery, cell projections, cell junctions and actin cytoskeleton. While GO-BP cell adhesion (GO:0007155) was not among top enriched terms, 40 out of 271 genes in that category were also down with Log_2FC(naïve)<-1, -log(q)= 5.06). Such a functional profile of downregulated genes suggests adaptive changes to reduced morphological complexity of OLs and / or OL disconnection from other cells/extracellular matrix.

Myelin sheath loss and disconnection from axons may be major drivers of these changes.

Although only 35 genes were highly downregulated in OLs on dpi 10, they showed significant overrepresentation of GO terms related to sterol biosynthesis (Figure 17b). When data for all 23 OL-expressed components of the cholesterol biosynthesis superpathway were analyzed, 15 genes were downregulated (median Log_2FC(naïve)=-1.14, $q<0.05$) and just one (*Hmgcs2*) was upregulated (Figure 16, Figure 17c). Importantly, downregulated genes included two critical regulators of cholesterol biosynthesis *Hmgcr* and *Sqle* (Figure 16, Figure 17c). Both genes remained downregulated on dpi 42 (Figure 17c). Importantly, all downregulated cholesterol biosynthesis genes showed OL-enriched expression in naïve, dpi 2, or dpi 10 mice with median log_2FC(Total)=1.55, 1.61, or 1.39, respectively ($q<0.05$, Figure 17c). Such an expression pattern is consistent with a critical role of cholesterol synthesis in long term maintenance of myelin and survival of mature OLs[214]. Therefore, downregulation of cholesterol biosynthesis may represent an adaptive response to loss of myelinated axons/myelin sheaths acutely post-SCI. It may also contribute to OL apoptosis subacutely post-SCI[107,108].

Top-enriched GOs for 224 transcripts that were highly downregulated on dpi 42 included several broadly defined terms such as development, biological regulation or binding (Figure 17d). In addition, cell adhesion, cell junction and glutamatergic synapse were also enriched (Figure 17d). This cell disconnection-like response resembles that observed among dpi 2-downregulated mRNAs.

Collectively, GO analysis of OL-specific gene expression suggests a bioenergetic shift towards oxidative phosphorylation and reduction of morphological complexity/cell connectivity both acutely and subchronically post-SCI. At least subchronically, stress adaptation and OL survival is the likely outcome of such changes as most OL loss occurs during acute/subacute phases of the SCI recovery[107,108]. However, those surviving OLs appear to undergo protracted degeneration including putative disconnection from axons.

Identifying candidate regulators of acute OL loss

After SCI, most OL loss occurs at the injury epicenter 24-48 hours post SCI[107,108]. Subacutely (dpi 7-dpi 21), additional OL loss via apoptosis is found in areas rostral and caudal from the epicenter[107,108]. No major OL loss has been reported beyond dpi 28[107,108]. Thus, OL mRNAs with acute post-SCI upregulation on dpi 2, but decreasing expression on dpi 42, may include major regulators of SCI-associated OL loss. Of 344 highly upregulated OL translatome mRNAs on dpi 2($Log_2FC(naïve) >1$, $q<0.05$, Figure 14), 148 were either not significantly upregulated on dpi 42, or their dpi 42 levels were at least two-fold lower than on dpi 2 (Figure 18a). In addition, 146 of those acutely-upregulated mRNAs showed their highest $Log_2FC(naïve)$ values on dpi 2 and only 2 reached maximal $Log_2FC(naïve)$ values on dpi 10. GO analysis of those OL loss-associated mRNAs revealed enrichment for GO-BP terms related to cell signaling (Figure 18b). Those included response to stimulus, regulation of cell communication, regulation of signaling, and signal transduction. Such an enrichment pattern corresponded well with overrepresentation of plasma membrane-associated GO-

CCs (Figure 18b). In addition, mRNAs encoding secreted proteins that are located in the extracellular region were overrepresented (Figure 18b). Cell death-associated GO-BP terms were also moderately enriched (*e.g.* GO:1901214, regulation of neuron death, 12/381 genes, -log(q)= 2.80). Finally, moderate enrichment of KEGG pathway terms related to amino acid biosynthesis was observed (Figure 18b).

Literature analysis was performed to identify which of 148 acute-phase-specific mRNAs are likely regulators of OL loss. Interestingly, several of those transcripts encoded components of the two major OL survival signaling cascades: the ERK1/2 MAP kinase pathway and the PI3K-AKT pathway[215–217] (Figure 18c,e,f). Of note, both positive and negative regulators of those pathways were upregulated (Figure 18c). In case of the ERK1/2 MAP kinase pathway, increased activity of the glutamate receptor (*Grik3*, *Cacng5*)[218] or receptor tyrosine kinase-mediated inputs (*Fgfr4*, *Fgfbp3*)[219] appeared to be opposed by upregulation of negative regulators of RAS/RAC1-mediated activation of MKK1/2 (*Syngap1*[220]*, Spry1, Spred3, Spry4*[221]*, Steap3*[222]*,* or the ERK1/2 phosphatase *Ptpn5*[223]. In the case of the PI3K-AKT pathway, enhanced inputs (*Fgfr4*, *Fgfbp3*, *Itgad*, *Bcat1/Bcat2*, *Pfkfb4*)[224–226] were opposed by upregulation of negative regulators including *Parvb*[227] and *Inpp4a*[228]. Interestingly, OL upregulation of the pro-survival cytokine *Il17b*[229] may represent an autocrine / paracrine stress survival mechanism as the IL17b receptor mRNA (*Il17rb*) is highly OL-enriched both in uninjured and contused spinal cord (Log_2FC(Total)= 2.40, 2.87, 2.34, or 2.51 for naïve, dpi 2, 10, or 42, respectively, $q<0.05$). Likewise, OLs appear as

the main source of *Il17b* expression (Figure 18e). Thus, pro-survival signaling networks are re-organized during the acute phase of OL response to SCI. Several of those changes may be adaptive and support survival under stress (*e.g*. activation of the ERK1/2-NFkB signaling by IL17B[229], AKT activation by PFKFB4 / BCAT1/2-mTOR[225,230], or PTPN5-mediated dephosphorylation of the activated ERK1/2 to limit the duration of ERK1/2 signaling)[231].

Several acutely upregulated genes were identified as potential regulators of the cell death machinery (Figure 18d-f). Activation of cell death may be promoted by: (i) reactive oxygen species (ROS) generating enzymes *Pcyox1l* and *Pla2g3*[232,233], (ii) an inhibitor of the death receptor-driven, pro-survival gene transcription, *Tifab*[234], (iii) a pro-excitotoxic inhibitor of JUN degradation, *Prr7*[235], and / or (iv) a positive regulator of pro-apoptotic MAP kinases JNK/p38, *Steap3*[236]. Conversely, cell death initiation may be negatively regulated by increased expression of (i) enzymes that antagonize accumulation of the pro-apoptotic second messenger ceramide (*Acsl5*, *Sphk1*)[237,238], (ii) *Sphk1* which stimulates production of the cytoprotective lipid mediator sphingosine-1-phosphate[238], (iii) negative regulators of ERK1/2 that may limit persistent, pro-necrotic activation of the ERK1/2 pathway in oxidative stress-exposed cells[231], (iv) several enzymes that contribute to anti-oxidant defenses reducing ROS toxicity (*Lpo*[239], *Apod*[240], *Bcat1/2*[241], *Aldh18a1*[242], *Pyccr1*[243], *Pfkfb4*[244], and (v) reduced ROS generation due to *Trf* (transferrin)-mediated chelation of iron[245]. Likewise, the lipid-peroxidation mediated effector phase of cell death cascades including ferroptosis may be antagonized by those positive regulators of anti-

oxidant defenses. Opposite effects on oxidative mechanisms of cell death execution are expected from upregulation of the potentially pro-ferroptotic lysosomal/endosomal ferroreductase *Steap3* which, by increasing the cytosolic Fe^{2+} pool, may promote lipid peroxidation[246–248]. Similar consequences may follow upregulation of the GSH-depleting enzyme *Chac1* as GSH is the key substrate for anti-ferroptosis lipid repair enzymes such as GPX4[248]. In addition, upregulation of the pro-apoptotic gene *Hrk* may promote SCI-induced OL apoptosis[249].

Several upregulated genes with a potential to modulate oxidative cell death (*Pla2g3*, *Apod*, *Trf*, *Lpo*) encode for secreted proteins[250]. In addition, on dpi 2, those transcripts are highly OL-enriched, suggesting OLs to be the main source of their respective protein products in the contused spinal cord tissue acutely post-SCI (Figure 18e). Other acutely OL-upregulated genes showing a similar pattern include those for secreted serine proteases (*Klk8*, *Klk9*) and secreted serine protease inhibitors (*Serpina3n*, *Serpina3c*, Figure 18e). Excessive extracellular serine protease activity may promote cell death and enhance white matter damage[193,251,252]. Therefore, OLs appear to activate autocrine/paracrine mechanisms that via regulation of oxidative stress and / or extracellular proteolysis may modify acute pathogenesis of SCI. Such a concept is supported by a report that SCI-associated OL death and axonal damage was reduced in *Klk8*$^{-/-}$ mice[193].

Epigenetic de-silencing as a potential regulator of the OL response to SCI

The current analysis of the OL translatome revealed extensive upregulation of genes in response to SCI. To identify transcriptional mechanisms that may contribute to such a response, overlaps between OL-upregulated genes and public datasets of ChIPSeq-confirmed mouse genome operons were determined using the ChIPSeq database module of the X2K suite[253]. At each post-SCI timepoint, top enriched operons included SUZ12 and MTF2, two components of the PRC2 chromatin repressive complex[254]. To further validate the specificity of these enrichments, z-scores were calculated for operon overlap gene counts of 344 dpi 2 upregulated genes vs. average overlap gene count for 10 random sets of 344 OL expressed genes. OL-upregulated genes showed overlaps with seven mouse genome operons that passed a stringent specificity criterion of z>5 (Figure 19a). Four of those operons (including three with top Z scores) were for the chromatin silencing factor SUZ12. Two other chromatin silencing factors including RCOR3 and MTF2 were also highly enriched. The specificity of those findings was further confirmed by weak operon enrichment among 289 acutely downregulated genes with a z-score range for top ten overlaps of 0.94-2.57.

As components of PRC2, SUZ12 and MTF2 promote repressive methylation of histones[254]. Noteworthy, SUZ12/PRC2-mediated gene repression is required for OL differentiation by downregulating differentiation inhibitory genes[255]. RCOR3 is a component of the KDM1A-RCOR1/2/3-HDAC complex that silences genes by opposing pro-transcriptional histone methylation and acetylation[256,257]. RCOR3 may be a negative regulator of those gene silencing

activities resulting in upregulation of genes that are repressed during cell differentiation[257]. *Suz12*, *Mtf2,* and *Rcor3* transcripts were detected both in total RNA and OL translatomes (Figure 19b). Their expression was unaffected by SCI. While *Suz12* and *Mtf2* showed similar expression in OLs and total RNA, *Rcor3* was moderately OL-enriched in all groups except dpi 42 (Figure 19b). Therefore, the identified operons are matched by continuous OL expression of their respective regulators.

Interestingly, the list of 129 unique SUZ12 target genes that were OL-upregulated acutely after SCI showed overrepresentation of GO terms related to signaling (Figure 19c). Moreover, it included such potential regulators of acute OL loss as *Ptpn5*, *Spry1*, *Spred3*, *Spry4*, *Fgfr4*, *Fgfbp3*, *Il17b*, *Grik2*, *Sphk1*, and *Hrk*. All but two of those PRC2 targets (*Ptpn5* and *Il17b*) overlapped with the RCOR3 operon. The current data suggest that de-silencing of the PRC2 and RCOR3 operons may contribute to acute upregulation of many SCI-response genes in OLs. Moreover, de-silencing of PRC2-repressed genes may also play a role in OL gene upregulation on dpi 10 and dpi 42.

STEAP3 as a novel marker of acute OL response to SCI

STEAP3 is a membrane protein that acts as a major endosomal/lysosomal metalloreductase that reduces Fe^{3+}/Cu^{3+} to Fe^{2+}/Cu^{2+} [246,258]. As Fe^{2+} is then exported from endosomes/lysosomes to cytoplasm, STEAP3 plays an important role in the cellular iron supply[246,247,259], but may also promote lipid peroxidation and ferroptosis[260]. In addition, STEAP3 binds to cell death effectors and signaling mediators to promote apoptosis and / or reduce activity of the pro-survival

pathways[222,236,261]. It is also required for stress-dependent exosome secretion[262,263]. Therefore, OL-upregulated *Steap3* may promote OL loss, but may also, via stimulation of exosome-mediated secretion, affect axons and / or other spinal cord cells.

In naïve mice, OL translatomes showed significant de-enrichment of *Steap3* (Figure 18e). High OL enrichment appeared on dpi 2 followed by similar expression in OL translatome and total RNA on dpi 10 and 42 (Figure 18e). In OLs, *Steap3* was sharply up on dpi 2 and remained elevated, albeit at reduced levels throughout the recovery period with Log_2FC(naive) ranging from 6.52 on dpi 2 to 3.67 on dpi 42 (Figure 18e). In total RNA samples, *Steap3* levels were also increased throughout the recovery period with an apparent peak on dpi 2 (Log_2FC(naive)=2.9, 2.7, or 1.89 on dpi 2, 10, or 42, respectively, $q<0.05$).

Increased expression of STEAP3 protein was confirmed by western blotting (Figure 20a). STEAP3 levels were significantly increased on dpi 2 but not dpi 10 or dpi 42 (Figure 20b). Therefore, at least acute OL tranlsatome upregulation of *Steap3* transcript correlates with increased bulk spinal cord expression of STEAP3 protein.

In naïve mice, faint STEAP3 immunofluorescence was observed in cell bodies of white matter OLs ($CC1^+$, Figure 21a, Figure 22). On dpi 1 or 2, such staining was also present throughout the spared ventral white matter at the injury epicenter as well as rostrally or caudally (Figure 21a, Figure 22 and 25). Seemingly nuclear localization of OL STEAP3 staining on transverse sections may represent perinuclear localization that is polarized mainly in the rostral-

caudal axis (Figure 21a). Unipolar, perinuclear STEAP3 immunofluorescence that reflects localizations to the endosomal/trans-Golgi network (TGN) has been reported in various cell types[246,258,262,263].

Acutely after SCI (dpi 1 or 2), a strong STEAP3 signal was also found in ring-like structures throughout the spared white matter (Figure 21a-b, Figure 22 and 25). Those structures were observed both at the injury epicenter as well as at the penumbra region rostrally and caudally from the injury site. They often showed partially overlapping and / or closely associated signals for the myelin marker MBP, as well as axonal marker phospho-NFH (p-NFH, Figure 21b). Importantly, those STEAP3^{+} structures likely represent a specific STEAP3 signal, as they were not observed with a control IgG (Figure 22 and 25).

Moreover, a different staining pattern was observed for PCYOX1L, whose mRNA is enriched in the OL translatome and is selectively upregulated in OLs but not total RNA samples on dpi 2 (Figure 18e, Figure 23, Figure 24 and 25). PCYOX1L is a close relative of the lysosomal cysteine deprenylase PCYOX1, which generates hydrogen peroxide and may contribute to oxidative stress[233,264,265]. In the white matter, PCYOX1L staining was observed in cell bodies and adjacent processes of CC1^{+} OLs (Figure 23a, Figure 22 and 24). Both control and SCI animals showed similar patterns of PCYOX1L expression that are consistent with a relatively moderate post-SCI increase of *Pcyox1l* in OLs (on dpi 2, Log2FC/naïve/=1.08, q<0.05). Unlike STEAP3, PCYOX1L immunofluorescence was observed in association with only a few damaged axons (Figure 23b, Figure 24 and 25). Therefore, acute upregulation of OL

STEAP3, but not PYCYOX1L, may be directly related to degeneration of myelinated axons.

Interestingly, STEAP3 was upregulated following treatment of cultured OL precursor cells (OPCs) or OPC-derived OLs with a mitochondrial uncoupling drug FCCP, but not the ER stress inducer tunicamycin (Figure 26). As FCCP uncouples mitochondrial respiration from ATP synthesis and increases mitochondrial ROS generation[266], upregulation of STEAP3 may represent a response of OL lineage cells to mitochondria dysfunction/mitochondrial oxidative stress. The latter form of cellular damage may upregulate expression of iron supply genes as mitochondrial biogenesis is a major driver of iron demand[267].

Discussion

The current data set represents the first comprehensive transcriptomic/translatomic description of OL gene expression response to SCI. Acutely, SCI-challenged OLs show translatomic changes indicative of a metabolic shift towards mitochondrial respiration that coincides with morphological simplification/cellular disconnection. Unexpectedly, a similar pattern reemerges subchronically. Acutely, OLs appear to undergo extensive re-organization of survival signaling networks. In addition, the acute OL translatome changes suggest an active role in regulation of cytotoxic mechanisms that contribute to secondary injury including extracellular proteolysis and oxidative stress. Epigenetic de-silencing appears to be a major driver of the SCI-activated OL gene expression. Lastly, STEAP3 is a novel marker of OL injury response that

may play a dual role as a positive, pleiotropic regulator of OL death/degeneration and an enhancer of exosome-mediated intercellular communication.

The current translatome analysis revealed OL-specific, SCI-mediated upregulation of several genes that were also identified as OL-upregulated in a recent scRNASeq analysis of the mouse spinal cord tissue acutely/subacutely after moderate contusive SCI[195]. Those include *Apod*, *Pla2g3*, *Trf*, *Klk8*, *Serpina3c*, *Serpina3n*, *Steap3*, *Pcyox1l*, *Itgad*, *Pfkfb4*, *Bact1/2* or *Spry1*. In addition, SCI-associated OL translatome changes show partial overlap with OL transcriptomic response to other types of CNS injury[268]. Recent analysis of multiple scRNASeq datasets from various mouse models of white matter damage including amyloidosis, tauopathy, EAE, and lysolecithin-induced demyelination has identified three major transcriptomic profiles of disease-associated OLs called DA1, DA2 and IFN. Of note, signature transcripts of all those profiles showed significant overlaps with SCI-upregulated OL mRNAs (Figure 27). The greatest overlaps were observed for the persistent, pro-inflammatory DA1 cluster. The overlap peaked on dpi 10, but was clearly present also on dpi 2 and dpi 42. The overlap with the transient cell injury response profile DA2 peaked on dpi 2. Interestingly, *Steap3* has been identified as a marker of DA1[268]. In addition, downregulation of cholesterol biosynthesis genes was identified as a major component of OL response to CNS injury throughout all those transcriptomic profiles[268]. The transient occurrence of such a response on dpi 10 suggests the greatest similarity between SCI-mediated OL gene expression changes at that time and those DA transcriptomic profiles.

While the current OL translatome dataset captures a large set of OL-expressed genes including those that are regulated by injury, it has important limitations that should be considered when choosing analysis tools or interpreting data. First, we observed apparent contamination of OL polysomes with mRNAs from non-OL cells including microglia/macrophages. We speculate that such a contamination originates from non-specific interactions between highly inducible non-OL mRNAs and IgG-coupled magnetic beads that occurs during sample preparation. Similar contamination has been recently reported in co-cultures of human and mouse neural cells[213]. The two-fold filtration process that took into account differential OL enrichment or constantly high level of OL enrichment reduced that contamination and identified high confidence components of the OL translatome that are regulated by SCI. However, while specificity of detection has improved, sensitivity likely suffered with over 60% of differentially expressed OL translatome mRNAs not passing the filtration criteria (Figure 14). Therefore, some components of OL response are likely missed in our analysis. Nevertheless, such a conservative analysis approach is justified in acute CNS injury models where dramatic changes in both tissue cellular composition and transcriptomes of inflammatory cells are major factors that determine bulk transcriptome readouts.

Another limitation is related to imperfect OL specificity of *Plp-CreERT2* expression. The *Plp-CreERT2* transgenic line that was used here to activate the RiboTag also drives Cre-ERT2 activity in Schwann cells[205]. As spinal cord samples my contain some short fragments of spinal nerve roots, it is possible

that a small fraction of OL polysomes is of Schwann cell origin. Such a contamination of the current dataset is suggested by an apparent OL enrichment and SCI upregulation of marker transcripts of Schwann cell nerve injury response including *Egfl8* or *Gdnf*[269]*.* Hence, at least some SCI-associated effects on OL gene expression may represent Schwann cell responses. Potential classification mistakes can be best avoided by confirming OL translatome mRNA changes using single cell level analysis of protein expression such as immunofluorescent or *in situ* hybridization-base approaches.

In myelinating glia, mitochondrial respiration is critical for myelination during development as myelin synthesis requires a large amount of ATP[69,270]. Conversely, in mature OLs, mitochondrial respiration is dispensable for OL survival, myelin sheath maintenance and axonal function[69]. Instead, OLs support axonal energy needs by providing lactate that is generated via aerobic glycolysis[69]. Therefore, OL mitochondria, some of which are also found in myelin sheaths, may be primarily involved in Ca^{2+} homeostasis and generation of anabolic metabolites for lipid synthesis[270].

As electrical activity of axons is a major consumer of OL-generated lactate[69], one could expect that OL disconnection from axons and / or axonal damage would lower lactate demand. Consequently, aerobic glycolysis would be reduced and mitochondrial respiration would increase producing a metabolic profile that resembles pre-myelinating/actively myelinating OLs. Our observed concomitant upregulation of respirasome genes, together with downregulation of

genes associated with morphological complexity/connectivity, supports such a scenario both acutely and subchronically after SCI.

Moreover, these data suggest that the first, acute wave of myelinated axon damage and reprogramming of OL metabolism is followed by a second, sub-chronic wave. After contusive SCI in rats, tracing experiments of the corticospinal tract showed acute axonal damage that is followed by chronic persistence of severed axons rostrally to the lesion[271]. In addition, a small portion of axons in the rubrospinal tract showed chronic damage and de/hypomyelination after mouse contusive SCI[272]. Therefore, while most axonal damage/myelin loss occurs acutely, continuing subchronic degeneration of myelinated axons is possible. As neuronal activity may affect both myelin sheath morphology and metabolic function[171], it is also possible that subchronic reorganization of OL respiration and connectivity may be a response to post-SCI reduction in activity of specific axonal tracts and / or spinal circuitries.

Core components, as well as regulators, of various intracellular signaling networks are highly represented among acutely upregulated OL genes. Several of those genes may have modulatory effects on survival signaling affecting acute loss of OLs. Those include increased expression of positive regulators of the core anti-apoptotic pathways ERK1/2 MAP kinase and PI3K-AKT. The former is often involved in Ca^{2+} sensing downstream of cell electrical activity[218] and the latter transduces survival signals from cell junctions[273]. Hence, post-SCI disconnection of OLs from axons may trigger a compensatory response due to reduced inputs of those pathways including lower activity of axonal-OL synapses

and reduced axonal laminin to OL integrin signaling. One could speculate that the net effects of those compensatory changes are pro-survival. Thus, PI3K-AKT activity seems to be mostly positively regulated, including upregulation of alternative inputs that activate AKT (Figure 18). Conversely, increased expression of many negative regulators of ERK1/2, including the ERK1/2-inactivating phosphatase *Ptpn5*, may limit oxidative stress-related, pro-necrotic overactivation of ERK1/2[231].

Lastly, SCI-mediated changes in OL gene expression indicate their active role in modifying the tissue environment to modulate secondary injury. Such effects may be mediated both by canonical secretion of signal-peptide containing proteins and non-canonical secretion by exosomes, as STEAP3 is a major regulator of exosome-mediated secretion[262,263]. Of note, significant enrichment of secreted proteins among upregulated genes on dpi 10 or dpi 42 suggests that OLs regulate not only acute damage, but also subacute/subchronic repair of the contused spinal cord.

In summary, this study establishes the first translatomic chart of OL response to thoracic contusive SCI. It uncovers previously unrecognized aspects of OL biology after SCI, including putative metabolic re-programming, re-organization of intracellular signaling and epigenetic de-silencing as a major driver of OL gene expression response to injury. These SCI-associated OL translatome data will be useful for design and / or interpretation of mechanistic studies of SCI-associated white matter damage as well as other types of white

matter pathology. Current data are available as a searchable database at SCI OL Gene Expression Database (scigenedatabase.com).

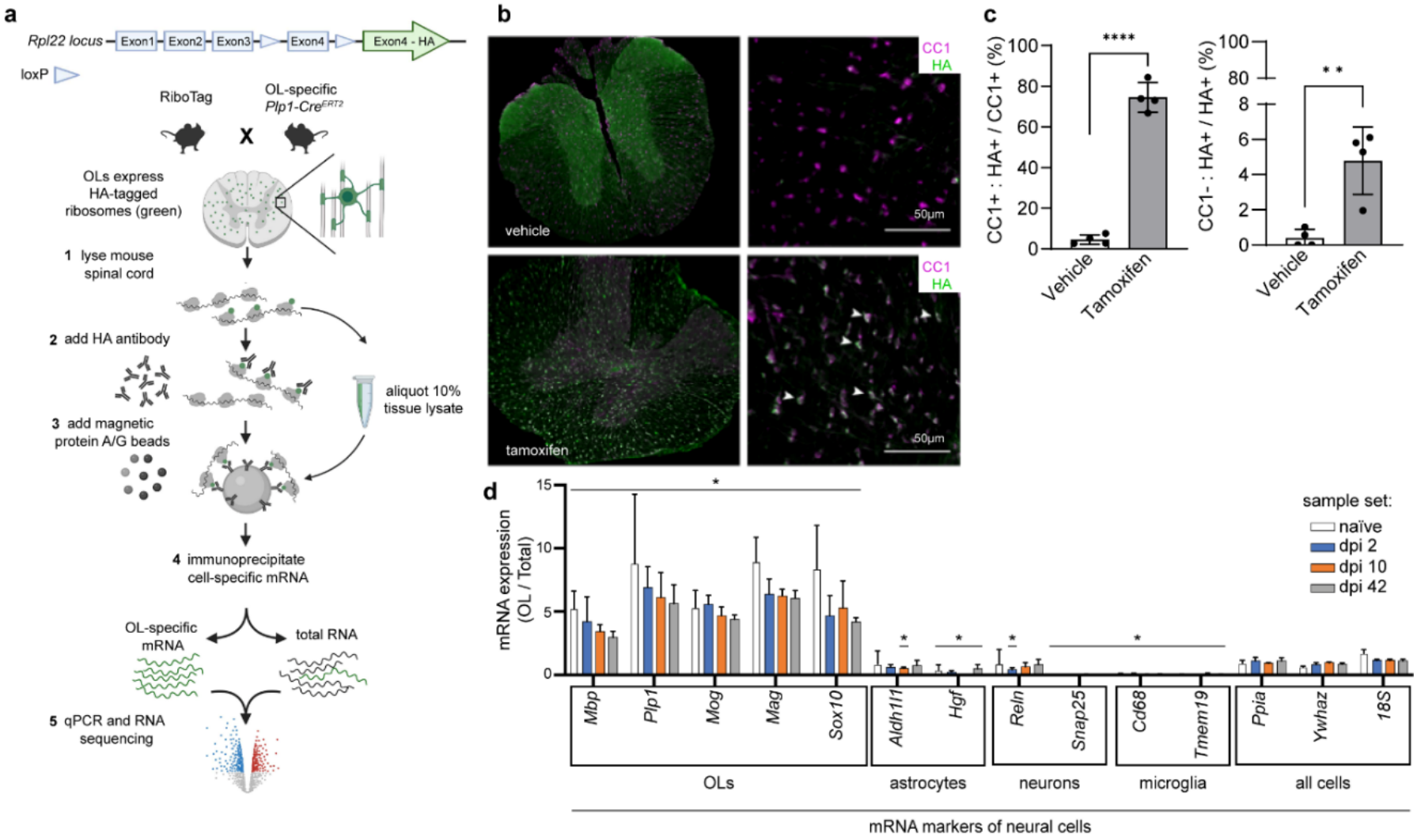
a
Rpl22 locus
Exon1
Exon2
Exon3
Exon4
Exon4 - HA
loxP
RiboTag
OL-specific
Plp1-CreERT2
OLs express
HA-tagged
ribosomes (green)
1 lyse mouse
spinal cord
2 add HA antibody
3 add magnetic
protein A/G beads
aliquot 10%
tissue lysate
4 immunoprecipitate
cell-specific mRNA
OL-specific
mRNA
total RNA
5 qPCR and RNA
sequencing
b
vehicle
tamoxifen
CC1
HA
50µm
c
CC1+ : HA+ / CC1+ (%)
CC1- : HA+ / HA+ (%)
****
**
Vehicle
Tamoxifen
d
mRNA expression
(OL / Total)
sample set:
naïve
dpi 2
dpi 10
dpi 42
Mbp
Plp1
Mog
Mag
Sox10
Aldh1l1
Hgf
Reln
Snap25
Cd68
Tmem19
Ppia
Ywhaz
18S
OLs
astrocytes
neurons
microglia
all cells
mRNA markers of neural cells

Figure 11. Successful induction of the OL-Ribotag and isolation the OL translatome.

(a) Design of the current OL-Ribotag study. OL-Ribotag mice are generated by combining the conditional Rpl22-HA knock in (Ribotag) with Plp1-driven CreERT2. After tamoxifen treatment, RPL22-HA is expressed selectively in mature OLs enabling immunoaffinity purification of their translatomes. OL or all cell (total RNA) mRNA expression is measured using qPCR or RNASeq. After normalization, OL enriched expression can be calculated as a fold total RNA sample. **(b)** Co-immunostaining for HA and the OL-specific CC1 epitope in thoracic spinal cord of vehicle- or tamoxifen-induced OL-Ribotag mice. Note the appearance of many HA^+ cells in the white matter of tamoxifen-treated animals. Most of those cells were also $CC1^+$ (arrowheads). **(c)** Quantitation of data obtained as in **(b)**. **(d)** Tamoxifen-induced OL-Ribotag mice received SCI and their contused spinal cord tissue was used for OL translatome isolation at the indicated days post-injury (dpi). Cell type marker transcripts were determined in OL and corresponding total RNA samples by qPCR. All cell-expressed housekeeping genes were used for normalization. Note the OL enrichment of OL marker mRNAs across all experimental groups. Conversely, several non-OL cell marker mRNAs were OL-depleted. Data on graphs represent averages ±SD from 3 individual animals (**c**) or 3 biological samples pooled from 2 mice each (**d**); *, $p<0.05$; **, $p<0.01$; ***, $p<0.001$ Mann-Whitney *u*-test).

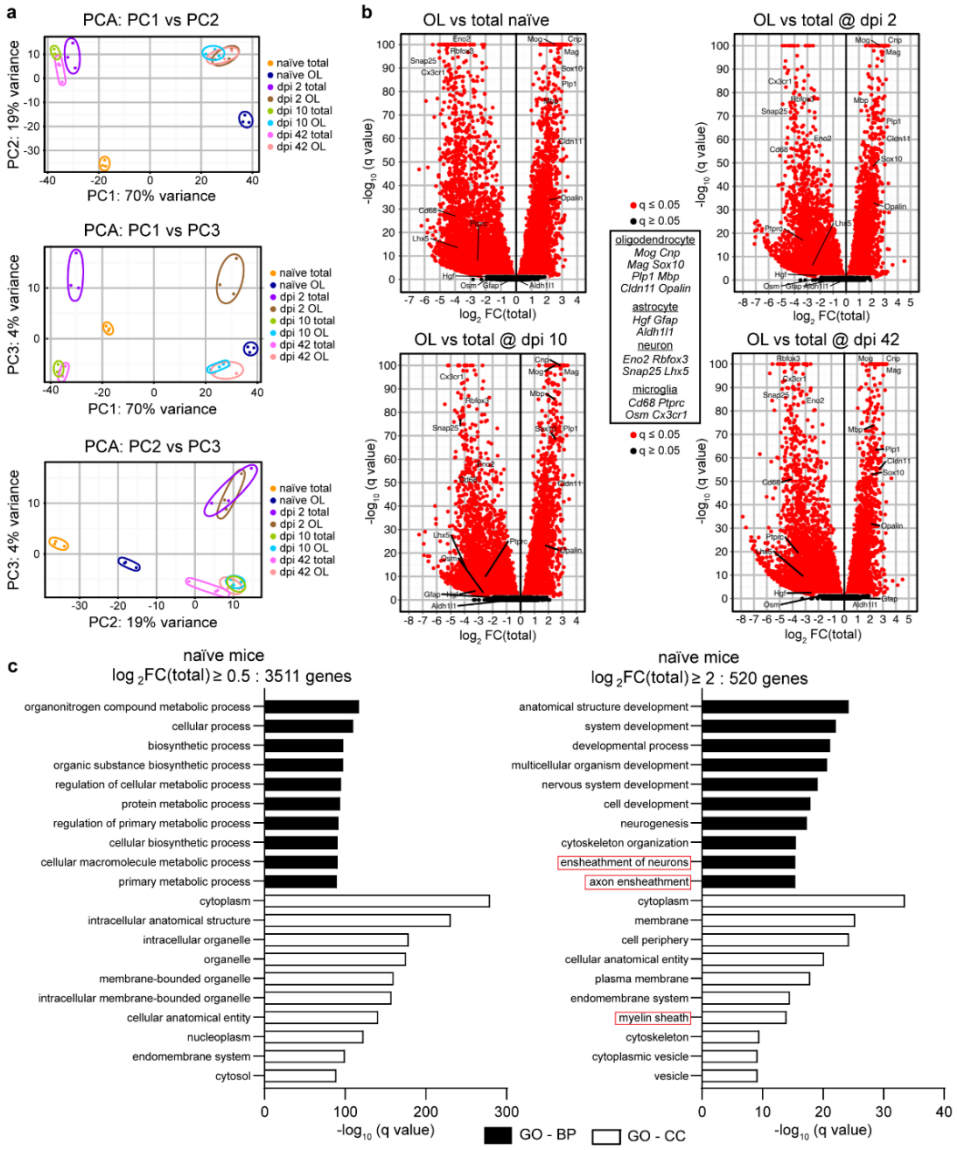

<u>Figure 12.</u> RNASeq confirms successful isolation of the OL translatome from intact or injured spinal cord tissue.

Tamoxifen-induced OL-Ribotag mice received SCI and OL translatomes were immunopurified as described in Figure 11. Following qPCR analysis of cell marker transcripts (Figure 11d), mRNA expression in the OL translatome and corresponding total RNA samples was analyzed by RNASeq. **(a)** Principal Component Analysis (PCA) was performed across all samples and included

mRNAs with a read count ≥10. Note that 70% of variance (PC1) was related to OL vs. total RNA origin followed by 19% (PC2) or 4% (PC3) due to effects of SCI across all time points or on dpi 2, respectively. **(b)** Volcano plots presenting all differentially expressed genes/mRNAs (DEGs) between OL vs. total RNA samples from the indicated groups. Note the significant OL enrichment or depletion of OL or microglia/neuron marker mRNAs across all groups, respectively. **(c)** The top 10 most overrepresented gene ontology biological process (GO-BP) or cellular component (GO-CC) terms among OL-enriched mRNAs from naïve mice as determined by q value ranking. GOs related to OL function (red boxes) show a high level of overrepresentation when highly, but not moderately, enriched OL mRNAs are analyzed. Similar GO overrepresentation patterns emerged in OL DEGs from SCI samples.

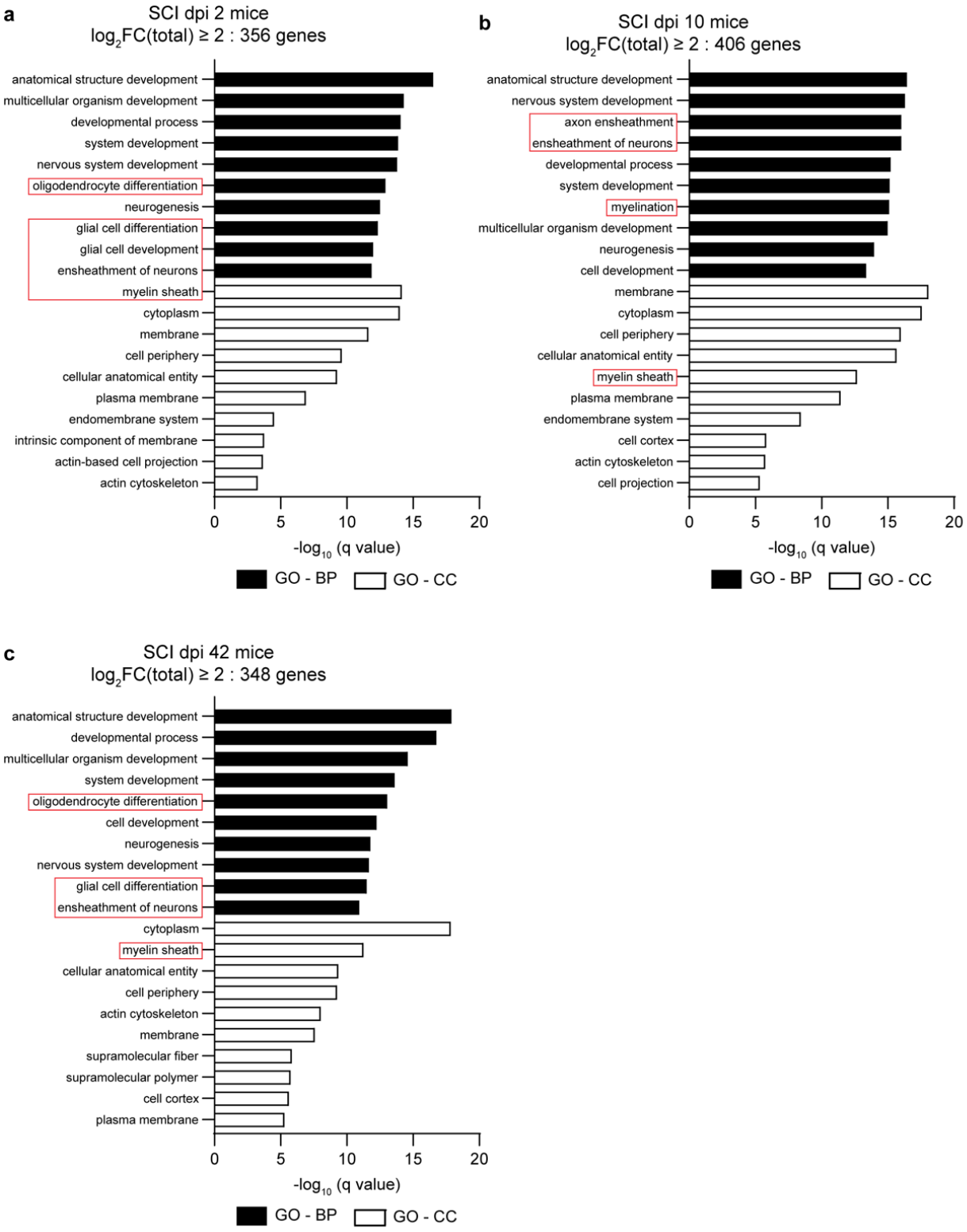
a
SCI dpi 2 mice
log2FC(total) ≥ 2 : 356 genes
anatomical structure development
multicellular organism development
developmental process
system development
nervous system development
oligodendrocyte differentiation
neurogenesis
glial cell differentiation
glial cell development
ensheathment of neurons
myelin sheath
cytoplasm
membrane
cell periphery
cellular anatomical entity
plasma membrane
endomembrane system
intrinsic component of membrane
actin-based cell projection
actin cytoskeleton
0 5 10 15 20
-log10 (q value)
GO - BP
GO - CC
b
SCI dpi 10 mice
log2FC(total) ≥ 2 : 406 genes
anatomical structure development
nervous system development
axon ensheathment
ensheathment of neurons
developmental process
system development
myelination
multicellular organism development
neurogenesis
cell development
membrane
cytoplasm
cell periphery
cellular anatomical entity
myelin sheath
plasma membrane
endomembrane system
cell cortex
actin cytoskeleton
cell projection
0 5 10 15 20
-log10 (q value)
GO - BP
GO - CC
c
SCI dpi 42 mice
log2FC(total) ≥ 2 : 348 genes
anatomical structure development
developmental process
multicellular organism development
system development
oligodendrocyte differentiation
cell development
neurogenesis
nervous system development
glial cell differentiation
ensheathment of neurons
cytoplasm
myelin sheath
cellular anatomical entity
cell periphery
actin cytoskeleton
membrane
supramolecular fiber
supramolecular polymer
cell cortex
plasma membrane
0 5 10 15 20
-log10 (q value)
GO - BP
GO - CC

Figure 13. Successful Isolation of OL translatome after SCI.

OL-enriched transcripts (Figure 12) with enrichment Log2FC(Total)>2, q<0.05 were analyzed for GO term overrepresentation. Top 10 most overrepresented gene ontology terms/category are shown for dpi 2 **(a)**, 10 **(b)** and 42 **(c)**. GOs related to OL function (red boxes) show high level of overrepresentation.

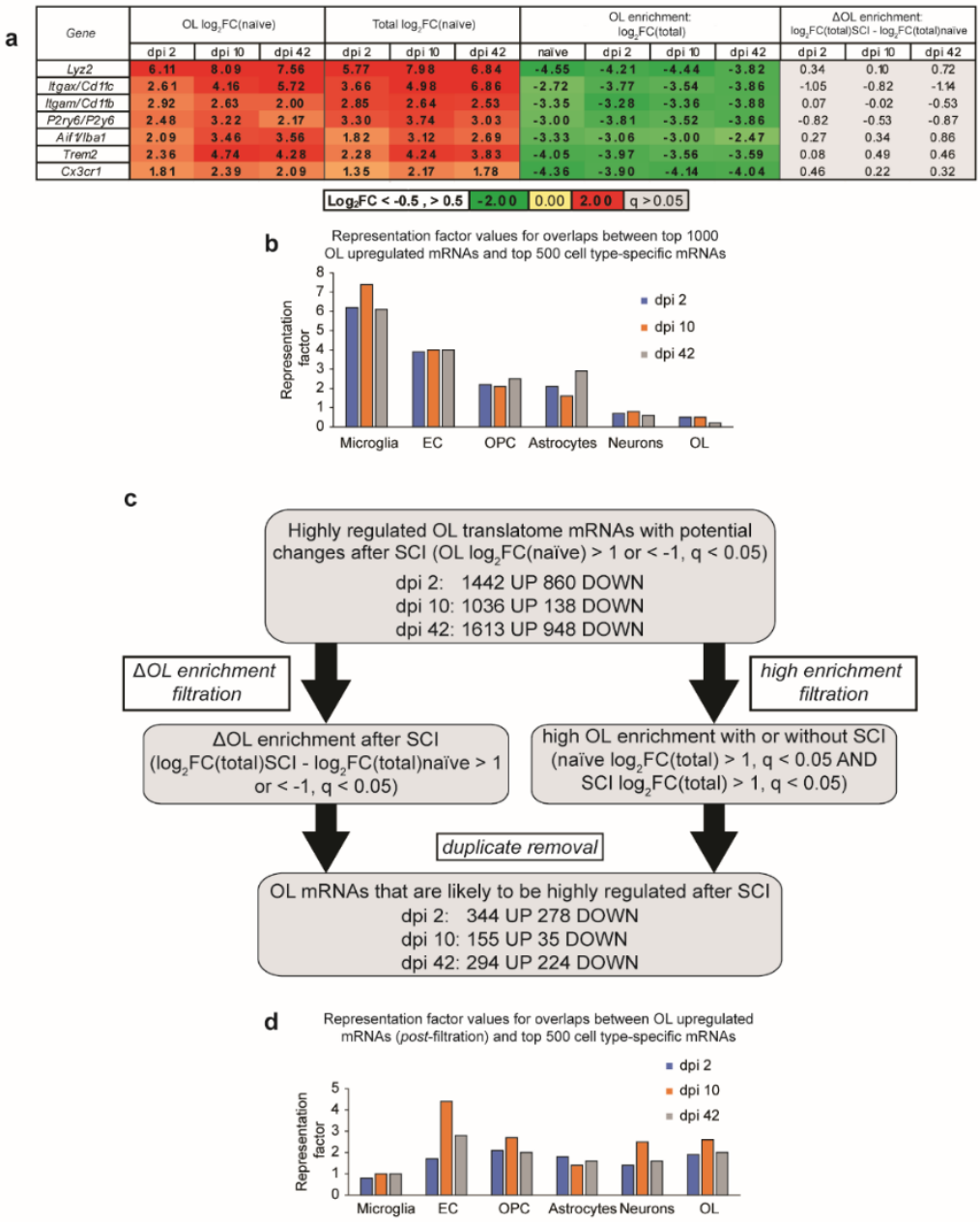

<u>Figure 14.</u> Determining OL gene expression response to SCI.

Differential gene expression was analyzed in OL translatomes from SCI vs. naïve samples. **(a,b)** SCI OL translatome contamination with marker mRNAs of microglia/monocyte-derived macrophages. At each timepoint after SCI, the top

1000 highly upregulated transcripts (Log_2FC/naïve/ >1, q<0.05) included several established markers of microglia and/or monocyte-derived macrophages **(a)**. While sharply upregulated in total RNA samples, those microglial mRNAs were OL depleted and their OL de-enrichment was unaffected after SCI. **(b)** Significant overrepresentation of the top 500 microglia marker transcripts (Brain RnaSeq database) among OL-upregulated mRNAs after SCI, representation factor = 1 if the number of overlapping genes is as expected by a random chance (OPC, oligodendrocyte precursor cells; EC, endothelial cells). **(c)** Flow chart of the filtration procedure for high confidence identification of the SCI-upregulated component of the OL translatome. The two-arm filtration process was based on (i) differential OL enrichment after SCI or (ii) constantly high OL enrichment before and after SCI. In each case, OL expression analysis took into account changes in total RNA (see Text for more details). **(d)** After filtration, no overrepresentation of microglial marker mRNAs is present among OL mRNAs that are upregulated after SCI.

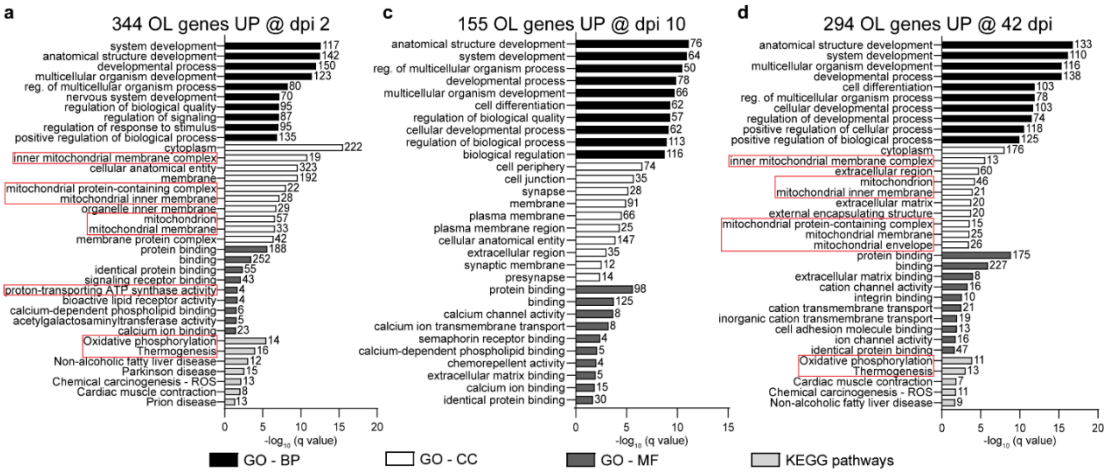

b

Respirasome genes: OL log_2FC(naïve) > 0.5 @ dpi 2 or dpi 42

	Gene	OL log_2FC(naïve)			Total log_2FC(naïve)			OL enrichment: log_2FC(total)			
		dpi 2	dpi 10	dpi 42	dpi 2	dpi 10	dpi 42	naïve	dpi 2	dpi 10	dpi 42
Complex I	*Dmac1*	**1.13**	0.38	**0.87**	**0.63**	0.36	0.52	0.03	**0.53**	0.06	0.39
	Dmac2	-0.03	0.34	**0.62**	**-0.67**	-0.25	0.09	**-1.24**	**-0.60**	**-0.65**	**-0.71**
	Ndufa1	**1.00**	0.32	**1.21**	-0.08	-0.12	0.45	**-1.42**	-0.34	**-0.98**	**-0.66**
	Ndufa11	**0.81**	0.39	**1.26**	-0.18	-0.40	0.22	**-0.80**	0.18	-0.02	0.25
	Ndufa12	0.37	0.12	**0.75**	-0.21	-0.44	0.13	**-1.31**	**-0.73**	**-0.75**	**-0.69**
	Ndufa13	**0.81**	0.29	**1.04**	0.02	-0.02	0.36	**-0.51**	0.29	-0.20	0.16
	Ndufa2	**1.11**	0.26	**1.21**	0.23	-0.03	0.34	**-0.75**	0.14	-0.45	0.12
	Ndufa3	**0.97**	0.28	**0.83**	0.08	-0.27	0.10	**-0.52**	0.37	0.04	0.22
	Ndufa4	**1.02**	0.31	**0.96**	-0.50	**-0.62**	-0.18	**-1.59**	-0.08	**-0.66**	-0.46
	Ndufa5	**0.69**	0.13	**0.81**	-0.27	**-0.52**	-0.14	**-0.88**	0.08	-0.23	0.07
	Ndufa6	**0.73**	0.19	**0.81**	-0.33	-0.45	0.02	**-0.95**	0.10	-0.31	-0.17
	Ndufa7	**0.75**	0.30	**0.77**	0.02	0.01	0.09	-0.27	0.46	0.03	0.41
	Ndufa8	**0.93**	0.32	**0.85**	-0.02	-0.31	0.15	**-0.78**	0.17	-0.15	-0.07
	Ndufab1	**0.80**	0.27	**0.93**	-0.21	-0.42	0.11	**-0.94**	0.08	-0.25	-0.13
	Ndufb10	0.37	0.20	**0.91**	-0.42	-0.37	0.25	**-0.67**	0.12	-0.11	-0.01
	Ndufb11	**0.81**	0.10	**0.93**	0.06	-0.12	0.34	-0.13	**0.61**	0.09	0.45
	Ndufb3	**0.68**	0.14	**1.06**	-0.30	-0.45	0.15	**-0.57**	0.41	0.02	0.34
	Ndufb5	**0.85**	0.17	**0.79**	-0.41	**-0.51**	-0.10	**-1.55**	-0.30	**-0.87**	**-0.66**
	Ndufb6	**0.74**	0.32	**0.92**	-0.48	**-0.75**	-0.12	**-1.26**	-0.04	-0.20	-0.22
	Ndufb7	**0.96**	0.28	**1.11**	0.27	-0.03	0.46	-0.22	0.48	0.10	0.44
	Ndufb8	0.36	0.08	**0.61**	**-0.52**	**-0.67**	-0.26	**-1.21**	-0.33	-0.47	-0.34
	Ndufb9	**0.68**	0.32	**0.89**	-0.26	-0.37	0.00	**-0.75**	0.19	-0.06	0.14
	Ndufc1	0.62	0.16	**0.71**	-0.24	-0.36	-0.22	**-1.30**	-0.44	**-0.78**	-0.37
	Ndufc2	**0.87**	0.08	**0.99**	-0.15	-0.37	0.12	-0.43	**0.58**	0.02	0.44
	Ndufs3	0.41	-0.02	**0.69**	-0.28	-0.47	0.08	**-0.62**	0.08	-0.16	-0.01
	Ndufs4	**0.57**	0.11	**0.71**	-0.39	-0.49	-0.10	-0.48	0.49	0.12	0.33
	Ndufs5	**1.14**	0.32	**1.34**	-0.01	-0.33	0.19	**-0.68**	0.48	-0.03	0.47
	Ndufs6	**0.89**	0.31	**0.81**	-0.24	-0.35	0.13	-0.48	0.45	0.18	0.19
	Ndufs7	0.45	0.06	**0.93**	-0.25	-0.37	0.28	-0.10	**0.60**	0.33	**0.55**
	Ndufs8	0.09	-0.06	**0.55**	-0.35	-0.35	0.15	-0.38	0.05	-0.08	0.02
	Ndufv2	0.48	-0.02	**0.54**	-0.44	**-0.59**	-0.28	**-0.99**	-0.08	-0.43	-0.17
C II	*Rab5if*	**0.93**	0.30	**0.58**	**0.76**	0.14	-0.20	-0.28	-0.11	-0.13	**0.51**
	Sdhb	0.19	0.11	**0.61**	-0.25	-0.26	0.03	-0.32	0.12	0.05	0.27
	Sdhc	**0.69**	0.23	**0.92**	0.18	0.14	0.47	0.15	**0.66**	0.23	**0.60**
	Sdhd	**0.68**	0.04	**0.69**	0.08	-0.28	-0.01	**-0.68**	-0.08	-0.36	0.02
C III	*Uqcc3*	**0.84**	0.49	**1.25**	0.33	0.22	**0.70**	-0.18	0.32	0.09	0.37
	Uqcr10	**0.98**	0.18	**1.00**	-0.04	-0.21	0.13	**-0.99**	0.02	**-0.60**	-0.12
	Uqcrb	**0.92**	0.34	**0.97**	0.05	-0.19	0.08	**-1.03**	-0.16	**-0.51**	-0.14
	Uqcrfs1	0.35	-0.02	**0.52**	-0.28	-0.42	-0.07	-0.13	**0.50**	0.28	0.46
	Uqcrh	**0.98**	0.16	**0.95**	-0.40	-0.47	-0.14	**-1.32**	0.06	**-0.69**	-0.23
	Uqcrq	**1.41**	0.43	**1.21**	0.23	-0.12	0.19	**-0.89**	0.30	-0.33	0.13
C IV	*AA467197*	**4.69**	2.02	1.15	**3.97**	1.82	-0.02	**-2.37**	-1.65	-2.17	-1.19
	Cox4i1	0.49	0.23	**0.95**	-0.41	**-0.56**	-0.09	**-0.57**	0.33	0.22	0.47
	Cox5a	**0.81**	0.23	**1.11**	-0.31	-0.50	0.09	**-1.55**	-0.43	**-0.82**	**-0.52**
	Cox6a1	**1.08**	0.27	**1.07**	0.05	-0.23	0.25	**-0.71**	0.32	-0.21	0.11
	Cox6a2	**5.59**	5.22	5.04	**7.91**	**7.86**	**9.77**	-0.08	**-2.40**	**-2.72**	**-4.80**
	Cox7a2	**0.87**	0.19	**0.77**	-0.29	-0.44	-0.17	**-1.30**	-0.14	**-0.67**	-0.36
	Cox7a2l	**0.58**	0.18	**0.72**	-0.17	0.06	0.25	**-1.14**	-0.38	**-1.02**	**-0.67**
	Cox7b	**1.10**	0.01	**1.11**	-0.37	**-0.81**	-0.22	**-1.94**	-0.48	**-1.12**	**-0.62**
	Cox7c	**1.44**	**0.58**	**1.44**	-0.08	-0.16	0.41	**-1.45**	0.07	**-0.71**	-0.42

Log_2FC < -0.5 , > 0.5 | -2.0 0 | 0.00 | 2.0 0 | q > 0.05

<u>Figure 15.</u> The OL response to SCI includes biphasic upregulation of mitochondrial respirasome genes.

(a,c,d) Overrepresented GOs (top 10/category) among high confidence OL translatome mRNAs that are highly upregulated after SCI (Log_2FC/naïve/>1, q<0.05, and two-arm filtration /Figure 14c/). Several GOs related to mitochondria are overrepresented on dpi 2 and 42, but not dpi 10 (red boxes). MF- molecular

function. **(b)** Fifty out of 68 mitochondrial respirasome genes that are OL-expressed are also OL upregulated on dpi 2 and/or 42 (Log_2FC/naïve/>0.5, q<0.05, bold). In most cases, their total spinal cord expression is unaffected (q>0.05, grey cells). Therefore, the biphasic upregulation of mitochondrial respirasome genes is OL-specific. In naïve mice, most of those upregulated genes are OL depleted (Log_2FC/Total/<-0.5, q<0.05, bold), which is consistent with reduced activity of oxidative phosphorylation in mature OLs.

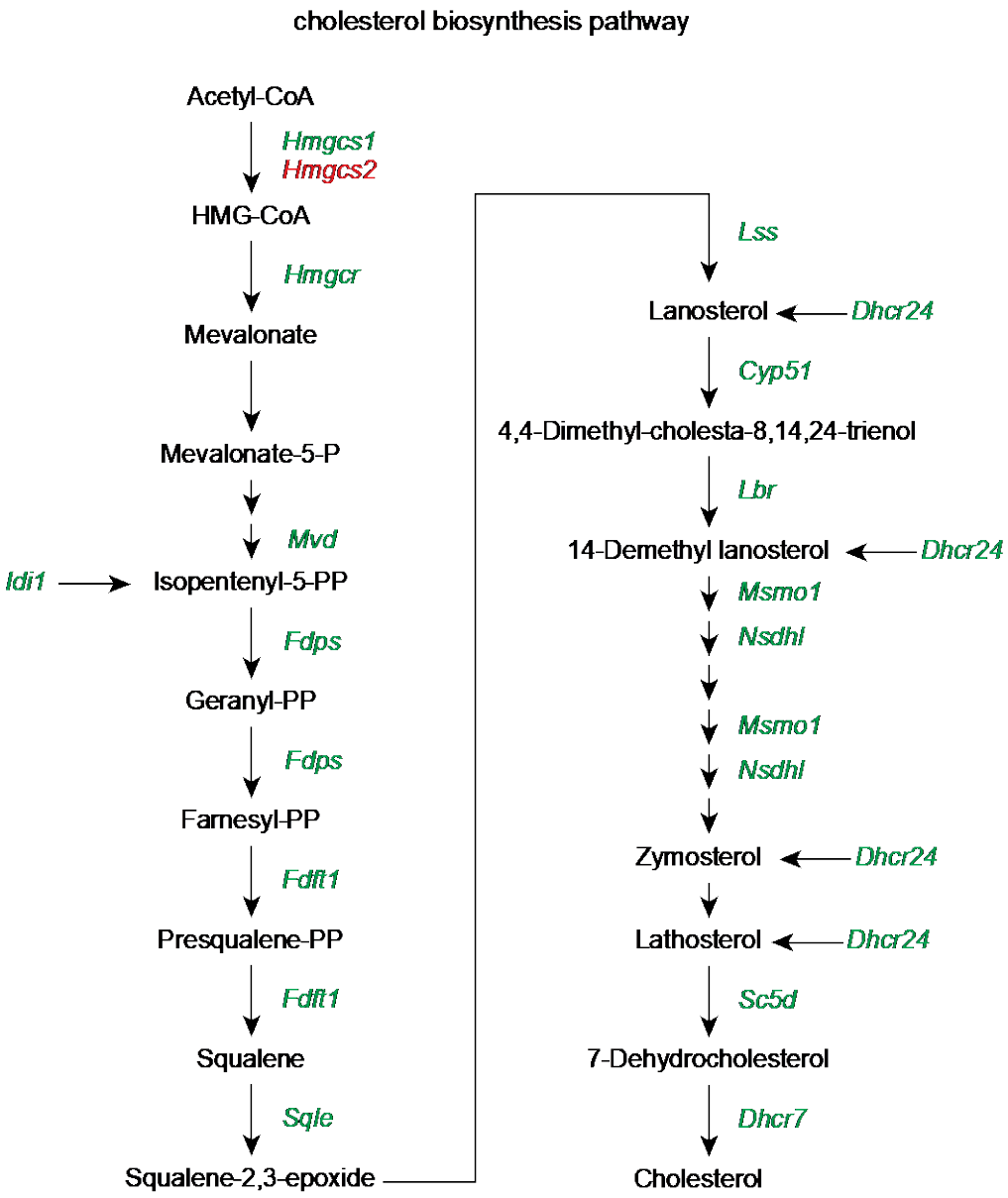

<u>Figure 16.</u> Cholesterol biosynthesis superpathway.

16 of 23 genes in the cholesterol biosynthesis superpathway are differentially expressed in OLs after SCI at dpi 10. All genes shown in green are downregulated after SCI (median Log_2FC(naïve)=-1.14, q<0.05). Only one gene, *Hmgcs2*, was upregulated (shown in red). Note *Hmgcr* and *Sqle* are

downregulated and are critical regulators of cholesterol biosynthesis. All downregulated cholesterol biosynthesis genes shown are OL-enriched at naïve, dpi 2 and dpi 10. Unlabeled arrows within the pathway are genes unaffected in OLs after SCI.

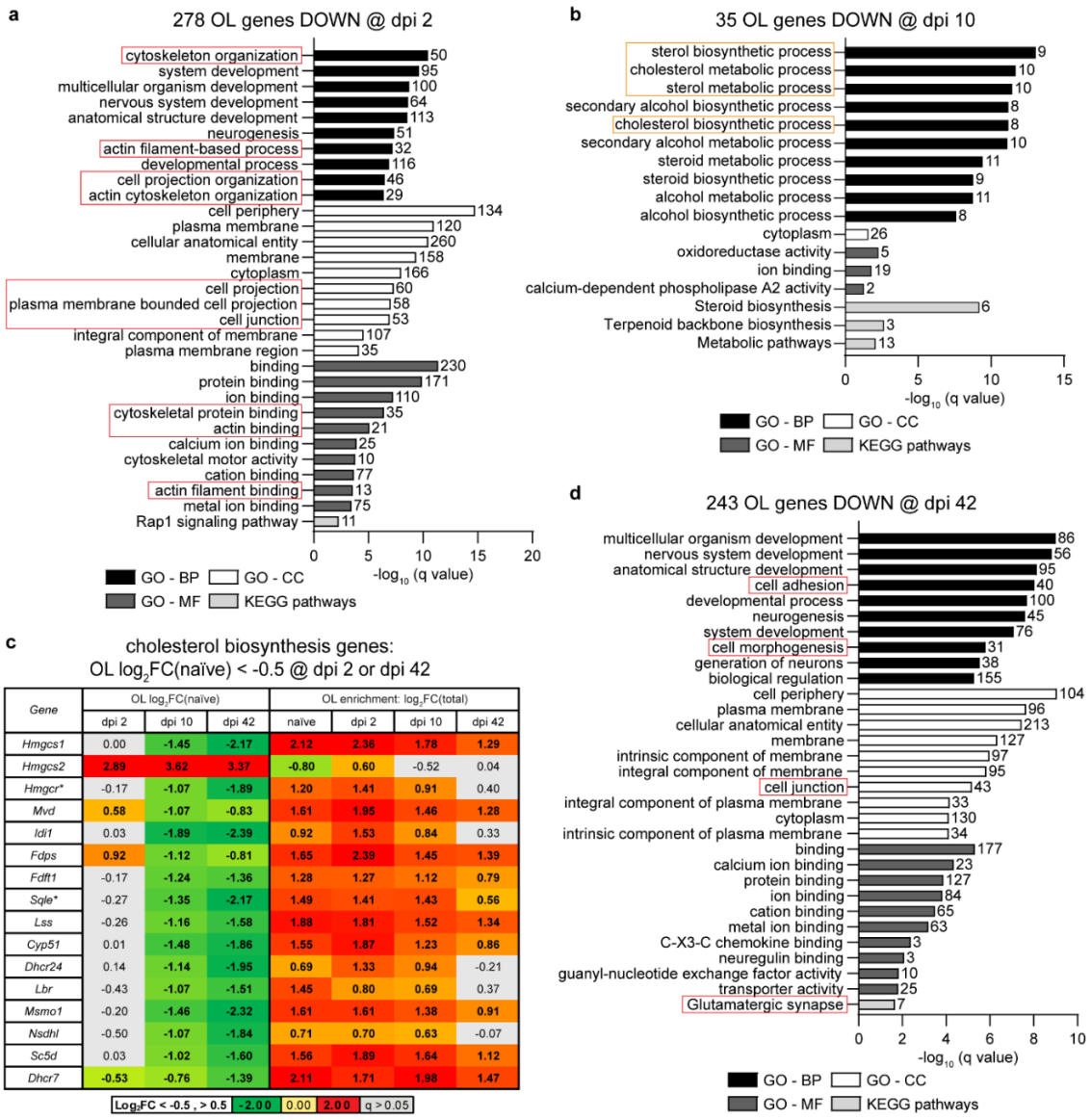

Figure 17. The OL response to SCI includes time-dependent downregulation of genes associated with morphological complexity, cell junctions, and cholesterol biosynthesis.

(a,b,d) Overrepresented GOs (top 10/category) among high confidence OL translatome mRNAs that are highly downregulated after SCI (Log_2FC/naïve/<-1, q<0.05, and two-arm filtration /Figure 14c/). On dpi 2 and 42, GOs associated

with morphological complexity and cell junctions/cell adhesion are overrepresented (red boxes). On dpi 10, the top overrepresented GOs are related to cholesterol biosynthesis (orange boxes). **(c)**. Fifteen out of 23 cholesterol biosynthesis genes that are OL-expressed are also OL downregulated on dpi 10 and 42 (Log_2FC/naïve/<-0.5, q<0.05, bold). All those downregulated genes are OL-enriched in naïve, dpi 2 and dpi 10 animals (Log_2FC/Total/>0.5, q<0.05, bold). For several of them, OL enrichment is lost by dpi 42 (q>0.05, grey cells). Genes whose products are critical regulators of cholesterol biosynthesis are indicated (*). The chart of the cholesterol biosynthesis pathway with post-SCI changes in OLs is shown in Figure 16.

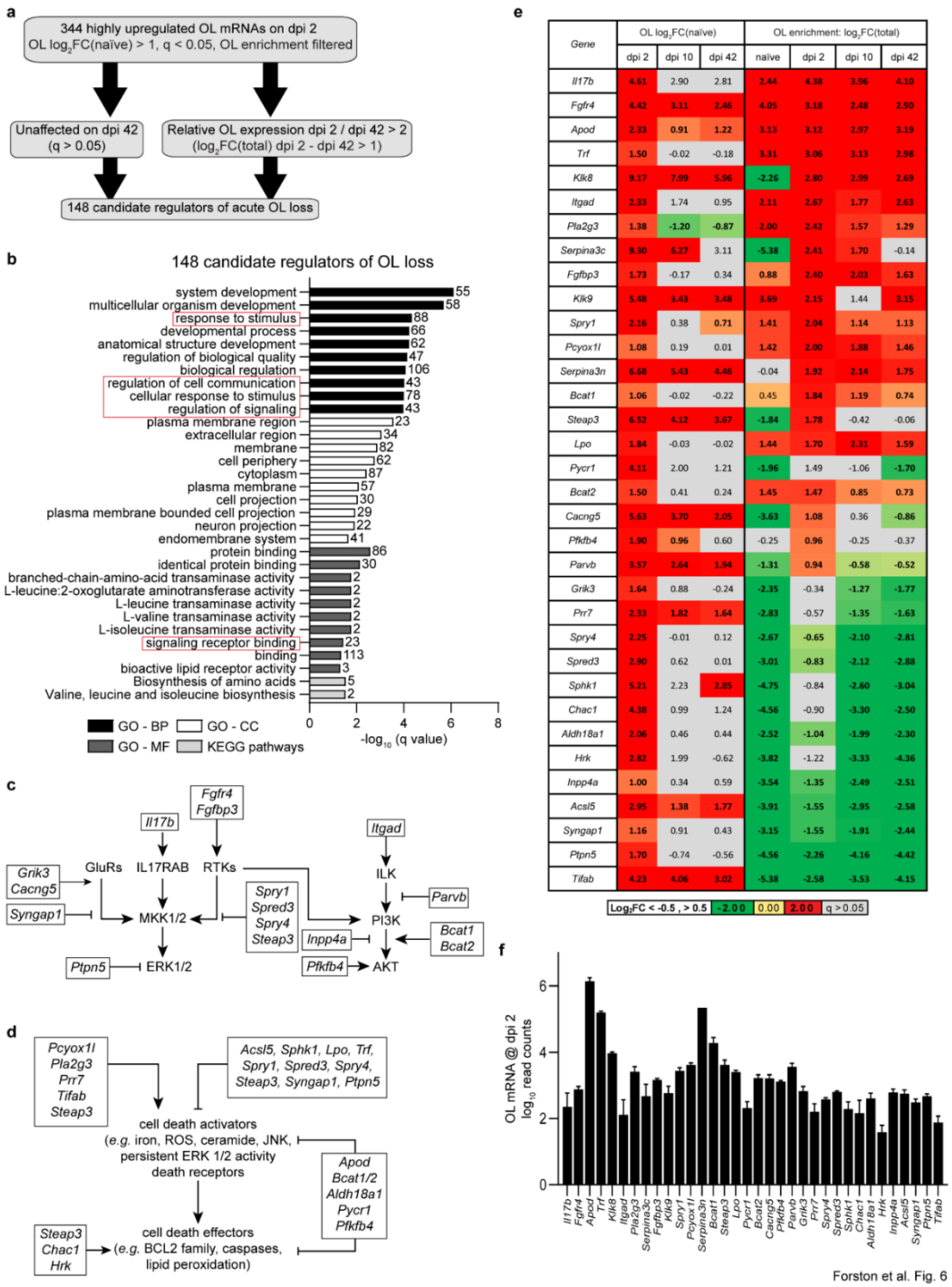

<u>Figure 18.</u> Identifying candidate regulators of OL loss after SCI.

(**a**) To identify likely candidate gene regulators of OL loss, OL translatome mRNAs that were highly upregulated on dpi 2 were further analyzed to identify those whose expression normalized or declined at least 2-fold on dpi 42 when OL

numbers stabilize and when little OL death has been reported (see text for details). **(b)** Overrepresented GOs (top 10/category) among candidate gene regulators of OL loss include several GO terms that are related to signaling (red boxes). **(c-d)** Literature-based analysis of candidate genes identified upregulated regulatory components of the survival signaling pathways including ERK and PI3K-AKT **(c)** as well as cell death activators and effectors **(d)**. OL-upregulated genes are marked by black boxes. **(e)** OL translatome expression and OL enrichment of potential OL loss regulators that are listed in (**c-d**). Their dpi 2 read counts are shown in (**f**). In (**e**), genes with SCI-associated expression change or OL enrichment/depletion $|Log_2FC|>0.5$ are in bold ($q<0.05$); non-significant effects are marked by grey cells ($q>0.05$). In (**f**), log_{10} averages ±SD are shown.

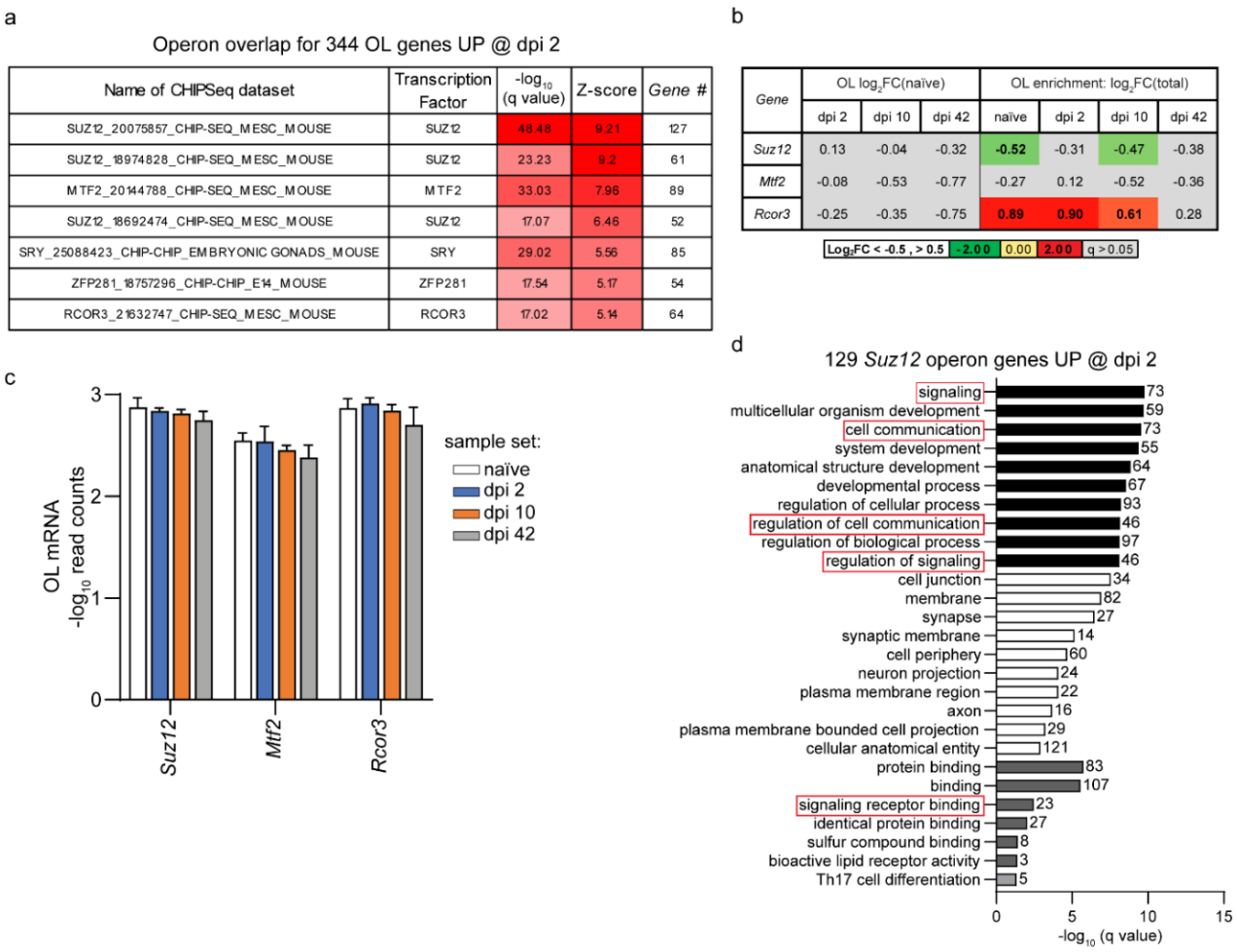

Figure 19. Epigenetic de-silencing as a potential regulator of the OL gene expression response to SCI.

(a) Overlaps between 344 OL translatome mRNAs that are highly upregulated on dpi 2 and CHIP-Seq-confirmed mouse operon genes from publicly available data sets. Five of seven overlaps with z-scores > 5 are for operons of epigenetic regulators including SUZ12, MTF2, and RCOR3. A similar pattern of top overlaps was observed on dpi 10 and dpi 42. **(b-c)** Relative (Log_2FC) or absolute (Log_{10}Read Count) expression of *Suz12, Mtf2, and Rcor3* in the OLs. In **(c)**, data represent averages ±SD. **(d)** GO analysis of 129 targets of SUZ12 targets that

are highly OL upregulated on dpi 2 (top 10 enriched GOs/category). Several GO terms related to cell signaling are also enriched.

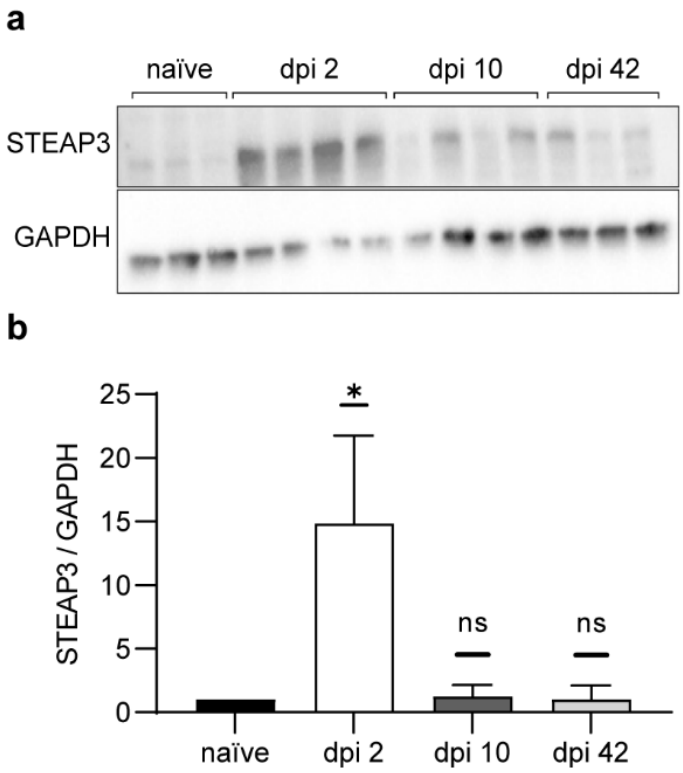

<u>Figure 20.</u> STEAP3, a candidate regulator of OL loss, is upregulated acutely after SCI.

Western blotting was performed using protein lysates from the contused spinal cord tissue of WT mice at the indicated post-injury times. GAPDH was used as a normalizing control. **(a)** A representative western blot. Each lane corresponds to an individual mouse. **(b)** Quantification of the blot shown in **(a)**. GAPDH-normalized STEAP3 expression is significantly elevated on dpi 2. Data are mean± SD (*, $p<0.05$; non-significant /ns/, $p>0.05$ Mann-Whitney *u*-test).

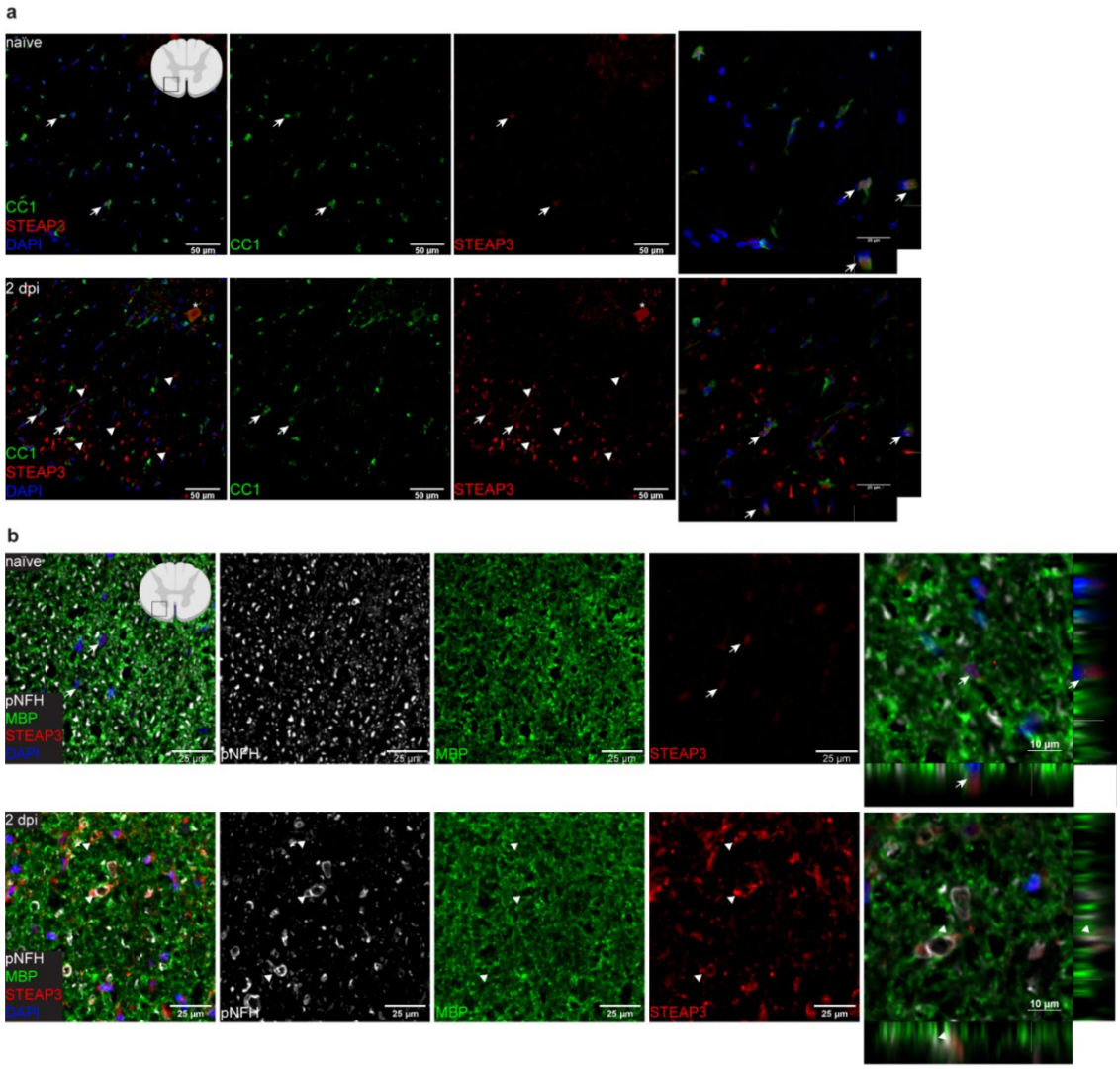

<u>Figure 21.</u> STEAP3 as a novel marker of myelin damage after SCI.

Transverse sections from WT mice with (dpi 2) or without SCI (naïve) were co-immunostained for STEAP3 and the indicated markers of OL cell somas (CC1), myelin sheaths (MBP) or axons (p-NFH). Cell nuclei were counterstained with Hoechst-33258 (DAPI). The SCI sections come from a region 1-2 mm rostral from the injury epicenter. **(a)** Representative confocal images of STEAP3 and CC1 co-staining in the ventral white matter (selected Z-axis projections are also shown). Arrows indicate $CC1^{+}$ OLs that show weak STEAP3 signal. Z axis

profiles of select double-positive cells (crosses) suggest peri-nuclear localization of STEAP3. Such cells are observed both in control tissue and on dpi 2. Arrowheads mark ring-like structures with a strong STEAP3 signal that do not overlap with cell nuclei and are only observed after SCI. A $STEAP3^{+}$ neuron-like cell in the grey matter is indicated by an asterisk. **(b)** Representative confocal images of STEAP3/MPB/p-NFH co-staining in the ventral white matter (selected Z-axis projections are also shown). Arrows indicate cells with perinuclear STEAP3 staining. Arrowheads identify damaged, distended axons that are associated with a strong STEAP3 signal. In those structures, lack of co-localization between STEAP3 and MBP or p-NFH indicates that STEAP3 may mark OL paranodes and/or a peri-axonal compartment adjacent to damaged axons. Similar $STEAP3^{+}$ structures were also observed on dpi 1 (Figure 22 and 25). Staining specificity controls are shown in Figure 22 and 25.

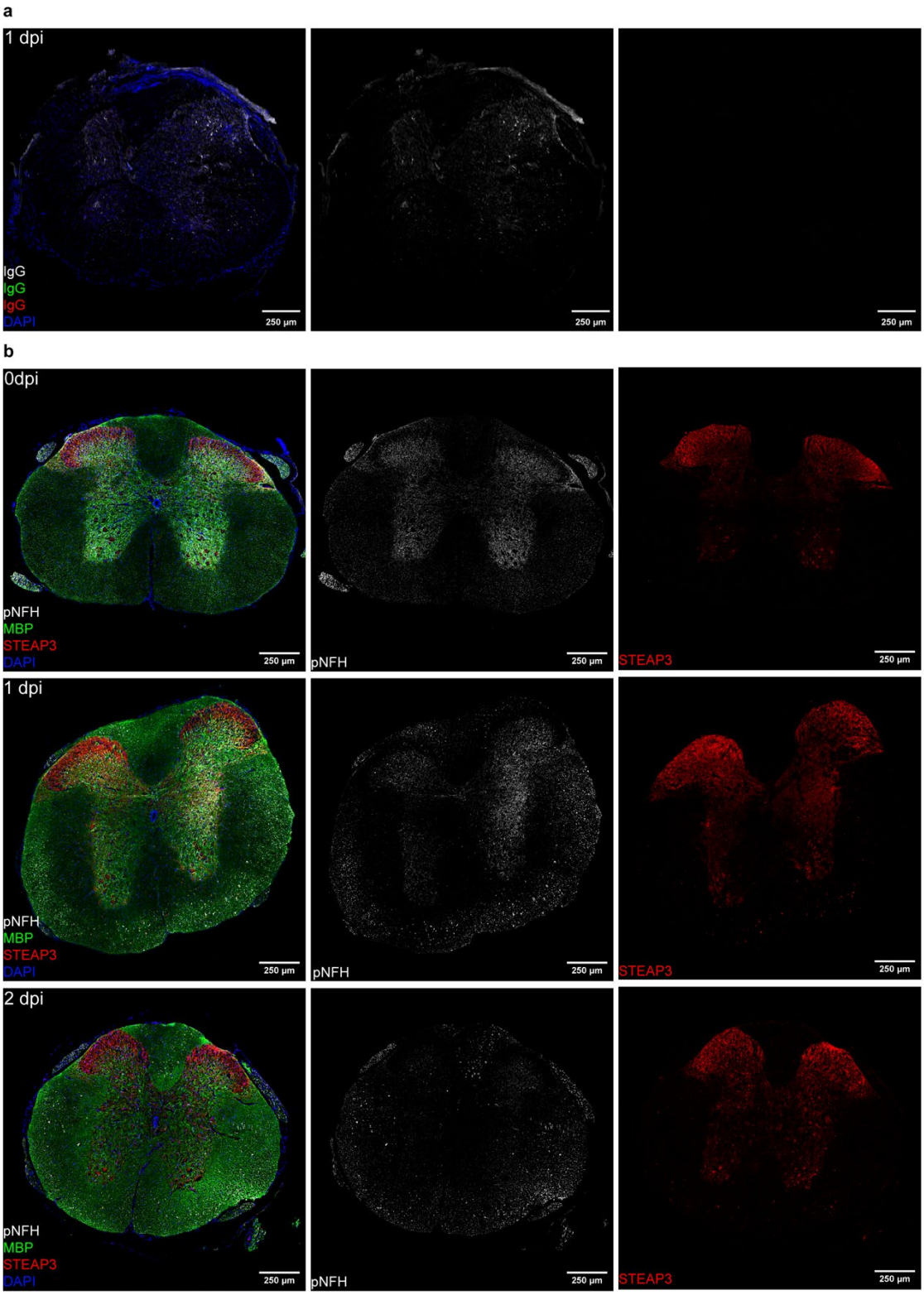

<u>Figure 22.</u> STEAP3 expression is upregulated in the ventral and lateral white matter after acute SCI.

Low magnification images of spinal cord sections with or without SCI that were stained for STEAP3 (tissue preparation and co-stainings as described for Figure 21). Specificity controls with non-immune IgGs that were used instead of primary antibodies are also shown.

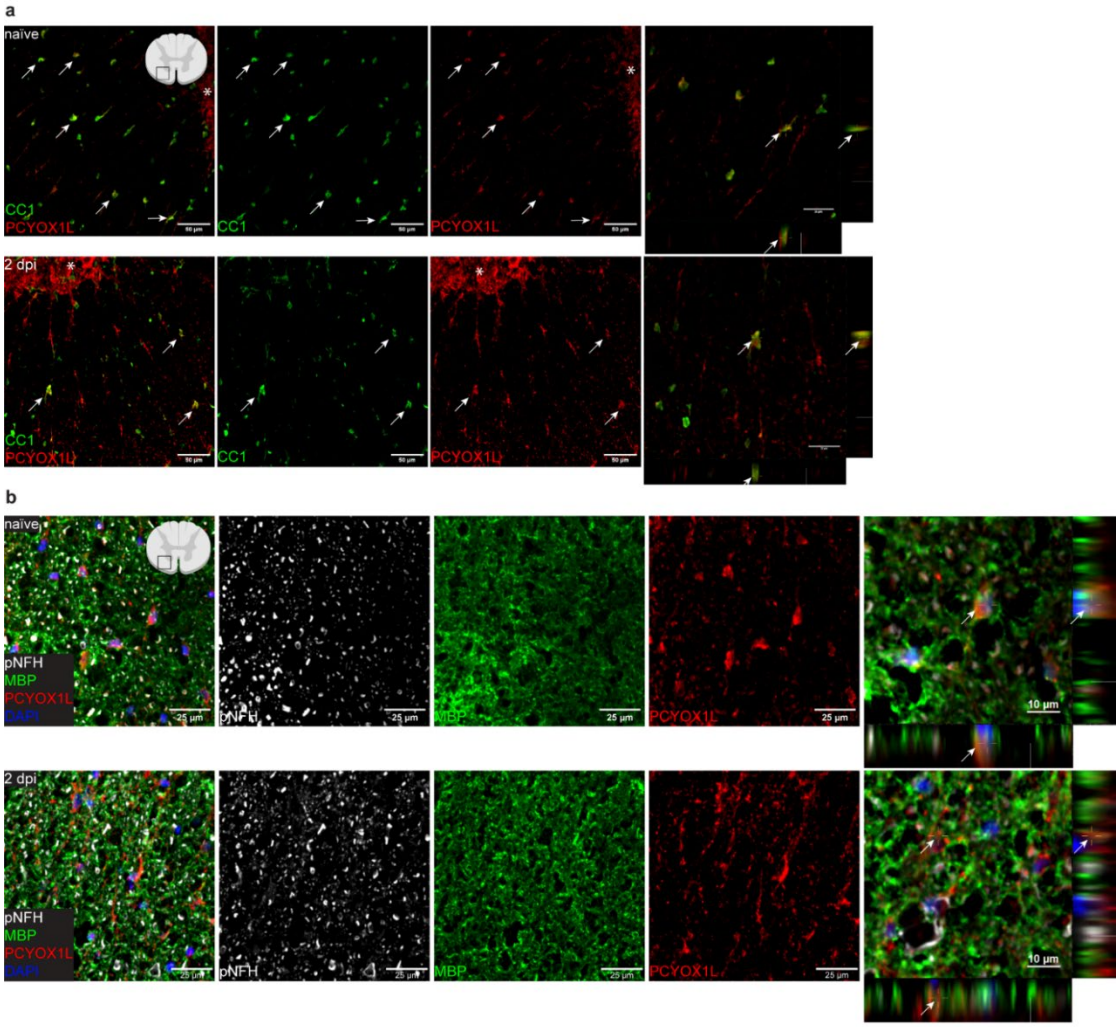

<u>Figure 23.</u> OL expression of PCYOX1L before and after SCI.

Preparation of spinal cord sections that were co-immunostained for PCYOX1L, CC1, MBP and p-NFH was as described for Figure 21. **(a)** Representative confocal images of PCYOX1L and CC1 co-immunostaining in the ventral white matter (selected Z-axis projections are also shown). Arrows indicate $CC1^{+}$ OLs that show positive PCYOX1L signal their cell somas and soma-proximal processes. Such cells are present in both control- and SCI tissue. A $PCYOX1L^{+}$ neuron-like cell in the grey matter is indicated by an asterisk. Somatic, vesicular/granule-like appearance of PCYOX1L signal is consistent with its

expected localization to lysosomes. **(b)** Representative confocal images of PCYOX1L/MPB/p-NFH co-staining in the ventral white matter (selected Z-axis projections are also shown). Arrows indicate cells with PCYOX1L^{+} somas/processes. Similar cell soma/process localization of PCYOX1L staining was also observed on dpi 1 (Figure 24 and 25). Staining specificity controls are shown in Figures 22 and 25.

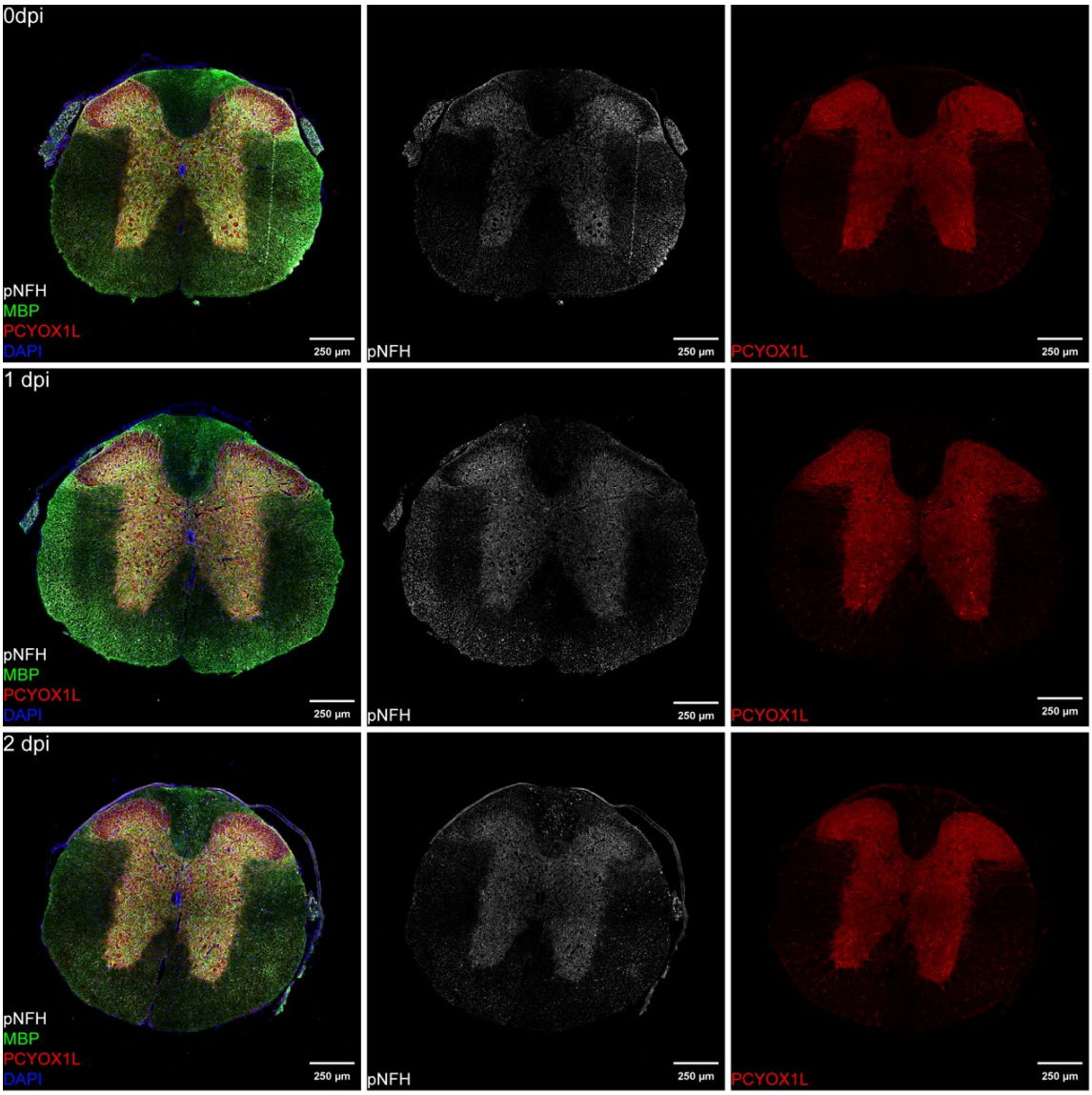

Figure 24. PCYOX1L expression in the spinal cord tissue with or without SCI.

Low magnification images of spinal cord sections with or without SCI that were stained for PCYOX1L (tissue preparation and co-stainings as described for Figure 21).

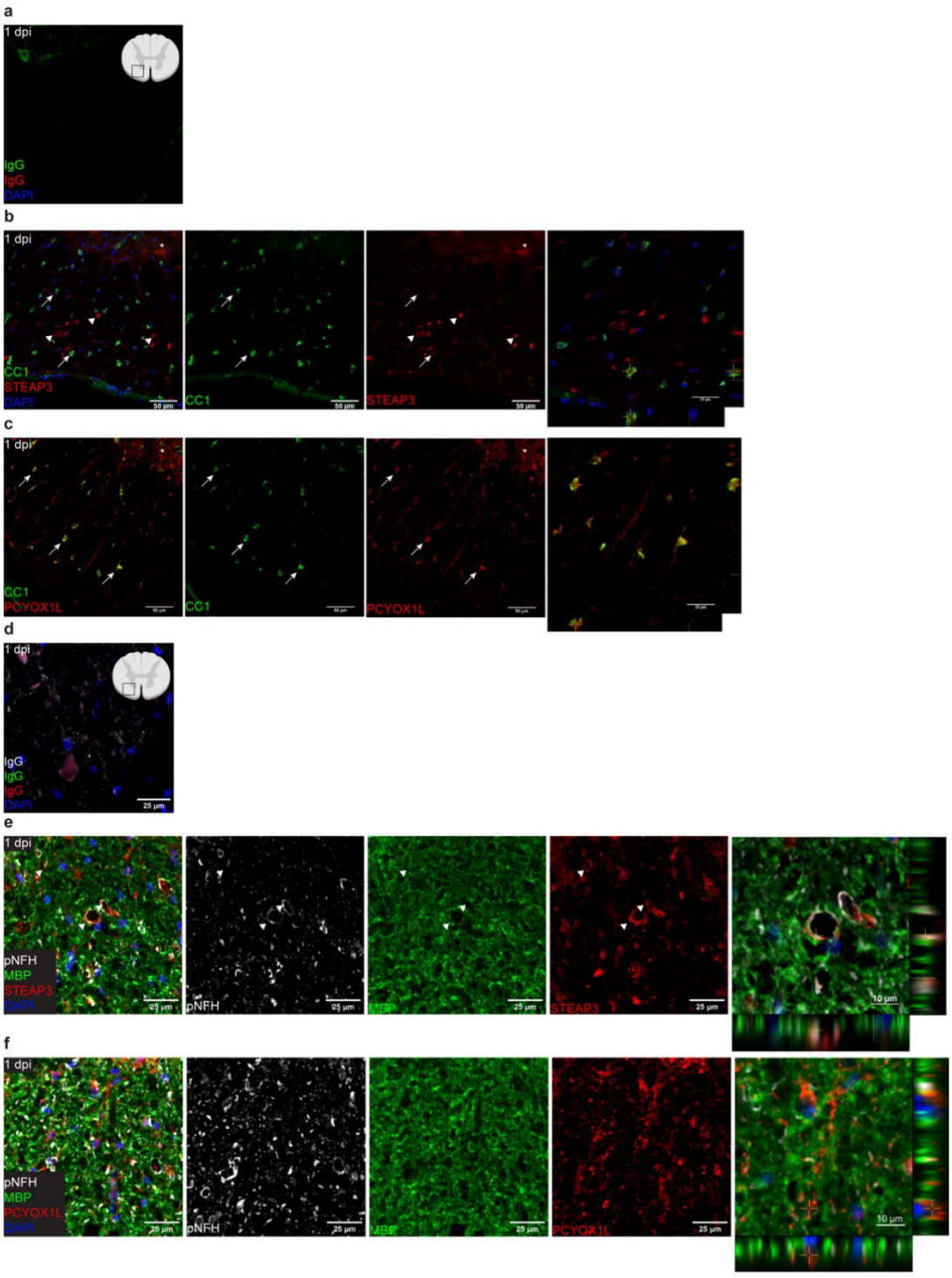

<u>Figure 25.</u> STEAP3 and PCYOX1L expression on dpi 1.

Tissue preparation and co-stainings as described for Fig. 9. **(a)** Arrows identify CC1+ cells with STEAP3 or PCYOX1L signals. Arrowheads mark STEAP3+

structures that are not associated with CC1+ cell somas and/or DAPI+ nuclei; such structures appear as the main source of increased STEAP3 staining in the white matter of the injured spinal cord. Z-axis profiles show representative CC1+ cell soma signals for STEAP3 or PCYOX1L (cross). **(b)** Most STEAP3 signal is found adjacent to distended, damaged axons that are identified by p-NFH (arrowheads). In contrast, most PCYOX1L is associated with cell somas (arrows). Specificity controls with non-immune IgGs that were used instead of primary antibodies are also shown.

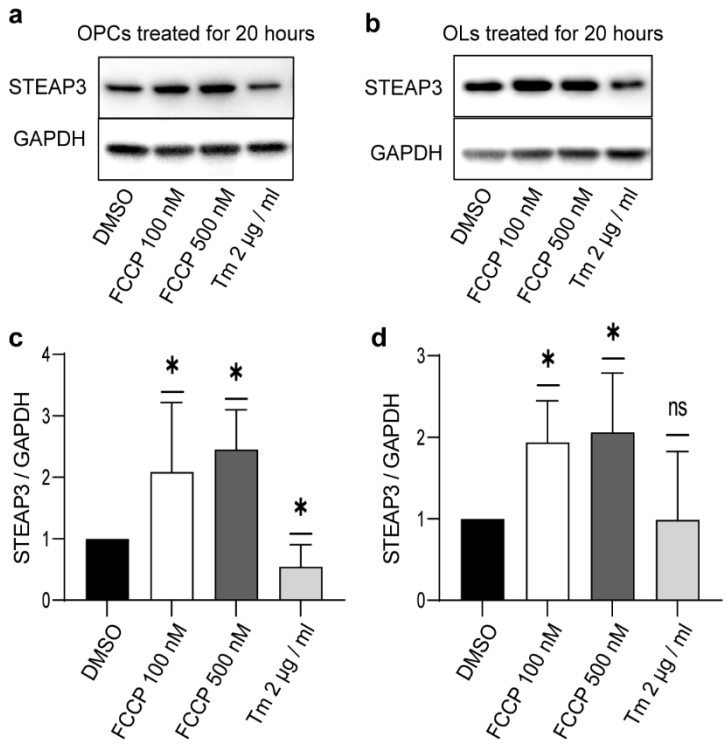

Figure 26. Mitochondrial dysfunction-associated upregulation of STEAP3 in cultured OL lineage cells.

Rat OPCs that were cultured in proliferation media (OPC) or OL-differentiated for 3 days (OLs) were treated with the mitochondrial oxidative phosphorylation uncoupler FCCP or the ER stress inducer tunicamycin (Tm) for 20 hours; 0.02% DMSO was used as a vehicle control (Veh). STEAP3 levels were analyzed by western blotting **(a-b)**. GAPDH-normalized STEAP3 expression was quantified using blots from 3 independent experiments **(c-d)**. STEAP3 expression increased in response to mitochondrial uncoupling but not ER stress. Data are mean ± SD (*, $p<0.05$; ns, $p>0.05$ Mann-Whitney *u*-test).

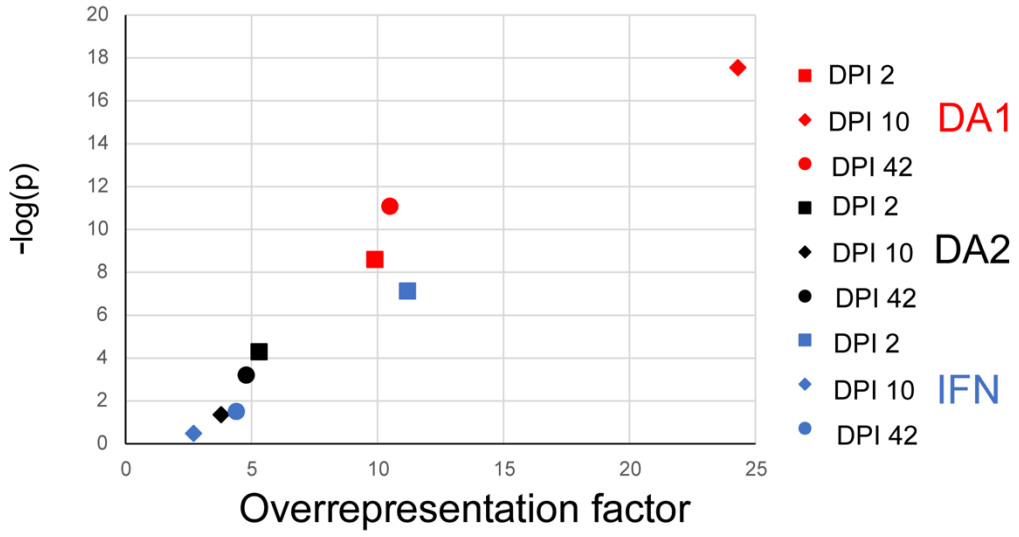

Figure 27. Unique disease-associated OL transcriptome profiles are overrepresented in OL translatome-upregulated mRNAs after SCI in a time-dependent manner.

Overrepresentation factor of OL translatome overlaps with single cell RNASeq-derived OL transcriptomic profiles that are common for various types of white matter damage[268] (http://research-pub.gene.com/OligoLandscape/, see Discussion for more details). The DA1 pro-inflammatory cluster shows greatest overlaps with the OL SCI translatome reaching a maximum on dpi 10.

CHAPTER IV
REVIEW OF FINDINGS

The presented data span developmental and injury contexts to better understand the proteostasis network and translational response to stress in the OL lineage. In Chapter II, we sought to identify the role of autophagy in OPCs during a critical period in mouse CNS development. Neonatal mice with conditional deletion of the essential autophagy gene *Atg5* in *Pdgfrα* expressing OPCs develop tremors by P12 and die by P15. Additionally, autophagy deficient OPCs in these animals undergo apoptotic death, reduced differentiation, and limited and abnormal myelination. Pharmacological and genetic inhibition or stimulation of autophagy blocked or enhanced myelination in OPC / DRG neuron co-cultures, respectively. These findings implicate autophagy as a critical regulator of OPC survival, maturation, and proper myelination.

In Chapter III we used RiboTag to isolate “actively translating”, ribosome-associated mRNAs specifically from myelinating OLs in the adult, thoracic spinal cord, and performed RNA sequencing to define the OL translatomic landscape across acute (dpi 2), subacute (dpi 10) and subchronic (dpi 42) SCI. The sequencing results reveal after SCI OLs experience higher mitochondrial respiration, reorganization of signaling, myelin sheath loss, lower cholesterol biosynthesis and epigenetic desilencing. It also identifies the metalloreductase

STEAP3 as a novel marker of OL-axon response to SCI. Such a dataset provides opportunities to generate novel hypotheses on an active role of OLs in neurotrauma-associated white matter damage.

Autophagy in OPCs is required for CNS development

The data presented in Chapter II point to a clear importance of autophagy in OPCs during development. In fact, in our model functional autophagy in OPCs is critical for the animal's survival. At first glance, this may appear unsurprising as autophagy is a fundamental catabolic process in most eukaryotic cells, and dysfunctional autophagy is implicated in many neurodegenerative diseases including white matter diseases[100,101,130]. Global deletion of many essential autophagy genes is embryonic or neonatal lethal[100,274]. Moreover, deletion of autophagy in select CNS cell populations, including neurons, astrocytes, and microglia can result in dysfunctional phenotypes during development and exacerbate neurodegenerative disease pathogenesis[118,145,175,177,275,276]. Although limited to myelinating glia, disruption in myelination by targeting myelin specific genes such as *Mbp* and *Plp1* can also lead to similar phenotypes we observed[277–280]. Therefore, the conditional deletion of autophagy in OPCs and subsequent failure of OPCs to myelinate is a likely reason for perinatal death.

Choosing our time of tamoxifen administration (P5-P9) relied on the fact that peak myelination in the mouse brain occurs between the first ~1-3 weeks after birth[29,281–283]. However, the timing of our inducible deletion is an important consideration. In mice, it is well established that during development OPCs populate the brain in three distinct waves – two waves during the embryonic

stage and a third cortical wave after birth[281]. Interestingly, soon after birth second wave OPCs derived from the medial ganglionic eminence (MGE) are eliminated from the cortex by an unknown mechanism and replaced by the third wave OPCs derived from the cortical ventricular zone (VZ)[23]. These VZ OPCs eventually make up 80% of the developed motor cortex[29]. The OPCs that myelinate the spinal cord arise during the embryonic stage, and do not display similar postnatal cortical waves seen in the brain[284]. Moreover, early SC OPCs differentiate and myelinate at the embryonic stage and continue to differentiate and myelinate postnatally[281,284].

It is possible that our postnatal deletion is targeting a majority of OPCs from the third cortical wave, as well as a subpopulation of first and second wave OPCs that have yet to differentiate[284]. Unfortunately, we did not quantitatively examine other regions of the CNS beyond the corpus callosum (CC). It would be interesting to know whether early myelinating regions, such as the SC or cerebellum, an early myelinated structure, display similar pathology as what we observed in the CC.

While studies exist of autophagy deficient animals displaying severe phenotypes[149,150], oftentimes cell specific deletion results in delayed pathogenesis. In contrast, pathogenesis in our animals was swift and lethal. Why did such a severe phenotype arise so quickly? One possible explanation could be that at our chosen time of deletion developing OPCs are in a heightened state of cellular stress and “primed” for programmed cell death. During development OPCs proliferate, migrate, differentiate, and myelinate; all which require

extensive translational control and protein synthesis[25,139,140,283]. Moreover, the OL lineage is particularly vulnerable to different cellular stresses including disruptions in proteostasis[25,283,285]. In some cases, varying levels of ER stress during development has been shown to influence cell differentiation[283]. Basal ER stress and expression of cellular stress related proteins may be important in the developmental programs of cells such as OPCs[283]. However, accumulation of pro-apoptotic proteins is likely enough to send the cell towards apoptosis. It is possible that inhibiting autophagy in PDGFRA+ OPCs during a critical period of development results in an imbalance in pro-apoptotic proteins that result in mass programmed death throughout the CNS.

OL development is a remarkable process that requires multiple steps to accomplish myelination[286]. Such processes include OPC generation from neural stem cells, proliferation, migration, differentiation, process extension and interaction with axons, timely initiation of myelin protein synthesis and membrane trafficking, spiral wrapping and compaction, and establishing the axo-myelinic synapse junctions[286]. Likewise, the OPC lineage can be classified into as many as 13 heterogenic molecular identities, suggesting a complex maturation program[287]. A simplified classification is by their ability to proliferate (OPC), exit the cell cycle but not yet produce myelin (premyelinating OL), and myelinating (mature, myelinating OL). As mentioned, previous reports in other cell types, including neurons and astrocytes have shown that autophagy regulates differentiation[144,145,288]. We found that ablating autophagy in OPCs *in vivo* and disrupting autophagy *in vitro* reduced differentiation and myelination. Similarly,

proteomics from progressive stages of human neural stem cells identified upregulated autophagy proteins during differentiation into OLs[289]. Interestingly, when knocking out *Atg5* in *CNP-Cre* mice, Aber et al. found that mice were viable into adulthood, suggesting autophagy is not required for maturation once the cell has reached the premyelinating OL stage[290]. However, by P56 mice display *hypermyelination* and begin to develop a tremor phenotype, followed by premature death[290]. Moreover, a recent study by Zhang et al. also found that *CNP-Cre:Atg5* mice were viable into adulthood, along with *CNP-Cre:Atg7, Olig2-Cre:Atg5* (entire OL lineage), and *Pdgfrα-CreERT2:Atg5* mice[291]. No observable phenotype was mentioned; however, mice were not kept alive passed P56, and the tremor phenotype may not have yet developed as seen by Aber et al[290,291].

In contrast to our findings, deleting *Atg5* in *Pdgfrα* expressing OPCs in mice did not lead to any observable phenotype or lethality but instead resulted in ectopic myelination in multiple brain regions[291]. However, in the study the mice received a one-time administration of tamoxifen at P4 with a dosage of 100 mg/kg, which may not have ablated *Atg5* from all OPCs. Indeed, previous data from our lab has shown that transgenic deletion of *Atg5* by Cre^{ERT2} is most effective over multiple days of tamoxifen administration[123,132]. Regardless, our data support the hypothesis that autophagy is critical for sufficient myelination during postnatal development.

Autophagy is implicated in regulating cytoskeletal dynamics in other cell types, including macrophages and neurons, and has been shown to modulate Rho-family GTPase activity[152,177]. Both actin[292–294] and tubulin[295,296] cytoskeletal

dynamics are essential for PNS myelination. During OL differentiation, changes in morphology unsurprisingly require extensive cytoskeletal regulation and rearrangement[134]. F-actin disassembly drives OL myelination, which is dependent on MBP[178,179]. Interestingly, CNP is involved in microtubule assembly, and overexpression of CNP in OPCs inhibits myelin compaction *in vitro* and *in vivo*[178,179]. CNP likely antagonizes MBP and acts as a barrier for MBP to compact myelin, thus CNP must be cleared for myelination to proceed[178,179]. The dynamics of CNP and MBP in myelin compaction is intriguing in the context of autophagy. Indeed, autophagy could regulate myelin growth through clearance of disassembled cytoskeletal elements. Moreover, CNP makes a logical target for autophagy to be degraded in a timely manner when production of MBP has reached levels ready to initiate myelin compaction. This tipping point between CNP and MBP could be an indirect trigger of autophagy and would be an interesting avenue to explore in future studies. Moreover, localization of *Mbp* mRNA translation is suspected to occur at axon-glia contact sites likely because MBP protein has a high affinity for compacting intracellular membranes[297–300]. Identifying the cargo of autophagosomes at different stages in the OL lineage would be an effective way to reveal stage-specific regulatory pathways and clarify its role in OL maturation.

Limitations

Monitoring and measuring autophagy requires careful consideration in experimental design. It is a highly dynamic process that is active at basal levels and can be regulated spatially and temporally based on the needs of the cell.

Steady state autophagy can be measured by direct observation of autophagic machinery via numerous techniques such as immunoblot, IHC, or TEM. However, such experiments are under static temporal constraints making interpretation difficult. Furthermore, autophagy occurs in stages including initiation, autophagosome formation, cargo sequestration, autophagosome maturation, autophagosome fusion with the lysosome and cargo degradation. Without perturbation of specific stages in the autophagic pathway, data can be misinterpreted. For example, increases in LC3-II, a well-known marker of autophagosomes, could be due to an increase in initiation, a decrease in lysosomal degradation, or perturbation in autophagosome fusion to the lysosome. Addition of multiple timepoints as well as use of pharmacological agents such as lysosomal inhibitors such as chloroquine or Bafilomycin A1 can aid in assessing autophagy function.

A more convincing report of autophagy is to measure *autophagic flux*, which refers to the overall activity of autophagy. This includes formation of the autophagosome, sequestration of its cargo, fusion with the lysosome, and release of degraded macromolecules back into the cytosol[101,102]. We measured autophagic flux by virally labeling autophagosomes with mCherry-EGFP-LC3B in differentiating OPCs. This approach takes advantage of the fact that GFP fluorescence is quenched in acidic environments such as the autolysosome (pH 4-5), while mCherry fluorescence does not[76,102,150,301]. Thus, an autophagosome should fluoresce yellow, and an autolysosome should fluoresce red. Differentiating OLs showed higher numbers of overall puncta compared to OPCs.

There was also an increase in red puncta, although not significant. Although there is a trending increase in the ratio of red / yellow (autolysosome / autophagosome), it was not significantly different from OPCs. This suggests the rate of autophagic degradation remains consistent across stages of differentiation, but there is an increase in overall autophagic flux. Identifying whether autophagic degradation increases or decreases could be monitored through live imaging[302,303]. Unfortunately, we did not perform such experiments. It would be interesting to see if there is a change in rate depending on the stage of development.

A cautionary note for pharmacological interventions targeting the autophagy pathway must be considered. Many pharmacological agents used in research lack specificity towards their proposed target. Pharmacological agents targeting autophagy are no exception. For example, rapamycin enhances autophagy through inhibition of mTORC1, and while autophagy may be stimulated, mTORC1 also acts as a master regulator of cell growth, translation, lipid synthesis, lysosomal biogenesis, energy metabolism, cell survival, and cytoskeletal organization[102,188]. Moreover, mTOR has been shown to be a critical positive regulator of OL differentiation and myelination[186,304–309]. To clearly determine the role of autophagy, we used myelination co-cultures treated with drugs that target the autophagy pathway directly. We found that enhancing autophagy using the Tat-beclin1 peptide, which stimulates autophagy by activating the Beclin-1 / Vps34 complex, promoted myelination around DRG axons. We next treated co-cultures with autophagy inhibitors KU55833, which

targets the PI3K / Beclin-1 / Vps34 complex and has some off target effects, and Verteporfin, which forces accumulation of p62 and failure for the autophagosome to mature. Treatment with autophagy inhibitors reduces myelination. However, the observed effects could also be due to activation or inhibition of autophagy in neurons thereby stimulating OPCs to myelinate independent of OPC autophagic activity. We found similar results in myelin capabilities in OPCs that stimulated autophagy via overexpressed wtATG5 or inhibited autophagy by dnATG5.

The study used *Pdgfr*α to drive Cre recombinase expression in early OPCs and delete *Atg5.* Although the goal of the study was to disrupt autophagy in OPCs alone, other cells expressing *Pdgfr*α could contribute to the observed phenotype. In fact, a subset of CNS pericytes, the cells responsible for blood brain barrier maintenance, capillary blood flow and microcirculation, also express *Pdgfr*α. Deletion of autophagy in *Pdgfr*α-expressing pericytes may contribute to the observed effects on OPC differentiation and animal health[174]. However, others have reported reduced differentiation when autophagy is inhibited in other cell types such as neurons and astrocytes[118,144,145,153]. These studies, along with our work both *in vivo* and *in vitro* argue autophagy deficient pericytes may contribute to the observed phenotype but are not the main drivers of reduced OPC differentiation, OPC loss, and aberrant myelination.

Autophagy has become a heavily researched topic in the past decade, meriting a Nobel Prize to its main discoverer Dr. Yoshinori Ohsumi in 2016. Numerous studies have confirmed its role in many diseases and injuries

including neurodegeneration and SCI[76,100]. However, varying severity of phenotypes resulting from perturbation in autophagy in select cell populations makes interpretation of its role in cell function(s) difficult. Our data identify autophagy as a key regulator of OL development. Furthermore, activating autophagy can enhance myelination, suggesting autophagy could be a promising therapeutic target in facilitating (re)myelination in delayed white matter development or white matter diseases. Future research must identify the cargo of autophagosomes during OL differentiation and myelination. Doing so will help us understand fundamental biological functions of autophagy that can be applied to cell health and disease as well as elucidate if or how autophagy can be utilized in specialized functions such as myelination. It may also identify novel therapeutic targets normally mediated by autophagy but are perturbed in white matter and neurodegenerative diseases.

The OL translatome after SCI

We used RiboTag to conditionally express HA-tagged ribosomes in *Plp1* expressing OLs. This comprehensive dataset captures the translatomic response of surviving OLs after SCI. As expected, qPCR of isolated mRNA from OLs was enriched in myelin specific proteins including *Mbp* and *Plp1.* Additionally, mRNAs associated with other neural cell types (*Hgf, Snap25, Cd68* etc) were depleted. This was observed in the intact spinal cord, as well as after 2-, 10-, and 42-days post-SCI. RNA sequencing results identified hundreds of significantly upregulated and downregulated genes at each time point, creating a genetic landscape for myelinating OLs in the intact cord and in response to SCI.

We found OLs upregulate respirasome genes and downregulate genes associated with morphological complexity and connectivity acutely and subchronically after SCI. Additionally, cholesterol biosynthesis is downregulated subacutely. These findings suggest mature OLs revert to similar metabolic programming as premyelinating OLs.

In the OL lineage, metabolic reprogramming during development and adulthood have been reported. During development, OPCs and premyelinating glia utilize mitochondrial respiration and oxidative phosphorylation to produce high amounts of ATP used for myelin synthesis and subsequent myelination[69,270]. Conversely, mature OLs do not require mitochondrial respiration, and instead shift towards aerobic glycolysis, generating lactate that is shuttled to support energetic demands of the axon[69,171,270]. In a seminal study by Fünfschilling and colleagues, knocking out OXPHOS during OL development results in severe dysmyelination, whereas knocking out OXPHOS in mature OLs after myelination is complete results in no visible phenotype in myelin or axon integrity[69]. Moreover, developing OLs are enriched with long mitochondria, while mature OLs have a lower density of mitochondria, and often fragmented in OL processes[270,310]. Mitochondria have also been found in myelin sheaths[270]. These observations support a shift towards less OXPHOS in mature cells.

Reverting to a premyelinating state could be a coping mechanism to help maintain survival of the OL and its remaining myelin sheaths after SCI. The OL may even be selectively removing myelin sheaths from damaged axons to save itself while also maintaining myelin sheaths on healthy axons. However, it is likely

the surviving OL is in a prolonged state of sublethal cellular stress as secondary damage can be observed as late as 6 weeks post-SCI[76,107,111,189]. A prolonged state of stress may push the OL to revert to a premyelinating OL, making it vulnerable to cell death. Indeed, accumulating reports suggest the premyelinating OL is more vulnerable to cell death than an OPC or myelinating OL[25,283,311]. If surviving OLs are reverting to a premyelinating stage, then they may be more vulnerable to chronic secondary damage characteristic of SCI. This could explain why the OL lineage undergoes more dynamic cell death after SCI compared to other cell types in the CNS[107].

Normally, remyelination in response to demyelination is mainly performed by differentiated OPCs, although resident myelinating OLs have some albeit limited capacity to myelinate local axons[25]. Remyelination by differentiated OPCs improves disease pathology such as MS, AD and PD[25]. However, adult OPCs ability to remyelinate is not as robust as the original intact myelin or from juvenile OPCs[25]. Regardless, remyelination by adult OPCs is sufficient in most disease models to restore some physiological function.

Remyelination also occurs in the spinal cord, including after SCI. However, its impact on functional recovery after SCI is controversial. While increased spared white matter correlates with improved functional recovery in thoracic injuries, neuron survival rather than spared white matter correlates with improved functional recovery in cervical and lumbar injuries[117]. However, strategies to target remyelination after SCI have not been as successful as those in other disease contexts. Moreover, the benefits of endogenous remyelination after SCI

has been challenged. Duncan et al. showed that inhibiting OPC remyelination by conditional deletion of *Myrf,* an essential transcription factor required for myelination, in *Pdgfrα* expressing cells does not affect locomotor outcomes (positive or negative) in mice after thoracic injury suggesting remyelination is not required for functional recovery after SCI. Although these results suggest remyelination is not required, it does not determine whether remyelination is not beneficial. It may be that remyelination is most effective depending on the injury severity and number of spared axons available to remyelinate. Furthermore, remyelination may help maintain axon structural integrity and prevent chronic axon degeneration. Further work is needed to better understand the role of remyelination after SCI. Inducing RiboTag in *Pdgfrα* mice before and after SCI may help bring to light some of the reasons why remyelination is not sufficient to promote functional recovery.

Additionally, damage to the axo-myelinic contact sites and to myelinated axons and metabolic reprogramming occurs acutely after SCI, followed by a subchronic wave with similar expected outcomes. Acute axonal damage followed by a subchronic wave of axonal damage has been shown in contusive SCI in rats[271,312]. Moreover, chronic demyelination in mouse contusive SCI is also documented[272]. Future studies investigating mitochondrial respiration in OLs after SCI could prove promising not only acutely, but also chronically. Furthermore, such a biphasic shift in metabolic programming suggests effectiveness of therapeutic interventions may be dependent on stage of recovery.

SCI-associated OL translatome changes show partial overlap with OL transcriptomic responses to other injuries[268]. Moreover, we further cross referenced our final gene lists with existing single-cell datasets[195,268] to confirm high confidence OL-specific genes that respond to SCI. Our conservative approach identified genes that have been implicated in pro-death pathways but not characterized in OLs after acute (dpi 2) SCI. These include *Apod, Pla2g3, Trf, Serpina3n, Serpina3c, Steap3, Pcyox1l, Itgad, Pfkfb4, Bact1/2* and *Spry.* A literature review of these genes led us to further investigate STEAP3 and PCYOX1L.

Few studies have investigated the role of PCYOX1L in cell biology. PCYOX1L is a relative of the lysosomal cysteine deprenylase PCYOX1, which generates hydrogen peroxide and has been implicated as a contributor to oxidative stress[233,264,265]. Recently PCYOX1L function has been described. Petenkova and colleagues show that loss of PCYOX1L protein reduces the mevalonate pathway, which impacted autophagy and cellular viability[313]. Moreover, *Pcyox1l* deficiency reduced protein prenylation in neutrophils[313]. Protein prenylation is a post-translational modification that typically promotes prenylated proteins to associate with plasma or endomembranes[314]. Interestingly, protein prenylation has been shown to be required for OPCs to correctly migrate to axon targets[315]. Likewise, CNP, a myelin protein involved in microtubule assembly and an antagonist to MBP-directed myelin compaction, is one of the few prenylated myelin proteins. It is suggested prenylation directs CNP to myelin membranes and modulates cell morphology[316]. Prenylation has been shown to

play a critical role in protein-protein interactions[314]. Given the relationship between CNP and MBP, one wonders whether prenylation and subsequent deprenylation by PCYOX1L influences their antagonistic relationship during myelination and remyelination. Thus, PCYOX1L expression in surviving OLs could contribute to chronic stress and may contribute to the chances of surviving OLs to maintain myelin or myelinate demyelinated axons.

STEAP3 or TSAP6 is an endosomal / lysosomal metalloreductase that reduces both insoluble ferric iron (Fe^{3+}) to soluble ferrous iron (Fe^{2+}) and Cu^{3+} to Cu^{2+} [222,258,317]. Ferrous iron (Fe^{2+}) is highly reactive and produces ROS via the Fenton reaction. Ferrous iron Fe^{2+} can then be exported from endosomes / lysosomes to the cytoplasm, which suggests STEAP3 plays an important role in cellular iron supply[246,247,259]. Due to this process, recent evidence suggests STEAP3 plays a role in lipid peroxidation and ferroptosis, a form of cell death mediated through iron homeostasis[222,260,263,317,318]. As mentioned previously, OLs contain the highest levels of iron in the CNS. Additionally, iron is directly required for myelination as a cofactor involved in ATP, cholesterol and lipid synthesis which confers with their high metabolic demands[81].

A meta-analysis performed by Pandey and colleagues identified *Steap3* as a marker of disease associated OLs[268]. STEAP3 has been implicated as an enhancer of cell death in p53 activated cancer cells[263], while knockdown has been shown to reduce apoptosis[246]. Not only is STEAP3 a contributor of oxidation through reduction of free iron, but it can also interact with members of the BH3-only apoptotic family of proteins, further intensifying apoptotic

death[259,261]. Additionally, STEAP3 is a major regulator of exosome-mediated secretion[262,263], suggesting non-canonical signaling by OLs could influence the tissue microenvironment. Moreover, canonical and non-canonical secreted proteins are among the upregulated genes at 10 and 42 dpi, suggesting OLs likely contribute to the tissue microenvironment throughout SCI recovery.

We verified STEAP3 expression at the protein level in acute SCI tissue via immunostaining. Interestingly, weak staining was present in OL cell bodies in the naïve mouse spinal cord, however after injury an interesting pattern emerged. After acute SCI, some spared myelinated axons rostral and caudal of the epicenter injury swell, resulting in abnormal myelin blebbing. We found that STEAP3 expression was present in cell bodies, but more so co-labeled with the swelling axons (pNFH) and myelin (MBP). The observed colocalization suggests that STEAP3 could be indicative of early axon damage, possibly through oxidative stress at or near the axo-myelinic synapse. Iron metabolism is essential for myelin production, and STEAP3 could be expressed to help maintain energy stores required for myelin protein synthesis near the myelin sheath. On the other hand, STEAP3 expression from OLs could be signaling to axons to rescue axon swelling.

We wanted to explore whether STEAP3 expression is affected by mitochondrial stress. Our *in vitro* data confirm STEAP3 is activated both in OPCs and OLs after treatment with the mitochondrial decoupler FCCP, but not the ER stress inducer tunicamycin. Uncoupling mitochondrial respiration from ATP synthesis increases ROS generation[266]. STEAP3 upregulation after mitochondrial

uncoupling in OL lineage cells may represent mitochondrial dysfunction or mitochondrial oxidative stress. Oxidative stress may activate expression of iron regulatory genes to mitigate ROS damage and support mitochondrial biogenesis as it requires iron and ATP production[267]. Future work exploring the role of STEAP3 in oxidative damage to OLs, as well as its role in the axon-myelinic pathology, looks promising. Would overexpression of STEAP3 exacerbate oxidative stress, or other forms of cellular stress?

Limitations

While the presented OL translatome dataset identifies many differentially expressed genes in OLs before and after progressive SCI, it has important limitations that must be considered. Extracting RNA from lipid rich tissue is difficult since lipids can interfere with clean separation of RNA. The spinal cord is particularly challenging due to its high levels of lipid rich myelin. Common extraction practices rely on strong lysis reagents such as TRIzol to degrade lipids and free up RNAs for isolation. However, RiboTag requires gentle tissue lysis using high salt buffers to maintain RNA-associated polysome complexes and does not fully degrade myelin-rich spinal cord tissue [129]. Localization of mRNA to different cellular compartments has been described for many mRNAs and cell types[298,319]. Indeed, *Mbp* mRNA was detected in purified myelin fractions nearly 40 years ago[320] and hundreds more mRNAs that localize to myelin have since been identified[321,322]. In line with this data, there is a distinct difference between the myelin and OL soma transcriptomes[322,323]. While we successfully isolated mRNAs from OLs, we may have missed many mRNAs trapped in undigested

myelin and tissue, and our data likely contain a biased pool of mRNAs residing mainly in the OL soma. Such a possibility unfortunately means we are missing an important pool of RNAs that could play significant roles in myelin maintenance and axon function, especially at the axo-myelinic synapse and in response to pathology. One possible method to indirectly identify genes trafficked to myelin sheaths (or other compartments of interest) would be to analyze our RNAseq dataset for subcellular localization mechanisms such as 3' untranslated regions (UTR) motifs of differentially expressed mRNAs[322]. 3' UTR motifs play a crucial role in temporal and spatial gene expression[322]. Such an analysis could be followed by *in situ* hybridization of identified genes to confirm spatial localization to the myelin sheath.

While mRNA isolation from spinal cord tissue via RiboTag likely results in loss of mRNAs from undigested tissue, it is also susceptible to contamination and signal artifacts from a few possible sources. Procedurally, immunoprecipitation methods rely on antibody binding to magnetic protein A / G beads that in theory should only isolate the antibody-tagged protein of interest. However, no method is perfect and non-specific binding does occur, especially when isolating protein from damaged tissue like acute SCI. The RiboTag protocols are transparent about this issue and suggest additional steps to limit such background noise[129].

Likewise, when using the RiboTag technique, it is important to consider mRNAs under differential translational control – not all mRNAs are translated equally. For example, one mRNA under translational control could have only 2-3 ribosomes in the repressed state and many more ribosomes during its active

state[129]. Unfortunately, RiboTag immunoprecipitation is probably not efficient enough to distinguish between the two states[129]. Moreover, ribosome pausing or stalling during elongation and subsequent repression of protein synthesis can occur when proteins require time to fold, are not yet needed, or mRNA is dysfunctional and needs to be degraded[324,325]. Importantly, such elongation kinetics can be modulated by cellular stress, such as heat shock or proteotoxic stress [325]. Therefore, some differential gene expression events within our dataset, especially acute timepoints where secondary damage is prevalent and most cells are under some state of stress, may be present due to changes in translational state rather than its preferential expression in response to SCI.

Another limitation is the animal model we used to express the RiboTag transgene. The *Plp1-Cre*^{ERT2} mouse line was used to activate ribosome tagging by HA in mature OLs, however *Plp1* is also expressed in Schwann cells[205]. While careful dissection of spinal cord tissue is done, it is difficult to limit fragments of dorsal and ventral nerve roots. Thus, it is a possibility that isolated ribosome-associated mRNAs are of Schwann cell origin. Indeed, in our dataset OL enrichment and SCI upregulation of known marker transcripts of Schwann cell nerve injury are found including *Egfl8* and *Gdnf*[269]. To avoid classification mistakes, genes of interest were confirmed to be expressed in OLs in other datasets[195], and were validated by immunofluorescence using OL specific protein markers.

Upon first review of our dataset, we observed possible contamination of OL polysomes with mRNAs involved in inflammation and immune response from

non-OL cells such as microglia and macrophages. We suspect the contamination is due to non-specific interactions between highly inducible non-OL mRNAs, especially those from immune cells, and the protein A / G magnetic beads during sample preparation. Additional studies using the RiboTag system have shown similar contamination making interpretation difficult[213,326].

To address these limitations, we developed a filtering strategy to identify differentially expressed ribosome-associated mRNA transcripts through stringent selection criteria[129,326]. In this case we applied a two-fold filtration process. Reducing the background noise can in part be done by normalizing the cell-specific mRNAs (OL translatome) to total cell mRNAs (input transcriptome) and filtering based on relative enrichment. However, this normalization is taking two distinctly different pools of mRNAs from cells (translatome vs transcriptome). Ideally, experiments would include constitutively expressed RiboTag animals, which could be used to identify differentially expressed genes in the cell-specific translatome compared to the total cell translatome. Our second criteria for filtration applied a common analysis used in RiboTag studies[129,327–329]; comparing the immunopurified, OL translatome of the experimental groups with the OL translatome of the control groups. This captures differential OL enrichment that would be masked if similar events occurred in the total mRNA pool. Thus, we pooled together two groups of genes: highly enriched OL transcripts (OL vs total mRNA) and differential OL enrichment (OL_{SCI} vs $OL_{naïve}$). These filtration criteria improve specificity of detection, but likely diminishes sensitivity to detect differentially expressed genes as over 60% of OL translatome mRNAs did not

pass our selection criteria. We are therefore missing many other biological pathways that are likely worth investigating.

The findings in Chapter III describe the OL translatome in response to progressive stages of SCI. Many differentially expressed genes were identified both in OLs (translatome) as well as all cells (transcriptome). These data are quite powerful as they present an unbiased approach to identify novel pathways previously not recognized in SCI in a cell-specific manner. However, most of the work presented is mainly descriptive. Like most sequencing datasets, there are still many differentially expressed genes and affected pathways to explore in how myelinating OLs and the total tissue respond to progressive stages of SCI recovery. Regardless, our findings highlight novel biological processes affected in OLs after SCI.

Concluding remarks

The presented studies used both developmental and injury models to uncover regulators in OL differentiation, myelination and survival. In development, OPCs undergo extensive translational regulation during differentiation. Such translational regulation is likely stage specific. Thus, maintaining proteostasis during periods of high protein synthesis, especially during critical periods of myelination, indicates a need for timely clearance of no longer needed proteins. Utilizing the OPC-specific *Atg5* knockout model, we found that autophagy is essential for OPC differentiation and myelination and produces a strong tremor phenotype. This study also highlights a role for

autophagy in facilitating myelination, possibly through myelin compaction. Future studies identifying targeted cargo of autophagy will prove invaluable in understanding the molecular mechanisms involved in OPC development. Likewise, such results suggest autophagy could be a promising therapeutic target in demyelinating diseases and SCI.

Despite OL contributions to functional outcomes after contusive, thoracic SCI, studies focused on OL transcriptional / translational response after injury are lacking compared to other CNS cell types. This discrepancy hinders development of therapeutic interventions targeting OL survival. Advances in unbiased omics technology and development of cell-specific transgenic animal models have enabled extensive understanding of biological responses after SCI in whole tissue and other neural cells (neurons, astrocytes, microglia). Using tools that target actively translating mRNAs, we describe the translatomic landscape of OLs in the intact spinal cord and in response to progressive stages of contusive SCI. It identifies previously unrecognized aspects of OL biology that may play a significant role in OL survival and myelin maintenance after SCI. The dataset is publicly available and will hopefully prove useful for future studies of white matter damage-associated injuries and diseases. Taken together, these studies provide insight into OPC / OL development and response after SCI, but also raises exciting questions that will hopefully inspire new hypotheses exploring OPC / OL biology in development and white matter pathology, such as SCI.

REFERENCES

1. Vesalius, A. De humani corporis fabrica libri septem (On the Fabric of the Human Body in Seven Books). (1543).
2. van Leeuwenhoek, A. Epistolae Physiologicae Super Compluribus Naturae Arcanis; *Epistola XXXII* 309–317 (1719).
3. Ehrenberg, C. G. Nothwendigkeit einer feineren mechanischen Zerlegung des Gehirns und der Nerven vor der chemischen, dargestellt aus Beobachtungen. *Ann Phys* 449–473 (1833).
4. Remak, R. Weitere mikroscopische Beobachtungen über die Primitivfasern des Nervensystems des Wirbelthiere. *Froriep's Neue Notizen* 35–41 (1837).
5. Boullerne, A. I. The history of myelin. *Experimental Neurology* vol. 283 431–445 Preprint at https://doi.org/10.1016/j.expneurol.2016.06.005 (2016).
6. Schwann, T. Microscopical Researches into the Accordance in the Structure and Growth of Animals and Plants . *Sydenham Society* (1839).
7. Kettenmann, H. & Ransom, B. The concept of neuroglia: a historical perspective. *Neuroglia* 1–16 (2005).
8. Virchow, R. L. Ueber das ausgebreitete Vorkommen einer dem Nervenmark analogen Substanz in den thierischen Geweben. *Virchows Arch* 562–572 (1854).
9. Ranvier, L.-A. Leçons sur l'Histologie du Système nerveux. *Librairie Savy* (1878).
10. Iglesias-Rozas, J. R. & Garrosa, M. Studies on neuroglia: Glia with very few processes (oligodendroglia) by pío del río-hortega. *Clin Neuropathol* **31**, 440–459 (2012).
11. Iglesias-Rozas, J. R. & Garrosa, M. Are the glia with very few processes homologous with Schwann cells? By Pí o del Rí o-Hortega. *Clin Neuropathol* **31**, 460–462 (2012).
12. Penfield, W. OLIGODENDROGLIA AND ITS RELATION TO CLASSICAL NEUROGLIA. *Brain* **47**, 430–452 (1924).
13. del Rio-Hortega, P. Tercera aportación al conocimiento morfologico e interpretación funcional de la oligodendroglia. *Memorias de la Real Sociedad Española de Historia Natural* **14**, 5–122 (1928).
14. Geren, B. Ben. The formation from the Schwann cell surface of myelin in the peripheral nerves of chick embryos. *Exp Cell Res* **7**, 558–562 (1954).
15. Bunge, M. B., Bunge, R. P. & Ris, H. Ultrastructural study of remyelination in an experimental lesion in adult cat spinal cord. *J Biophys Biochem Cytol* **10**, 67–94 (1961).

16. Bunge, R. P., Bunge, M. B. & RIS, H. Electron microscopic study of demyelination in an experimentally induced lesion in adult cat spinal cord. *J Biophys Biochem Cytol* **7**, 685–696 (1960).
17. Bunge, M. B., Bunge, R. P. & Pappas, G. D. Electron microscopic demonstration of connections between glia and myelin sheaths in the developing mammalian central nervous system. *J Cell Biol* **12**, 448–453 (1962).
18. Bunge, R. P. Glial cells and the central myelin sheath. *Physiol Rev* **48**, 197–251 (1968).
19. Warf, B. C., Fok-Seang, J. & Miller, R. H. Evidence for the ventral origin of oligodendrocyte precursors in the rat spinal cord. *J Neurosci* **11**, 2477–2488 (1991).
20. Pringle, N. P. & Richardson, W. D. A singularity of PDGF alpha-receptor expression in the dorsoventral axis of the neural tube may define the origin of the oligodendrocyte lineage. *Development* **117**, 525–533 (1993).
21. Huang, W., Guo, Q., Bai, X., Scheller, A. & Kirchhoff, F. Early embryonic NG2 glia are exclusively gliogenic and do not generate neurons in the brain. *Glia* **67**, 1094–1103 (2019).
22. Vallstedt, A., Klos, J. M. & Ericson, J. Multiple dorsoventral origins of oligodendrocyte generation in the spinal cord and hindbrain. *Neuron* **45**, 55–67 (2005).
23. Kessaris, N. *et al.* Competing waves of oligodendrocytes in the forebrain and postnatal elimination of an embryonic lineage. *Nat Neurosci* **9**, 173–179 (2006).
24. Richardson, W. D., Kessaris, N. & Pringle, N. Oligodendrocyte wars. *Nat Rev Neurosci* **7**, 11–18 (2006).
25. Kuhn, S., Gritti, L., Crooks, D. & Dombrowski, Y. Oligodendrocytes in Development, Myelin Generation and Beyond. *Cells* **8**, (2019).
26. Miller, R. H. Regulation of oligodendrocyte development in the vertebrate CNS. *Prog Neurobiol* **67**, 451–467 (2002).
27. Zhu, Q. *et al.* Dorsally-derived oligodendrocytes in the spinal cord contribute to axonal myelination during development and remyelination following focal demyelination. *Glia* **59**, 1612–1621 (2011).
28. Barres, B. A. *et al.* Cell death and control of cell survival in the oligodendrocyte lineage. *Cell* **70**, 31–46 (1992).
29. Tripathi, R. B. *et al.* Dorsally and ventrally derived oligodendrocytes have similar electrical properties but myelinate preferred tracts. *J Neurosci* **31**, 6809–6819 (2011).
30. Fu, H. *et al.* Dual origin of spinal oligodendrocyte progenitors and evidence for the cooperative role of Olig2 and Nkx2.2 in the control of oligodendrocyte differentiation. *Development* **129**, 681–693 (2002).
31. Lu, Q. R. *et al.* Common developmental requirement for Olig function indicates a motor neuron/oligodendrocyte connection. *Cell* **109**, 75–86 (2002).

32. Takebayashi, H. *et al.* The basic helix-loop-helix factor olig2 is essential for the development of motoneuron and oligodendrocyte lineages. *Curr Biol* **12**, 1157–1163 (2002).
33. Zhou, Q. & Anderson, D. J. The bHLH transcription factors OLIG2 and OLIG1 couple neuronal and glial subtype specification. *Cell* **109**, 61–73 (2002).
34. Hall, A., Giese, N. A. & Richardson, W. D. Spinal cord oligodendrocytes develop from ventrally derived progenitor cells that express PDGF alpha-receptors. *Development* **122**, 4085–4094 (1996).
35. Pringle, N. P., Guthrie, S., Lumsden, A. & Richardson, W. D. Dorsal spinal cord neuroepithelium generates astrocytes but not oligodendrocytes. *Neuron* **20**, 883–893 (1998).
36. Nishiyama, A., Lin, X. H., Giese, N., Heldin, C. H. & Stallcup, W. B. Interaction between NG2 proteoglycan and PDGF alpha-receptor on O2A progenitor cells is required for optimal response to PDGF. *J Neurosci Res* **43**, 315–330 (1996).
37. Sommer, I. & Schachner, M. Cell that are O4 antigen-positive and O1 antigen-negative differentiate into O1 antigen-positive oligodendrocytes. *Neurosci Lett* **29**, 183–188 (1982).
38. Bansal, R., Stefansson, K. & Pfeiffer, S. E. Proligodendroblast antigen (POA), a developmental antigen expressed by A007/O4-positive oligodendrocyte progenitors prior to the appearance of sulfatide and galactocerebroside. *J Neurochem* **58**, 2221–2229 (1992).
39. Hartman, B. K., Agrawal, H. C., Agrawal, D. & Kalmbach, S. Development and maturation of central nervous system myelin: comparison of immunohistochemical localization of proteolipid protein and basic protein in myelin and oligodendrocytes. *Proc Natl Acad Sci U S A* **79**, 4217–4220 (1982).
40. Monge, M., Kadiiski, D., Jacque, C. M. & Zalc, B. Oligodendroglial expression and deposition of four major myelin constituents in the myelin sheath during development. An in vivo study. *Dev Neurosci* **8**, 222–235 (1986).
41. Tsai, H. H. *et al.* Oligodendrocyte precursors migrate along vasculature in the developing nervous system. *Science* **351**, 379–384 (2016).
42. Tsai, H. H. *et al.* The chemokine receptor CXCR2 controls positioning of oligodendrocyte precursors in developing spinal cord by arresting their migration. *Cell* **110**, 373–383 (2002).
43. Hughes, A. N. & Appel, B. Oligodendrocytes express synaptic proteins that modulate myelin sheath formation. *Nat Commun* **10**, (2019).
44. Xia, W. & Fancy, S. P. J. Mechanisms of oligodendrocyte progenitor developmental migration. *Dev Neurobiol* **81**, 985–996 (2021).
45. Su, Y. *et al.* Astrocyte endfoot formation controls the termination of oligodendrocyte precursor cell perivascular migration during development. *Neuron* **111**, 190-201.e8 (2023).

46. Hughes, E. G., Kang, S. H., Fukaya, M. & Bergles, D. E. Oligodendrocyte progenitors balance growth with self-repulsion to achieve homeostasis in the adult brain. *Nat Neurosci* **16**, 668–676 (2013).
47. Gibson, E. M. *et al.* Neuronal activity promotes oligodendrogenesis and adaptive myelination in the mammalian brain. *Science* **344**, (2014).
48. Bloom, M. S., Orthmann-Murphy, J. & Grinspan, J. B. Motor Learning and Physical Exercise in Adaptive Myelination and Remyelination. *ASN Neuro* **14**, (2022).
49. Knowles, J. K., Batra, A., Xu, H. & Monje, M. Adaptive and maladaptive myelination in health and disease. *Nat Rev Neurol* **18**, 735–746 (2022).
50. Hill, R. A., Li, A. M. & Grutzendler, J. Lifelong cortical myelin plasticity and age-related degeneration in the live mammalian brain. *Nat Neurosci* **21**, 683–695 (2018).
51. Hughes, E. G., Orthmann-Murphy, J. L., Langseth, A. J. & Bergles, D. E. Myelin remodeling through experience-dependent oligodendrogenesis in the adult somatosensory cortex. *Nat Neurosci* **21**, 696–706 (2018).
52. Charcot, J.-M. Histologie de la Sclérose en Plaques. *Gazette des hopitaux civils et militaires* **41**, 557-558,566 (1868).
53. Compston, A. & Coles, A. Multiple sclerosis. *Lancet* **372**, 1502–1517 (2008).
54. Lassmann, H., Van Horssen, J. & Mahad, D. Progressive multiple sclerosis: pathology and pathogenesis. *Nat Rev Neurol* **8**, 647–656 (2012).
55. Bankston, A. N., Mandler, M. D. & Feng, Y. Oligodendroglia and neurotrophic factors in neurodegeneration. *Neuroscience Bulletin* Preprint at https://doi.org/10.1007/s12264-013-1321-3 (2013).
56. Ghasemi, N., Razavi, S. & Nikzad, E. Multiple Sclerosis: Pathogenesis, Symptoms, Diagnoses and Cell-Based Therapy. *Cell J* **19**, 1–10 (2017).
57. Williams, A. *et al.* Semaphorin 3A and 3F: key players in myelin repair in multiple sclerosis? *Brain* **130**, 2554–2565 (2007).
58. Piaton, G. *et al.* Class 3 semaphorins influence oligodendrocyte precursor recruitment and remyelination in adult central nervous system. *Brain* **134**, 1156–1167 (2011).
59. Bin, J. M. *et al.* Full-length and fragmented netrin-1 in multiple sclerosis plaques are inhibitors of oligodendrocyte precursor cell migration. *Am J Pathol* **183**, 673–680 (2013).
60. Boyd, A., Zhang, H. & Williams, A. Insufficient OPC migration into demyelinated lesions is a cause of poor remyelination in MS and mouse models. *Acta Neuropathol* **125**, 841–859 (2013).
61. Tepavčevič, V. *et al.* Early netrin-1 expression impairs central nervous system remyelination. *Ann Neurol* **76**, 252–268 (2014).
62. Tepavčević, V. & Lubetzki, C. Oligodendrocyte progenitor cell recruitment and remyelination in multiple sclerosis: the more, the merrier? *Brain* **145**, 4178–4192 (2022).
63. Prineas, J. W. *et al.* Multiple sclerosis. Pathology of recurrent lesions. *Brain* **116 (Pt 3)**, 681–693 (1993).

64. Rosenberg, S. S., Kelland, E. E., Tokar, E., De La Torre, A. R. & Chan, J. R. The geometric and spatial constraints of the microenvironment induce oligodendrocyte differentiation. *Proc Natl Acad Sci U S A* **105**, 14662–14667 (2008).
65. Cooper, J. J. M. *et al.* Chronic demyelination of rabbit lesions is attributable to failed oligodendrocyte progenitor cell repopulation. *Glia* **71**, 1018–1035 (2023).
66. Byravan, S., Foster, L. M., Phan, T., Verity, A. N. & Campagnoni, A. T. Murine oligodendroglial cells express nerve growth factor. *Proc Natl Acad Sci U S A* **91**, 8812–8816 (1994).
67. Du, Y. & Dreyfus, C. F. Oligodendrocytes as providers of growth factors. *J Neurosci Res* **68**, 647–654 (2002).
68. Wilkins, A., Majed, H., Layfield, R., Compston, A. & Chandran, S. Oligodendrocytes promote neuronal survival and axonal length by distinct intracellular mechanisms: A novel role for oligodendrocyte-derived glial cell line-derived neurotrophic factor. *Journal of Neuroscience* **23**, 4967–4974 (2003).
69. Fünfschilling, U. *et al.* Glycolytic oligodendrocytes maintain myelin and long-term axonal integrity. *Nature* **485**, 517–521 (2012).
70. Lee, Y. *et al.* Oligodendroglia metabolically support axons and contribute to neurodegeneration. *Nature* **487**, 443–448 (2012).
71. Falcão, A. M. *et al.* Disease-specific oligodendrocyte lineage cells arise in multiple sclerosis. *Nat Med* **24**, 1837–1844 (2018).
72. Witte, M. E. *et al.* Enhanced number and activity of mitochondria in multiple sclerosis lesions. *J Pathol* **219**, 193–204 (2009).
73. Witte, M. E., Mahad, D. J., Lassmann, H. & van Horssen, J. Mitochondrial dysfunction contributes to neurodegeneration in multiple sclerosis. *Trends Mol Med* **20**, 179–187 (2014).
74. Zhou, P. *et al.* Monocarboxylate transporter 1 and the vulnerability of oligodendrocyte lineage cells to metabolic stresses. *CNS Neurosci Ther* **24**, 126–134 (2018).
75. Tepavčević, V. Oligodendroglial Energy Metabolism and (re)Myelination. *Life (Basel)* **11**, (2021).
76. Whittemore, S. R., Saraswat Ohri, S., Forston, M. D., Wei, G. Z. & Hetman, M. The Proteostasis Network: A Global Therapeutic Target for Neuroprotection after Spinal Cord Injury. *Cells* **11**, (2022).
77. Hoffman-Zacharska, D., Kmieć, T., Poznański, J., Jurek, M. & Bal, J. Mutations in the PLP1 gene residue p. Gly198 as the molecular basis of Pelizeaus-Merzbacher phenotype. *Brain Dev* **35**, 877–880 (2013).
78. Inoue, K. Cellular pathology of pelizaeus-merzbacher disease involving chaperones associated with endoplasmic reticulum stress. *Front Mol Biosci* **4**, 7 (2017).
79. Nobuta, H. *et al.* Oligodendrocyte Death in Pelizaeus-Merzbacher Disease Is Rescued by Iron Chelation. *Cell Stem Cell* **25**, 531-541.e6 (2019).
80. Dixon, S. J. *et al.* Ferroptosis: an iron-dependent form of nonapoptotic cell death. *Cell* **149**, 1060–1072 (2012).

81. Cheli, V. T., Correale, J., Paez, P. M. & Pasquini, J. M. Iron Metabolism in Oligodendrocytes and Astrocytes, Implications for Myelination and Remyelination. *ASN Neuro* **12**, (2020).
82. Cheli, V. T. *et al.* H-ferritin expression in astrocytes is necessary for proper oligodendrocyte development and myelination. *Glia* **69**, 2981–2998 (2021).
83. Rosas, H. D. *et al.* Diffusion tensor imaging in presymptomatic and early Huntington's disease: Selective white matter pathology and its relationship to clinical measures. *Mov Disord* **21**, 1317–1325 (2006).
84. Martins-de-Souza, D. *et al.* Proteome analysis of the thalamus and cerebrospinal fluid reveals glycolysis dysfunction and potential biomarkers candidates for schizophrenia. *J Psychiatr Res* **44**, 1176–1189 (2010).
85. Bohnen, N. I. & Albin, R. L. White matter lesions in Parkinson disease. *Nat Rev Neurol* **7**, 229–236 (2011).
86. Di Paola, M. *et al.* Multimodal MRI analysis of the corpus callosum reveals white matter differences in presymptomatic and early Huntington's disease. *Cereb Cortex* **22**, 2858–2866 (2012).
87. Gold, B. T., Johnson, N. F., Powell, D. K. & Smith, C. D. White matter integrity and vulnerability to Alzheimer's disease: preliminary findings and future directions. *Biochim Biophys Acta* **1822**, 416–422 (2012).
88. Meissner, W. G. *et al.* Multiple System Atrophy: Recent Developments and Future Perspectives. *Mov Disord* **34**, 1629–1642 (2019).
89. Ahmed, Z., Asi, Y. T., Lees, A. J., Revesz, T. & Holton, J. L. Identification and quantification of oligodendrocyte precursor cells in multiple system atrophy, progressive supranuclear palsy and Parkinson's disease. *Brain pathology* **23**, 263–273 (2013).
90. Hetz, C., Chevet, E. & Oakes, S. A. Proteostasis control by the unfolded protein response. *Nature Cell Biology* Preprint at https://doi.org/10.1038/ncb3184 (2015).
91. Jackson, M. P. & Hewitt, E. W. Cellular proteostasis: degradation of misfolded proteins by lysosomes. *Essays Biochem* **60**, 173–180 (2016).
92. Klaips, C. L., Jayaraj, G. G. & Hartl, F. U. Pathways of cellular proteostasis in aging and disease. *Journal of Cell Biology* **217**, 51–63 (2018).
93. Lottes, E. N. & Cox, D. N. Homeostatic Roles of the Proteostasis Network in Dendrites. *Front Cell Neurosci* **14**, (2020).
94. Labbadia, J. & Morimoto, R. I. The Biology of Proteostasis in Aging and Disease. *Annu Rev Biochem* **84**, 435–464 (2015).
95. Shen, M., Schmitt, S., Buac, D. & Dou, Q. P. Targeting the ubiquitin-proteasome system for cancer therapy. *Expert Opin Ther Targets* **17**, 1091–1108 (2013).
96. Kurtishi, A., Rosen, B., Patil, K. S., Alves, G. W. & Møller, S. G. Cellular Proteostasis in Neurodegeneration. *Mol Neurobiol* **56**, 3676–3689 (2019).
97. Costa-Mattioli, M. & Walter, P. The integrated stress response: From mechanism to disease. *Science* **368**, (2020).
98. Meusser, B., Hirsch, C., Jarosch, E. & Sommer, T. ERAD: the long road to destruction. *Nat Cell Biol* **7**, 766–772 (2005).

99. Dikic, I. & Elazar, Z. Mechanism and medical implications of mammalian autophagy. *Nat Rev Mol Cell Biol* **19**, 349–364 (2018).
100. Mizushima, N. & Levine, B. Autophagy in Human Diseases. *N Engl J Med* **383**, 1564–1576 (2020).
101. Reggiori, F. & Klionsky, D. J. Autophagy in the eukaryotic cell. *Eukaryot Cell* **1**, 11–21 (2002).
102. Klionsky, D. J. *et al.* Guidelines for the use and interpretation of assays for monitoring autophagy (4th edition)1. *Autophagy* **17**, 1–382 (2021).
103. National Spinal Cord Injury Statistical Center. Traumatic Spinal Cord Injury Facts and Figures at a Glance 2023 SCI Data Sheet. *University of Alabama at Birmingham* (2023).
104. Jain, N. B. *et al.* Traumatic spinal cord injury in the United States, 1993-2012. *JAMA* **313**, 2236–2243 (2015).
105. NSCISC National Spinal Cord Injury Statistical Center. Spinal Cord Injury Model Systems. *Birmingham, Alabama* (2021).
106. Almad, A., Sahinkaya, F. R. & McTigue, D. M. Oligodendrocyte fate after spinal cord injury. *Neurotherapeutics* **8**, 262–273 (2011).
107. Pukos, N., Goodus, M. T., Sahinkaya, F. R. & McTigue, D. M. Myelin status and oligodendrocyte lineage cells over time after spinal cord injury: What do we know and what still needs to be unwrapped? *Glia* **67**, 2178–2202 (2019).
108. Duncan, G. J. *et al.* The fate and function of oligodendrocyte progenitor cells after traumatic spinal cord injury. *Glia* **68**, 227–245 (2020).
109. Crowe, M. J., Bresnahan, J. C., Shuman, S. L., Masters, J. N. & Beattie, M. S. Apoptosis and delayed degeneration after spinal cord injury in rats and monkeys. *Nat Med* **3**, 73–76 (1997).
110. Norenberg, M. D., Smith, J. & Marcillo, A. The pathology of human spinal cord injury: defining the problems. *J Neurotrauma* **21**, 429–440 (2004).
111. Hilton, B. J., Moulson, A. J. & Tetzlaff, W. Neuroprotection and secondary damage following spinal cord injury: concepts and methods. *Neurosci Lett* **652**, 3–10 (2017).
112. Giacci, M. K. *et al.* Oligodendroglia Are Particularly Vulnerable to Oxidative Damage after Neurotrauma In Vivo. *J Neurosci* **38**, 6491–6504 (2018).
113. de Rivero Vaccari, J. P. *et al.* P2X4 receptors influence inflammasome activation after spinal cord injury. *J Neurosci* **32**, 3058–3066 (2012).
114. Ravindran, R. *et al.* The amino acid sensor GCN2 controls gut inflammation by inhibiting inflammasome activation. *Nature* **531**, 523–527 (2016).
115. Ohri, S. S. *et al.* Attenuating the endoplasmic reticulum stress response improves functional recovery after spinal cord injury. *Glia* **59**, 1489–1502 (2011).
116. Mekhail, M., Almazan, G. & Tabrizian, M. Oligodendrocyte-protection and remyelination post-spinal cord injuries: a review. *Prog Neurobiol* **96**, 322–339 (2012).

117. Magnuson, D. S. K. *et al.* Comparing deficits following excitotoxic and contusion injuries in the thoracic and lumbar spinal cord of the adult rat. *Exp Neurol* **156**, 191–204 (1999).
118. Hara, T. *et al.* Suppression of basal autophagy in neural cells causes neurodegenerative disease in mice. *Nature* **441**, 885–889 (2006).
119. Han, J. *et al.* ER-stress-induced transcriptional regulation increases protein synthesis leading to cell death. *Nat Cell Biol* **15**, 481–490 (2013).
120. Ohri, S. S., Hetman, M. & Whittemore, S. R. Restoring endoplasmic reticulum homeostasis improves functional recovery after spinal cord injury. *Neurobiol Dis* (2013) doi:10.1016/j.nbd.2013.04.021.
121. Han, J. *et al.* ER stress signalling through eIF2α and CHOP, but not IRE1α, attenuates adipogenesis in mice. *Diabetologia* **56**, 911–924 (2013).
122. Ohri, S. S. *et al.* Deletion of the Pro-Apoptotic Endoplasmic Reticulum Stress Response Effector CHOP Does Not Result in Improved Locomotor Function after Severe Contusive Spinal Cord Injury. *J Neurotrauma* **29**, 579–588 (2012).
123. Ohri, S. S. *et al.* Blocking autophagy in oligodendrocytes limits functional recovery after spinal cord injury. *Journal of Neuroscience* **38**, 5900–5912 (2018).
124. Guo, L., Lv, J., Huang, Y.-F., Hao, D.-J. & Liu, J.-J. Bioinformatics analyses of differentially expressed genes associated with spinal cord injury: A microarray-based analysis in a mouse model. *Neural Regen Res* **14**, 1262–1270 (2019).
125. Li, Y. *et al.* RNA sequencing screening of differentially expressed genes after spinal cord injury. *Neural Regen Res* **14**, 1583–1593 (2019).
126. Chen, K. *et al.* RNA-seq characterization of spinal cord injury transcriptome in acute/subacute phases: a resource for understanding the pathology at the systems level. *PLoS One* **8**, (2013).
127. Squair, J. W. *et al.* Integrated systems analysis reveals conserved gene networks underlying response to spinal cord injury. *Elife* **7**, (2018).
128. Titlow, J. S. *et al.* Systematic analysis of YFP traps reveals common mRNA/protein discordance in neural tissues. *J Cell Biol* **222**, (2023).
129. Sanz, E., Bean, J. C., Carey, D. P., Quintana, A. & McKnight, G. S. RiboTag: Ribosomal Tagging Strategy to Analyze Cell Type Specific mRNA Expression In Vivo. *Curr Protoc Neurosci* **88**, e77 (2019).
130. Trelford, C. B. & Di Guglielmo, G. M. Molecular mechanisms of mammalian autophagy. *Biochem J* **478**, 3395–3421 (2021).
131. Jiang, P. & Mizushima, N. Autophagy and human diseases. *Cell Res* **24**, 69–79 (2014).
132. Bankston, A. N. *et al.* Autophagy is essential for oligodendrocyte differentiation, survival, and proper myelination. *Glia* **67**, (2019).
133. Quarles, R., Macklin, W. & Morell, P. Myelin formation, Structure and Biochemistry. *Basic neurochemistry: molecular, cellular and medical aspects.* (2006).

134. Bauer, N. G., Richter-Landsberg, C. & Ffrench-Constant, C. Role of the oligodendroglial cytoskeleton in differentiation and myelination. *Glia* **57**, 1691–1705 (2009).
135. Miller, R. H. Control of oligodendrocyte development and myelination in the vertebrate CNS. in *The Biology of Oligodendrocytes* 49–63 (Cambridge University Press, 2010). doi:10.1017/CBO9780511782121.004.
136. Wegner, M. A matter of identity: Transcriptional control in oligodendrocytes. *Journal of Molecular Neuroscience* (2008) doi:10.1007/s12031-007-9008-8.
137. Simons, M. & Lyons, D. A. Axonal selection and myelin sheath generation in the central nervous system. *Curr Opin Cell Biol* **25**, 512–519 (2013).
138. Franklin, R. J. M. & Ffrench-Constant, C. Remyelination in the CNS: from biology to therapy. *Nat Rev Neurosci* **9**, 839–855 (2008).
139. Emery, B. Transcriptional and post-transcriptional control of CNS myelination. *Curr Opin Neurobiol* **20**, 601–607 (2010).
140. Emery, B. Regulation of oligodendrocyte differentiation and myelination. *Science* **330**, 779–782 (2010).
141. Patel, J. R. & Klein, R. S. Mediators of oligodendrocyte differentiation during remyelination. *FEBS Lett* **585**, 3730–3737 (2011).
142. Kawachi, I. & Lassmann, H. Neurodegeneration in multiple sclerosis and neuromyelitis optica. *J Neurol Neurosurg Psychiatry* **88**, 137–145 (2017).
143. Münzel, E. J. & Williams, A. Promoting remyelination in multiple sclerosis-recent advances. *Drugs* **73**, 2017–2029 (2013).
144. Vázquez, P. *et al.* Atg5 and Ambra1 differentially modulate neurogenesis in neural stem cells. *Autophagy* (2012) doi:10.4161/auto.8.2.18535.
145. Wang, S. *et al.* Autophagy-related gene Atg5 is essential for astrocyte differentiation in the developing mouse cortex. *EMBO Rep* (2014) doi:10.15252/embr.201338343.
146. Kundu, Mondira, Thompson, C. B. Autophagy : Basic Principles and Relevance to Disease. *The Annual Review of Pathology: Mechanisms of Disease* (2008) doi:10.1146/annurev.pathol.2.010506.091842.
147. Hale, A. N., Ledbetter, D. J., Gawriluk, T. R. & Rucker, E. B. Autophagy: Regulation and role in development. *Autophagy* **9**, 951–972 (2013).
148. Pankiv, S. *et al.* p62/SQSTM1 binds directly to Atg8/LC3 to facilitate degradation of ubiquitinated protein aggregates by autophagy. *J Biol Chem* **282**, 24131–24145 (2007).
149. Yue, Z., Jin, S., Yang, C., Levine, A. J. & Heintz, N. Beclin 1, an autophagy gene essential for early embryonic development, is a haploinsufficient tumor suppressor. *Proc Natl Acad Sci U S A* **100**, 15077–15082 (2003).
150. Kuma, A. *et al.* The role of autophagy during the early neonatal starvation period. *Nature* (2004) doi:10.1038/nature03029.
151. Mariño, G., Madeo, F. & Kroemer, G. Autophagy for tissue homeostasis and neuroprotection. *Current Opinion in Cell Biology* Preprint at https://doi.org/10.1016/j.ceb.2010.10.001 (2011).

152. Kadandale, P., Stender, J. D., Glass, C. K. & Kiger, A. A. Conserved role for autophagy in Rho1-mediated cortical remodeling and blood cell recruitment. *Proc Natl Acad Sci U S A* **107**, 10502–10507 (2010).
153. Jang, S. Y. *et al.* Autophagy is involved in the reduction of myelinating Schwann cell cytoplasm during myelin maturation of the peripheral nerve. *PLoS One* **10**, (2015).
154. Eppig, J. T. & Shimoyama, M. Gene and protein nomenclature follow the guidelines of Mouse Genomic Informatics. *http://www.informatics.jax.org/mgihome/nomen/gene.shtml* (2015).
155. Smith, C. M., Mayer, J. A. & Duncan, I. D. Autophagy promotes oligodendrocyte survival and function following dysmyelination in a long-lived myelin mutant. *The Journal of Neuroscience* **33**, 8088–8100 (2013).
156. Shoji-Kawata, S. *et al.* Identification of a candidate therapeutic autophagy-inducing peptide. *Nature* **494**, 201–206 (2013).
157. Donohue, E., Balgi, A. D., Komatsu, M. & Roberge, M. Induction of Covalently Crosslinked p62 Oligomers with Reduced Binding to Polyubiquitinated Proteins by the Autophagy Inhibitor Verteporfin. *PLoS One* **9**, (2014).
158. Donohue, E. *et al.* Inhibition of autophagosome formation by the benzoporphyrin derivative verteporfin. *J Biol Chem* **286**, 7290–7300 (2011).
159. National Research Council. Guide for the Care and Use of Laboratory Animals. *Guide for the Care and Use of Laboratory Animals* (2011) doi:10.17226/12910.
160. Dincman, T. A., Beare, J. E., Ohri, S. S. & Whittemore, S. R. Isolation of cortical mouse oligodendrocyte precursor cells. *J Neurosci Methods* **209**, 219–226 (2012).
161. Plant, G. W. *et al.* Purified adult ensheathing glia fail to myelinate axons under culture conditions that enable Schwann cells to form myelin. *J Neurosci* **22**, 6083–6091 (2002).
162. Cao, Q. *et al.* Transplantation of Ciliary Neurotrophic Factor-Expressing Adult Oligodendrocyte Precursor Cells Promotes Remyelination and Functional Recovery after SpinalCord Injury. *Journal of Neuroscience* (2010) doi:10.1523/JNEUROSCI.3174-09.2010.
163. Pearse, D. D. *et al.* cAMP and Schwann cells promote axonal growth and functional recovery after spinal cord injury. *Nat Med* **10**, 610–616 (2004).
164. Cheng, X. *et al.* Bone Morphogenetic Protein Signaling and Olig1/2 Interact to Regulate the Differentiation and Maturation of Adult Oligodendrocyte Precursor Cells. *Stem Cells* (2007) doi:10.1634/stemcells.2007-0284.
165. Hetman, M., Kanning, K., Cavanaugh, J. E. & Xia, Z. Neuroprotection by brain-derived neurotrophic factor is mediated by extracellular signal-regulated kinase and phosphatidylinositol 3-kinase. *J Biol Chem* **274**, 22569–22580 (1999).
166. Kimura, S., Noda, T. & Yoshimori, T. Dissection of the autophagosome maturation process by a novel reporter protein, tandem fluorescent-tagged LC3. *Autophagy* **3**, 452–460 (2007).

167. N'Diaye, E. N. *et al.* PLIC proteins or ubiquilins regulate autophagy-dependent cell survival during nutrient starvation. *EMBO Rep* **10**, 173–179 (2009).
168. Loos, B., Du Toit, A. & Hofmeyr, J. H. S. Defining and measuring autophagosome flux - Concept and reality. *Autophagy* Preprint at https://doi.org/10.4161/15548627.2014.973338 (2014).
169. Farkas, T., Daugaard, M. & Jäättelä, M. Identification of small molecule inhibitors of phosphatidylinositol 3-kinase and autophagy. *J Biol Chem* **286**, 38904–38912 (2011).
170. Trapp, B. D., Nishiyama, A., Cheng, D. & Macklin, W. Differentiation and death of premyelinating oligodendrocytes in developing rodent brain. *Journal of Cell Biology* **137**, 459–468 (1997).
171. Simons, M. & Nave, K. A. Oligodendrocytes: Myelination and Axonal Support. *Cold Spring Harb Perspect Biol* **8**, (2015).
172. Tang, A. H. & Rando, T. A. Induction of autophagy supports the bioenergetic demands of quiescent muscle stem cell activation. *EMBO J* **33**, 2782–2797 (2014).
173. Maday, S., Wallace, K. E. & Holzbaur, E. L. F. Autophagosomes initiate distally and mature during transport toward the cell soma in primary neurons. *Journal of Cell Biology* (2012) doi:10.1083/jcb.201106120.
174. Montagne, A. *et al.* Pericyte degeneration causes white matter dysfunction in the mouse central nervous system. *Nat Med* **24**, 326–337 (2018).
175. Komatsu, M. *et al.* Loss of autophagy in the central nervous system causes neurodegeneration in mice. *Nature* **441**, 880–884 (2006).
176. Lv, X. *et al.* The crucial role of Atg5 in cortical neurogenesis during early brain development. *Sci Rep* **4**, (2014).
177. Ban, B.-K. *et al.* Autophagy negatively regulates early axon growth in cortical neurons. *Mol Cell Biol* **33**, 3907–3919 (2013).
178. Nawaz, S. *et al.* Actin filament turnover drives leading edge growth during myelin sheath formation in the central nervous system. *Dev Cell* **34**, 139–151 (2015).
179. Zuchero, J. B. *et al.* CNS myelin wrapping is driven by actin disassembly. *Dev Cell* **34**, 152–167 (2015).
180. Corcelle, E. *et al.* Control of the autophagy maturation step by the MAPK ERK and p38: Lessons from environmental carcinogens. *Autophagy* Preprint at https://doi.org/10.4161/auto.3424 (2007).
181. Jackman, N., Ishii, A. & Bansal, R. Oligodendrocyte development and myelin biogenesis: parsing out the roles of glycosphingolipids. *Physiology (Bethesda)* **24**, 290–297 (2009).
182. Mao, K., Wang, K., Zhao, M., Xu, T. & Klionsky, D. J. Two MAPK-signaling pathways are required for mitophagy in Saccharomyces cerevisiae. *Journal of Cell Biology* (2011) doi:10.1083/jcb.201102092.
183. Dall'Armi, C., Devereaux, K. A. & Di Paolo, G. The role of lipids in the control of autophagy. *Curr Biol* **23**, (2013).
184. Rubio, N. *et al.* P38MAPK-regulated induction of p62 and NBR1 after photodynamic therapy promotes autophagic clearance of ubiquitin

aggregates and reduces reactive oxygen species levels by supporting Nrf2-antioxidant signaling. *Free Radic Biol Med* (2014) doi:10.1016/j.freeradbiomed.2013.11.010.
185. Haines, J. D., Fulton, D. L., Richard, S. & Almazan, G. P38 mitogen-activated protein kinase pathway regulates genes during proliferation and differentiation in oligodendrocytes. *PLoS One* (2015) doi:10.1371/journal.pone.0145843.
186. Gaesser, J. M. & Fyffe-Maricich, S. L. Intracellular signaling pathway regulation of myelination and remyelination in the CNS. *Experimental Neurology* Preprint at https://doi.org/10.1016/j.expneurol.2016.03.008 (2016).
187. Rangaraju, S. *et al.* Rapamycin activates autophagy and improves myelination in explant cultures from neuropathic mice. *J Neurosci* **30**, 11388–11397 (2010).
188. Laplante, M. *et al.* mTOR signaling in growth control and disease. *Cell* (2012) doi:10.1016/j.cell.2012.03.017.
189. Ahuja, C. S. *et al.* Traumatic spinal cord injury. *Nat Rev Dis Primers* **3**, (2017).
190. Basso, D. M., Beattie, M. S. & Bresnahan, J. C. Graded histological and locomotor outcomes after spinal cord contusion using the NYU weight-drop device versus transection. *Exp Neurol* **139**, 244–256 (1996).
191. Beattie, M. S. *et al.* ProNGF induces p75-mediated death of oligodendrocytes following spinal cord injury. *Neuron* **36**, 375–386 (2002).
192. Dong, H. *et al.* Enhanced oligodendrocyte survival after spinal cord injury in Bax-deficient mice and mice with delayed Wallerian degeneration. *J Neurosci* **23**, 8682–8691 (2003).
193. Terayama, R. *et al.* Neuropsin promotes oligodendrocyte death, demyelination and axonal degeneration after spinal cord injury. *Neuroscience* **148**, 175–187 (2007).
194. Floriddia, E. M. *et al.* Distinct oligodendrocyte populations have spatial preference and different responses to spinal cord injury. *Nat Commun* **11**, (2020).
195. Milich, L. M. *et al.* Single-cell analysis of the cellular heterogeneity and interactions in the injured mouse spinal cord. *J Exp Med* **218**, (2021).
196. Potter, S. S. Single-cell RNA sequencing for the study of development, physiology and disease. *Nat Rev Nephrol* **14**, 479–492 (2018).
197. Young, M. D. & Behjati, S. SoupX removes ambient RNA contamination from droplet-based single-cell RNA sequencing data. *Gigascience* **9**, (2020).
198. Kapur, M., Monaghan, C. E. & Ackerman, S. L. Regulation of mRNA Translation in Neurons-A Matter of Life and Death. *Neuron* **96**, 616–637 (2017).
199. Elbaz, B. & Popko, B. Molecular Control of Oligodendrocyte Development. *Trends Neurosci* **42**, 263–277 (2019).
200. Kats, I. R. & Klann, E. Translating from cancer to the brain: regulation of protein synthesis by eIF4F. *Learn Mem* **26**, 332–342 (2019).

201. Heiman, M. *et al.* A translational profiling approach for the molecular characterization of CNS cell types. *Cell* **135**, 738–748 (2008).
202. Sanz, E. *et al.* Cell-type-specific isolation of ribosome-associated mRNA from complex tissues. *Proc Natl Acad Sci U S A* **106**, 13939–13944 (2009).
203. Anderson, M. A. *et al.* Astrocyte scar formation aids central nervous system axon regeneration. *Nature* **532**, 195–200 (2016).
204. Zhu, Y. *et al.* Macrophage transcriptional profile identifies lipid catabolic pathways that can be therapeutically targeted after spinal cord injury. *Journal of Neuroscience* **37**, 2362–2376 (2017).
205. Doerflinger, N. H., Macklin, W. B. & Popko, B. Inducible site-specific recombination in myelinating cells. *Genesis* **35**, 63–72 (2003).
206. Raudvere, U. *et al.* g:Profiler: a web server for functional enrichment analysis and conversions of gene lists (2019 update). *Nucleic Acids Res* **47**, W191–W198 (2019).
207. Karp, P. D. *et al.* Pathway Tools version 23.0 update: software for pathway/genome informatics and systems biology. *Brief Bioinform* **22**, 109–126 (2021).
208. Zhang, Y. *et al.* An RNA-Sequencing Transcriptome and Splicing Database of Glia, Neurons, and Vascular Cells of the Cerebral Cortex. *Journal of Neuroscience* **34**, 11929–11947 (2014).
209. Milich, L. M., Ryan, C. B. & Lee, J. K. The origin, fate, and contribution of macrophages to spinal cord injury pathology. *Acta Neuropathol* **137**, (2019).
210. Dawson, M. R. L., Polito, A., Levine, J. M. & Reynolds, R. NG2-expressing glial progenitor cells: An abundant and widespread population of cycling cells in the adult rat CNS. *Molecular and Cellular Neuroscience* **24**, 476–488 (2003).
211. Valério-Gomes, B., Guimarães, D. M., Szczupak, D. & Lent, R. The Absolute Number of Oligodendrocytes in the Adult Mouse Brain. *Front Neuroanat* **12**, (2018).
212. David, S. & Kroner, A. Repertoire of microglial and macrophage responses after spinal cord injury. *Nat Rev Neurosci* **12**, 388–399 (2011).
213. Gregory, J. A. *et al.* Cell Type-Specific In Vitro Gene Expression Profiling of Stem Cell-Derived Neural Models. *Cells* **9**, (2020).
214. Miron, V. E. *et al.* Statin therapy inhibits remyelination in the central nervous system. *Am J Pathol* **174**, 1880–1890 (2009).
215. Vemuri, G. S. & McMorris, F. A. Oligodendrocytes and their precursors require phosphatidylinositol 3-kinase signaling for survival. *Development* **122**, 2529–2537 (1996).
216. Flores, A. I. *et al.* Akt-mediated survival of oligodendrocytes induced by neuregulins. *J Neurosci* **20**, 7622–7630 (2000).
217. Lee, J. Y., Oh, T. H. & Yune, T. Y. Ghrelin inhibits hydrogen peroxide-induced apoptotic cell death of oligodendrocytes via ERK and p38MAPK signaling. *Endocrinology* **152**, 2377–2386 (2011).

218. Wiegert, J. S. & Bading, H. Activity-dependent calcium signaling and ERK-MAP kinases in neurons: a link to structural plasticity of the nucleus and gene transcription regulation. *Cell Calcium* **49**, 296–305 (2011).
219. McKay, M. M. & Morrison, D. K. Integrating signals from RTKs to ERK/MAPK. *Oncogene* **26**, 3113–3121 (2007).
220. Rumbaugh, G., Adams, J. P., Kim, J. H. & Huganir, R. L. SynGAP regulates synaptic strength and mitogen-activated protein kinases in cultured neurons. *Proc Natl Acad Sci U S A* **103**, 4344–4351 (2006).
221. Cabrita, M. A. & Christofori, G. Sprouty proteins, masterminds of receptor tyrosine kinase signaling. *Angiogenesis* **11**, 53–62 (2008).
222. Li, P. L. *et al.* STEAP3 (Six-Transmembrane Epithelial Antigen of Prostate 3) Inhibits Pathological Cardiac Hypertrophy. *Hypertension* **76**, 1219–1230 (2020).
223. Choi, Y. S. *et al.* Status epilepticus-induced somatostatinergic hilar interneuron degeneration is regulated by striatal enriched protein tyrosine phosphatase. *J Neurosci* **27**, 2999–3009 (2007).
224. Hemmings, B. A. & Restuccia, D. F. PI3K-PKB/Akt pathway. *Cold Spring Harb Perspect Biol* **4**, (2012).
225. Pegoraro, C. *et al.* PFKFB4 controls embryonic patterning via Akt signalling independently of glycolysis. *Nat Commun* **6**, (2015).
226. Sivanand, S. & Vander Heiden, M. G. Emerging Roles for Branched-Chain Amino Acid Metabolism in Cancer. *Cancer Cell* **37**, 147–156 (2020).
227. Mongroo, P. S. *et al.* Beta-parvin inhibits integrin-linked kinase signaling and is downregulated in breast cancer. *Oncogene* **23**, 8959–8970 (2004).
228. Ivetac, I. *et al.* Regulation of PI(3)K/Akt signalling and cellular transformation by inositol polyphosphate 4-phosphatase-1. *EMBO Rep* **10**, 487–493 (2009).
229. Bastid, J., Dejou, C., Docquier, A. & Bonnefoy, N. The Emerging Role of the IL-17B/IL-17RB Pathway in Cancer. *Front Immunol* **11**, (2020).
230. Neinast, M., Murashige, D. & Arany, Z. Branched Chain Amino Acids. *Annu Rev Physiol* **81**, 139–164 (2019).
231. Chu, C. T., Levinthal, D. J., Kulich, S. M., Chalovich, E. M. & DeFranco, D. B. Oxidative neuronal injury. The dark side of ERK1/2. *Eur J Biochem* **271**, 2060–2066 (2004).
232. Yagami, T., Yamamoto, Y. & Koma, H. The role of secretory phospholipase A_2 in the central nervous system and neurological diseases. *Mol Neurobiol* **49**, 863–876 (2014).
233. Banfi, C. *et al.* Prenylcysteine oxidase 1, an emerging player in atherosclerosis. *Commun Biol* **4**, (2021).
234. Niederkorn, M., Agarwal, P. & Starczynowski, D. T. TIFA and TIFAB: FHA-domain proteins involved in inflammation, hematopoiesis, and disease. *Exp Hematol* **90**, 18–29 (2020).
235. Kravchick, D. O. *et al.* Synaptonuclear messenger PRR7 inhibits c-Jun ubiquitination and regulates NMDA-mediated excitotoxicity. *EMBO J* **35**, 1923–1934 (2016).

236. Guo, W. Z. *et al.* Six-Transmembrane Epithelial Antigen of the Prostate 3 Deficiency in Hepatocytes Protects the Liver Against Ischemia-Reperfusion Injury by Suppressing Transforming Growth Factor-β-Activated Kinase 1. *Hepatology* **71**, 1037–1054 (2020).
237. Senkal, C. E. *et al.* Ceramide Is Metabolized to Acylceramide and Stored in Lipid Droplets. *Cell Metab* **25**, 686–697 (2017).
238. Ueda, N. A Rheostat of Ceramide and Sphingosine-1-Phosphate as a Determinant of Oxidative Stress-Mediated Kidney Injury. *Int J Mol Sci* **23**, (2022).
239. Yamakaze, J. & Lu, Z. Deletion of the lactoperoxidase gene causes multisystem inflammation and tumors in mice. *Sci Rep* **11**, (2021).
240. Elliott, D. A., Weickert, C. S. & Garner, B. Apolipoproteins in the brain: implications for neurological and psychiatric disorders. *Clin Lipidol* **51**, 555–573 (2010).
241. Wang, K. *et al.* Branched-chain amino acid aminotransferase 2 regulates ferroptotic cell death in cancer cells. *Cell Death Differ* **28**, 1222–1236 (2021).
242. Coutelier, M. *et al.* Alteration of ornithine metabolism leads to dominant and recessive hereditary spastic paraplegia. *Brain* **138**, 2191–2205 (2015).
243. Hollinshead, K. E. R. *et al.* Oncogenic IDH1 Mutations Promote Enhanced Proline Synthesis through PYCR1 to Support the Maintenance of Mitochondrial Redox Homeostasis. *Cell Rep* **22**, 3107–3114 (2018).
244. Yi, M. *et al.* 6-Phosphofructo-2-kinase/fructose-2,6-biphosphatase 3 and 4: A pair of valves for fine-tuning of glucose metabolism in human cancer. *Mol Metab* **20**, 1–13 (2019).
245. Daruich, A. *et al.* Iron is neurotoxic in retinal detachment and transferrin confers neuroprotection. *Sci Adv* **5**, (2019).
246. Ohgami, R. S. *et al.* Identification of a ferrireductase required for efficient transferrin-dependent iron uptake in erythroid cells. *Nat Genet* **37**, 1264–1269 (2005).
247. Lambe, T. *et al.* Identification of a Steap3 endosomal targeting motif essential for normal iron metabolism. *Blood* **113**, 1805–1808 (2009).
248. Ratan, R. R. The Chemical Biology of Ferroptosis in the Central Nervous System. *Cell Chem Biol* **27**, 479–498 (2020).
249. Yin, K. J. *et al.* JNK activation contributes to DP5 induction and apoptosis following traumatic spinal cord injury. *Neurobiol Dis* **20**, 881–889 (2005).
250. Kaspric, N., Picard, B., Reichstadt, M., Tournayre, J. & Bonnet, M. ProteINSIDE to Easily Investigate Proteomics Data from Ruminants: Application to Mine Proteome of Adipose and Muscle Tissues in Bovine Foetuses. *PLoS One* **10**, (2015).
251. Radulovic, M. *et al.* Kallikrein cascades in traumatic spinal cord injury: in vitro evidence for roles in axonopathy and neuron degeneration. *J Neuropathol Exp Neurol* **72**, 1072–1089 (2013).
252. Bando, Y. *et al.* Kallikrein 6 secreted by oligodendrocytes regulates the progression of experimental autoimmune encephalomyelitis. *Glia* **66**, 359–378 (2018).

253. Clarke, D. J. B. *et al.* eXpression2Kinases (X2K) Web: linking expression signatures to upstream cell signaling networks. *Nucleic Acids Res* **46**, W171–W179 (2018).
254. Loh, C. H. & Veenstra, G. J. C. The Role of Polycomb Proteins in Cell Lineage Commitment and Embryonic Development. *Epigenomes* **6**, (2022).
255. He, D. *et al.* lncRNA Functional Networks in Oligodendrocytes Reveal Stage-Specific Myelination Control by an lncOL1/Suz12 Complex in the CNS. *Neuron* **93**, 362–378 (2017).
256. Barrios, Á. P. *et al.* Differential properties of transcriptional complexes formed by the CoREST family. *Mol Cell Biol* **34**, 2760–2770 (2014).
257. Upadhyay, G., Chowdhury, A. H., Vaidyanathan, B., Kim, D. & Saleque, S. Antagonistic actions of Rcor proteins regulate LSD1 activity and cellular differentiation. *Proc Natl Acad Sci U S A* **111**, 8071–8076 (2014).
258. Kleven, M. D., Dlakić, M. & Lawrence, C. M. Characterization of a single b-type heme, FAD, and metal binding sites in the transmembrane domain of six-transmembrane epithelial antigen of the prostate (STEAP) family proteins. *J Biol Chem* **290**, 22558–22569 (2015).
259. Zhang, F. *et al.* Metalloreductase Steap3 coordinates the regulation of iron homeostasis and inflammatory responses. *Haematologica* **97**, 1826–1835 (2012).
260. Howie, H. L. *et al.* Differences in Steap3 expression are a mechanism of genetic variation of RBC storage and oxidative damage in mice. *Blood Adv* **3**, 2272–2285 (2019).
261. Passer, B. J. *et al.* The p53-inducible TSAP6 gene product regulates apoptosis and the cell cycle and interacts with Nix and the Myt1 kinase. *Proc Natl Acad Sci U S A* **100**, 2284–2289 (2003).
262. Amzallag, N. *et al.* TSAP6 facilitates the secretion of translationally controlled tumor protein/histamine-releasing factor via a nonclassical pathway. *J Biol Chem* **279**, 46104–46112 (2004).
263. Lespagnol, A. *et al.* Exosome secretion, including the DNA damage-induced p53-dependent secretory pathway, is severely compromised in TSAP6/Steap3-null mice. *Cell Death Differ* **15**, 1723–1733 (2008).
264. Tschantz, W. R., Digits, J. A., Pyun, H. J., Coates, R. M. & Casey, P. J. Lysosomal prenylcysteine lyase is a FAD-dependent thioether oxidase. *J Biol Chem* **276**, 2321–2324 (2001).
265. Lu, J. Y. & Hofmann, S. L. Thematic review series: lipid posttranslational modifications. Lysosomal metabolism of lipid-modified proteins. *J Lipid Res* **47**, 1352–1357 (2006).
266. Demine, S., Renard, P. & Arnould, T. Mitochondrial Uncoupling: A Key Controller of Biological Processes in Physiology and Diseases. *Cells* **8**, (2019).
267. Horowitz, M. P. & Greenamyre, J. T. Mitochondrial iron metabolism and its role in neurodegeneration. *J Alzheimers Dis* **20 Suppl 2**, (2010).
268. Pandey, S. *et al.* Disease-associated oligodendrocyte responses across neurodegenerative diseases. *Cell Rep* **40**, (2022).

269. Weiss, T. *et al.* Schwann cell plasticity regulates neuroblastic tumor cell differentiation via epidermal growth factor-like protein 8. *Nat Commun* **12**, (2021).
270. Meyer, N. & Rinholm, J. E. Mitochondria in Myelinating Oligodendrocytes: Slow and Out of Breath? *Metabolites* **11**, (2021).
271. Hill, C. E. A view from the ending: Axonal dieback and regeneration following SCI. *Neurosci Lett* **652**, 11–24 (2017).
272. Lasiene, J., Shupe, L., Perlmutter, S. & Horner, P. No evidence for chronic demyelination in spared axons after spinal cord injury in a mouse. *J Neurosci* **28**, 3887–3896 (2008).
273. Colognato, H. & Tzvetanova, I. D. Glia unglued: how signals from the extracellular matrix regulate the development of myelinating glia. *Dev Neurobiol* **71**, 924–955 (2011).
274. Doria, A., Gatto, M. & Punzi, L. Autophagy in human health and disease. *New England Journal of Medicine* vol. 368 1845–1846 Preprint at https://doi.org/10.1056/NEJMc1303158 (2013).
275. Lin, M., Yu, H., Xie, Q., Xu, Z. & Shang, P. Role of microglia autophagy and mitophagy in age-related neurodegenerative diseases. *Front Aging Neurosci* **14**, (2023).
276. Plaza-Zabala, A., Sierra-Torre, V. & Sierra, A. Autophagy and Microglia: Novel Partners in Neurodegeneration and Aging. *Int J Mol Sci* **18**, (2017).
277. Brady, S. T. *et al.* Formation of compact myelin is required for maturation of the axonal cytoskeleton. *J Neurosci* **19**, 7278–7288 (1999).
278. Readhead, C. & Hood, L. The dysmyelinating mouse mutations shiverer (shi) and myelin deficient (shimld). *Behav Genet* **20**, 213–234 (1990).
279. Mikoshiba, K. *et al.* Oligodendrocyte abnormalities in shiverer mouse mutant are determined in primary chimaeras. *Nature* **299**, 357–359 (1982).
280. Wolf, M. K. & Billings-Gagliardi, S. CNS hypomyelinated mutant mice (jimpy, shiverer, quaking): in vitro evidence for primary oligodendrocyte defects. *Adv Exp Med Biol* **181**, 115–133 (1984).
281. Rivers, L. E. *et al.* PDGFRA/NG2 glia generate myelinating oligodendrocytes and piriform projection neurons in adult mice. *Nat Neurosci* **11**, 1392–1401 (2008).
282. Baumann, N. & Pham-Dinh, D. Biology of oligodendrocyte and myelin in the mammalian central nervous system. *Physiol Rev* **81**, 871–927 (2001).
283. Stone, S., Wu, S., Nave, K. A. & Lin, W. The UPR preserves mature oligodendrocyte viability and function in adults by regulating autophagy of PLP. *JCI Insight* **5**, (2020).
284. Cristobal, C. D. & Lee, H. K. Development of myelinating glia: An overview. *Glia* **70**, 2237 (2022).
285. Barateiro, A., Brites, D. & Fernandes, A. Oligodendrocyte Development and Myelination in Neurodevelopment: Molecular Mechanisms in Health and Disease. *Curr Pharm Des* **22**, 656–679 (2016).
286. Snaidero, N. & Simons, M. The logistics of myelin biogenesis in the central nervous system. *Glia* **65**, 1021–1031 (2017).

287. Marques, S. *et al.* Oligodendrocyte heterogeneity in the mouse juvenile and adult central nervous system. *Science* **352**, 1326–1329 (2016).
288. Wang, Z.-Y., Lin, J.-H., Muharram, A. & Liu, W.-G. Beclin-1-mediated autophagy protects spinal cord neurons against mechanical injury-induced apoptosis. *Apoptosis* **19**, 933–945 (2014).
289. Pooyan, P. *et al.* The Dynamic Proteome of Oligodendrocyte Lineage Differentiation Features Planar Cell Polarity and Macroautophagy Pathways. *Gigascience* **9**, 1–23 (2020).
290. Aber, E. R. *et al.* Oligodendroglial macroautophagy is essential for myelin sheath turnover to prevent neurodegeneration and death. *Cell Rep* **41**, (2022).
291. Zhang, T. *et al.* Autophagy collaborates with apoptosis pathways to control myelination specificity and function. *bioRxiv* (2023) doi:10.1101/2022.12.31.522394.
292. Sparrow, N. *et al.* The actin-severing protein cofilin is downstream of neuregulin signaling and is essential for Schwann cell myelination. *J Neurosci* **32**, 5284–5297 (2012).
293. O'Meara, R. W. *et al.* Integrin-linked kinase regulates process extension in oligodendrocytes via control of actin cytoskeletal dynamics. *J Neurosci* **33**, 9781–9793 (2013).
294. Montani, L. *et al.* Profilin 1 is required for peripheral nervous system myelination. *Development* **141**, 1553–1561 (2014).
295. Larson, T. A., Gordon, T. N., Lau, H. E. & Parichy, D. M. Defective adult oligodendrocyte and Schwann cell development, pigment pattern, and craniofacial morphology in puma mutant zebrafish having an alpha tubulin mutation. *Dev Biol* **346**, 296–309 (2010).
296. Lehotzky, A. *et al.* Tubulin polymerization-promoting protein (TPPP/p25) is critical for oligodendrocyte differentiation. *Glia* **58**, 157–168 (2010).
297. Staugaitis, S. M., Smith, P. R. & Colman, D. R. Expression of myelin basic protein isoforms in nonglial cells. *J Cell Biol* **110**, 1719–1727 (1990).
298. Müller, C., Bauer, N. M., Schäfer, I. & White, R. Making myelin basic protein -from mRNA transport to localized translation. *Front Cell Neurosci* **7**, (2013).
299. Torvund-Jensen, J., Steengaard, J., Reimer, L., Fihl, L. B. & Laursen, L. S. Transport and translation of MBP mRNA is regulated differently by distinct hnRNP proteins. *J Cell Sci* **127**, 1550–1564 (2014).
300. Hoch-Kraft, P., Trotter, J. & Gonsior, C. Missing in Action: Dysfunctional RNA Metabolism in Oligodendroglial Cells as a Contributor to Neurodegenerative Diseases? *Neurochem Res* **45**, 566–579 (2020).
301. Iwai-Kanai, E. *et al.* A method to measure cardiac autophagic flux in vivo. *Autophagy* **4**, 322–9 (2008).
302. Walker, S. A., Karanasios, E. & Ktistakis, N. T. Correlative Live Cell and Super Resolution Imaging of Autophagosome Formation. *Methods Enzymol* **587**, 1–20 (2017).
303. Cerrato, G., Sauvat, A., Kepp, O. & Kroemer, G. Live cell imaging of LC3 dynamics. *Methods Cell Biol* **164**, 27–38 (2021).

304. Tyler, W. A. *et al.* Activation of the mammalian target of rapamycin (mTOR) is essential for oligodendrocyte differentiation. *J Neurosci* **29**, 6367–6378 (2009).
305. Wood, T. L. *et al.* mTOR: a link from the extracellular milieu to transcriptional regulation of oligodendrocyte development. *ASN Neuro* **5**, 63–79 (2013).
306. Figlia, G., Gerber, D. & Suter, U. Myelination and mTOR. *Glia* **66**, 693–707 (2018).
307. Musah, A. S. *et al.* Mechanistic Target of Rapamycin Regulates the Oligodendrocyte Cytoskeleton during Myelination. *J Neurosci* **40**, 2993–3007 (2020).
308. Jeffries, M. A. *et al.* mTOR Signaling Regulates Metabolic Function in Oligodendrocyte Precursor Cells and Promotes Efficient Brain Remyelination in the Cuprizone Model. *J Neurosci* **41**, 8321–8337 (2021).
309. Khandker, L. *et al.* Cholesterol biosynthesis defines oligodendrocyte precursor heterogeneity between brain and spinal cord. *Cell Rep* **38**, (2022).
310. Rinholm, J. E. *et al.* Movement and structure of mitochondria in oligodendrocytes and their myelin sheaths. *Glia* **64**, 810–825 (2016).
311. Duncan, G. J. *et al.* Myelin regulatory factor drives remyelination in multiple sclerosis. *Acta Neuropathol* **134**, 403–422 (2017).
312. Pukos, N. *et al.* Chronic demyelination and myelin repair after spinal cord injury in mice: A potential link for glutamatergic axon activity. *Glia* **71**, (2023).
313. Petenkova, A. *et al.* Prenylcysteine oxidase 1 like protein is required for neutrophil bactericidal activities. *Nat Commun* **14**, 2761 (2023).
314. Zhang, F. L. & Casey, P. J. Protein prenylation: molecular mechanisms and functional consequences. *Annu Rev Biochem* **65**, 241–269 (1996).
315. Mathews, E. S. *et al.* Mutation of 3-Hydroxy-3-Methylglutaryl CoA Synthase I Reveals Requirements for Isoprenoid and Cholesterol Synthesis in Oligodendrocyte Migration Arrest, Axon Wrapping, and Myelin Gene Expression. *The Journal of Neuroscience* **34**, 3402 (2014).
316. De Angelis, D. A. & Braun, P. E. Isoprenylation of brain 2',3'-cyclic nucleotide 3'-phosphodiesterase modulates cell morphology. *J Neurosci Res* **39**, 386–397 (1994).
317. Ohgami, R. S., Campagna, D. R., McDonald, A. & Fleming, M. D. The Steap proteins are metalloreductases. *Blood* **108**, 1388–1394 (2006).
318. Smirnova, E. V. *et al.* Identification of Myelin Basic Protein Proximity Interactome Using TurboID Labeling Proteomics. *Cells* **12**, (2023).
319. Shahbabian, K. & Chartrand, P. Control of cytoplasmic mRNA localization. *Cell Mol Life Sci* **69**, 535–552 (2012).
320. Colman, D. R., Kreibich, G., Frey, A. B. & Sabatini, D. D. Synthesis and incorporation of myelin polypeptides into CNS myelin. *J Cell Biol* **95**, 598–608 (1982).
321. Thakurela, S. *et al.* The transcriptome of mouse central nervous system myelin. *Sci Rep* **6**, (2016).

322. Yergert, K. M., Doll, C. A., O'Rouke, R., Hines, J. H. & Appel, B. Identification of 3' UTR motifs required for mRNA localization to myelin sheaths in vivo. *PLoS Biol* **19**, (2021).
323. De Vries, H., Schrage, G. & Hoekstra, D. An apical-type trafficking pathway is present in cultured oligodendrocytes but the sphingolipid-enriched myelin membrane is the target of a basolateral-type pathway. *Mol Biol Cell* **9**, 599–609 (1998).
324. Veltri, A. J. *et al.* Distinct elongation stalls during translation are linked with distinct pathways for mRNA degradation. *Elife* **11**, (2022).
325. Chandrasekaran, V. *et al.* Mechanism of ribosome stalling during translation of a poly(A) tail. *Nature Structural & Molecular Biology 2019 26:12* **26**, 1132–1140 (2019).
326. Haimon, Z. *et al.* Re-evaluating microglia expression profiles using RiboTag and cell isolation strategies /631/1647/2017 /631/1647/2017/2079 technical-report. *Nat Immunol* **19**, 636–644 (2018).
327. Itoh, N. *et al.* Cell-specific and region-specific transcriptomics in the multiple sclerosis model: Focus on astrocytes. *Proc Natl Acad Sci U S A* **115**, E302–E309 (2018).
328. Tassoni, A. *et al.* The astrocyte transcriptome in EAE optic neuritis shows complement activation and reveals a sex difference in astrocytic C3 expression. *Sci Rep* **9**, (2019).
329. Voskuhl, R. R. *et al.* Gene expression in oligodendrocytes during remyelination reveals cholesterol homeostasis as a therapeutic target in multiple sclerosis. *Proc Natl Acad Sci U S A* **116**, 10130–10139 (2019).

ABBREVIATIONS

ABBREVIATION	
AD	Alzheimer's disease
Aif1/Iba1	Allograft inflammatory factor 1
ALDH1L1	Aldehyde dehydrogenase 1 family member L1
AMPK	5' AMP-activated protein kinase
APC	Adenomatous Polyposis Coli
ATF4	Activating transcription factor 4
ATG12	Autophagy related 12
ATG16L	Autophagy related 16 like 1
Atg5	Autophagy related 5
Atg7	Autophagy related 7
ATG8	Autophagy related 8
ATP	Adenosine triphosphate
Bax	Bcl2 associated X, apoptosis regulator
BP	Biological process
BSA	Bovine serum albumin
CC	Corpus callosum
CC	Cellular component
CC1	Adenomatous polyposis coli clone CC1

CC3	Cleaved-caspase 3
CD68	Cluster of differentiation 68
CDNA	Complementary deoxyriboneucleic acid
CGE	Caudal ganglionic eminence
CHOP	C/EBP (CCAAT enhancer binding protein) homologous protein
CNP	2',3'-cyclic nucleotide 3' phosphodiesterase
CNS	Central nervous system
CNTF	Ciliary neurotrophic factor
Cx3cr1	C-X3-C motif chemokine receptor 1
DMSO	Dimethylsulfoxide
Dn	Dominant-negative
DPBS	Dulbecco's phosphate buffer saline
Dpi	Days post-injury
DRG	Dorsal root ganglion (neurons)
E##.#	Embryonic day ##.#
EGFP	Enhanced green fluorescent protein
EIF2alpha	Eukaryotic translation initiation factor 2 subunit 1 (alpha)
ER	Endoplasmic reticulum
ERMN	Ermin
ERSR	endoplasmic reticulum stress response
ERT2	Estrogen receptor with mutated ligand binding domain for tamoxifen
EV	Empty vector
FA2H	Fatty acid 2-hydroxylase

FC	Fold change
FCCP	Carbonyl cyanide 4-(trifluoromethoxy)phenylhydrazone
FGF-2	Fibroblast growth factor
Flp	Flippase
GAPDH	Glyceraldehyde-3-phosphate dehydrogenase
GAPR-1	Google-Associated plant Pathogenesis Related protein 1
GEO	Gene expression omnibus
GFAP	Glial fibrillary acidic protein
GJB1	Gap junction protein beta 1
GJC2	Gap junction protein gamma 2
GO	Gene ontology
HA	Hemagglutinin
HBSS	Hanks buffered saline solution
HD	Huntington's disease
HGF	Hepatocyte growth factor
HIV-1	Human immunodeficiency virus 1
HPRT	Hypoxanthine phosphoribosyltransferase 1
HSR	Heat shock response
I.p.	Intraperitoneal
IACUC	Insititutional animal care and use
IBC	Institutional bio safety committee
ICC	Immunocytochemistry
IgG	Immunoglobulin G

IgM	Immunoglobulin M
IH	Infinite horizons
IHC	Immunohistochemistry
IL-1beta	Interleukin 1 beta
ISR	Integrated stress response
Itgam/Cd11b	Integrin subunit alpha M
Kdyn	Kilodyne
KLK6	Kallikrein related peptidase 6
Klk8	Kallikrein related peptidase 8
LC3B	Light chain 3 beta
Les	Long-Evans shaker
LGE	Lateral ganglionic eminence
LHX5	LIM homeobox 5
Log2FC	Log base 2 fold change
MAG	Myelin associated glycoprotein
MBP	Myelin basic protein
MF	Molecular function
MGE	Medial ganglionic eminence
MOG	Myelin oligodendrocyte glycoprotein
MRNA	Messenger ribonucleic acid
MS	Multiple sclerosis
MSA	Multiple systems atrophy
MTOR	Mammalian target of rapamycin

MTT	3-[4,5-dimethylthiazole-2-yl]-2-5-diphenyltetrazolium bromide
NDS	Normal donkey serum
NF-M	Neurofilament protein M
NG2	Neural/glial antigen 2
O1	O antigen 1
O4	O antigen 4
OL	Oligodendroglia or oligodendrocyte
Olig2	Oligodendrocyte transcription factor 2
Opalin	Oligodendrocytic myelin para nodal and inner loop protein
OPC	Oligodendrocyte progenitor cell
OSM	Oncostatin M
OsO4	Osmium tetraoxide
OXPHOS	Oxidative phosphorylation
P#	Postnatal day #
P62	Squestosome 1, protein 62 kDa
P75/NGFR	Nerve growth factor receptor
PBS	Phosphate buffer saline
PCA	Principal component analysis
PCYOX1L	Prenylcysteine oxidase 1 like
PD	Parkinson's disease
PDGF	Platelet derived growth factor receptor alpha
PDGFRalpha	Platelet derived growth factor receptor alpha
PDL	Poly-D-lysine

PEIF2alpha	Phosphorylated eukaryotic translation initiation factor 2 alpha
PFA	Paraformaldehyde
PI3K	Phosphor osito de 3-kinase
PLP1	Proteolipid protein 1
PMD	Pelizeus-Merzbacher Disease
pMN	Progenitor motor neuron
PNF-H	Phosphorylated neurofilament heavy subunit
PNS	peripheral nervous system
PPIA	Peptidylprolyl isomerase A
QPCR	Quantitative polymerase chain reaction
RELN	Reelin
RLE	Relative Log Expression
RNA	Ribonucleic acid
RNASeq	RNA sequencing
ROPC	Rat Oligodendrocyte progenitor cell
ROS	Reactive oxygen species
RPL22	Ribosomal protein L22
RRNA	Ribosomal RNA
RTTA	Reverse tetracycline-controlled transactivator
Sc(RNAseq)	Single cell RNA sequencing
SCI	Spinal cord injury
SNAP25	Synaptosome associated protein 25
SOX10	SRY-box transcription factor 10

STEAP3 / TSAP6	Six transmembrane epithelial antigen of the prostate 3 / Tumor suppressor-activated pathway protein 6
T3	Triiodothyronine
T9	Thoracic spinal segment 9
TEM	Transmission electron microscopy
TF	Transcription factor
TMEM19	Transmembrane protein 19
TNFalpha	Tumor necrosis factor alpha
TRAP	Translating ribosome affinity purification
TRE	Tet-responsive element
UPR	Unfold protein response
UPS	Ubiquitin-proteasome system
VPS34	Vacuolar protein-sorting 34
WT	Wildtype

CURRICULUM VITA

Michael David Forston
1724 Edenside Ave, Apt 1, Louisville, KY 40204 (812) 431-2532
mdfors01@louisville.edu

EDUCATION

University of Louisville, Louisville, KY May 2023
Ph.D. in Anatomical Sciences and Neurobiology
Mentors: Dr. Scott R. Whittemore & Dr. Michal Hetman
Dissertation: *Novel insights into oligodendrocyte biology from developmental myelination studies in autophagy deficient mice and analysis of the oligodendrocyte translatome response to contusive spinal cord injury*

University of Louisville, Louisville, KY December 2019
M.S. in Anatomical Sciences and Neurobiology
Mentor: Dr. Scott R. Whittemore
Thesis: *Oligodendrocyte proteostasis during development and disease*

Concordia College, Morehead, MN May 2014
B.A. in Biology

HONORS AND AWARDS

Keynote Selection Committee 2019, 2022
27th Annual Kentucky Spinal Cord and Head Injury Research Trust Symposium, Louisville, KY — Chair

25th Annual Kentucky Spinal Cord and Head Injury Research Trust Symposium, Louisville KY — Member

1st Place Excellence in Neuroscience Research April 2022
Neuroscience Day, University of Louisville

3rd Place Excellence in Neuroscience Research April 2018
Neuroscience Day, University of Louisville

PUBLICATIONS

Bankston AN*, **Forston MD***, Howard RM, Andres KR, Smith AE, Ohri SS, Bates ML, Bunge MB, Whittemore SR. 2019*. Autophagy is essential for oligodendrocyte differentiation, survival, and proper myelination*. Glia 67.
*co-first authors

Forston MD*, Wei G*, Chariker JH, Stephenson T, Andres K, Glover C, Rouchka EC, Whittemore SR, Hetman M. 2023. *Enhanced oxidative phosphorylation, re-organization of intracellular signaling, and epigenetic de-silencing as revealed by oligodendrocyte translatome analysis after contusive spinal cord injury*.
(to be submitted)
*co-first authors

Whittemore SR, Saraswat Ohri S, **Forston MD**, Wei GZ, Hetman M. 2022. *The Proteostasis Network: A Global Therapeutic Target for Neuroprotection after Spinal Cord Injury*. Cells 11.

Saraswat Ohri S, Andres KR, Howard RM, Brown BL, **Forston MD**, Hetman M, Whittemore SR. 2023. *Acute Pharmacological Inhibition of Protein Kinase R-Like Endoplasmic Reticulum Kinase Signaling after Spinal Cord Injury Spares Oligodendrocytes and Improves Locomotor Recovery.* J Neurotrauma.

Gao Y, Wei G, **Forston MD**, Hodges ER, Burke D, Andres K, Morehouse J, Armstrong C, Glover C, Slomnicki LP, Ding J, Chariker JH, Rouchka EC, Ohri SS, Whittemore SR, Hetman M. 2023. *Opposite modulation of functional recovery following contusive spinal cord injury in mice with oligodendrocyte-selective deletions in Atf4 and Chop/Ddit3.* Scientific Reports.

RESEARCH EXPERIENCE

Animal models: mouse (neonatal, adult), rat (neonatal)

Surgical technique: Spinal cord injury (IH impactor); pre- and post-operative animal care; CNS cell isolation from brain tissue.

Histology: transcardial perfusions; brain and spinal cord dissection (fresh and fixed tissues); tissue preparation for electron microscopy, tissue sectioning with cryostat and microtome; immunofluorescence, immunohistochemistry, immunocytochemistry.

Microscopy: inverted (Nikon); confocal (Nikon), live imaging (Zeiss)

Molecular biology: DNA, RNA, and protein isolation; PCR; qPCR; RNA sequencing sample preparation; plasmid cloning; immunoprecipitation; lentiviral and retroviral viral vector construction; transfections and viral titering; *in vitro*

pharmacological treatments; cell death and cell viability assays; immunocytochemistry; primary CNS mono and co-cultures.

Computer software: image analysis (Nikon Elements, ImageJ); Adobe Suite; Microsoft Office Suite; statistical analyses (SPSS, SigmaPlot, GraphPad); R; RNAseq bioinformatics analysis; Gene Ontology programs (gProfiler, Metascape, PantherDB).

SCIENTIFIC WRITING

Manuscript reviews: significantly contributed to peer review process for GLIA and Journal of Neurotrauma

Research protocols: wrote protocols for IACUC approval.

Grant preparation and review: participated in trainee and faculty specific aims review and summary statement evaluations.

ABSTRACTS

Forston MD, Wei GZ, Stephenson TL, Andres KR, Howard RM, Chariker JH, Rouhcka EC, Whittemore SR, Hetman M. (2023). *Enhanced oxidative phosphorylation, re-organization of intracellular signaling, and epigenetic de-silencing as revealed by oligodendrocyte translatome analysis after spinal cord injury.* 19th International Symposium for Neural Regeneration. Skamania, WA April 2023.

Forston MD, Wei GZ, Chariker JH, Stephenson TL, Howard RM, Andres KR, Myers SA, Burke DA, Stoll BA, Rouchka EC, Whittemore SR, Hetman M. (2022). *Ribotag analysis of oligodendrocyte response to spinal cord injury identifies novel candidate regulators of oligodendrocyte death and survival.* 27th Annual Kentucky Spinal Cord and Head Injury Research Trust Symposium. Louisville, KY 2022.

Stephenson TL, **Forston MD**, Wei GZ, Chariker JH, Rouchka EC, Whittemore SR. (2022). *A searchable database of the oligodendrocyte translatome from contused mouse spinal cord tissue.* 27th Annual Kentucky Spinal Cord and Head Injury Research Trust Symposium. Louisville, KY 2022.

Forston MD, Wei GZ, Chariker JH, Howard RM, Andres KR, Myers SA, Burke DA, Stephenson TL, Stoll BA, Rouchka EC, Whittemore SR, Hetman M. (2021). *Post-spinal cord injury oligodendrocyte translatome analysis reveals paracrine contributions to white matter repair.* 50th Annual Society for Neuroscience Conference. Virtual presentation. Chicago, IL 2021.

Forston MD, Wei GZ, Chariker JH, Howard RM, Andres KR, Myers SA, Burke DA, Stephenson TL, Rouchka EC, Whittemore SR, Hetman M. (2021). *Post-*

spinal cord injury oligodendrocyte translatome analysis reveals paracine contributions to white matter repair. Research!Louisville. Louisville, KY 2021.

Stoll BA, **Forston MD**, Wei GZ, Stephenson TL, Hetman M. (2021). *Validating Changes in Oligodendrocyte Translatome after Spinal Cord Injury.* KY IDeA Networks of Biomedical Research Excellence Poster Day. Louisville, KY 2021.

Forston MD, Howard RM, Siladi A, Newton J, Shoup J, Ohri SS, Whittemore SR, Hetman M. (2018). *An unbiased screen to identify FDA approved drugs for novel use to treat spinal cord injury.* Neuroscience Day, University of Louisville. Louisville, KY 2018.

Forston MD, Bankston AN, Howard RM, Whittemore SR. (2017). *Autophagy targets potential key proteins involved in oligodendrocyte differentiation and myelination.* 23rd Annual Kentucky Spinal Cord and Head Injury Research Trust Symposium. Louisville, KY 2017.

Bankston AN, **Forston MD**, Smith AE, Howard RM, Whittemore SR. (2017). *Autophagy regulates myelin compaction in the final stages of CNS myelination*. 23rd Annual Kentucky Spinal Cord and Head Injury Research Trust Symposium. Louisville, KY 2017.

Bankston AN, **Forston MD**, Smith AE, Howard RM, Whittemore SR. (2016). *Autophagy regulates myelin compaction in the final stages of CNS myelination.* American Society for Cell Biology Annual Meeting, Louisville, KY 2016.

Bankston AN, **Forston MD**, Smith AE, Howard RM, Whittemore SR. (2016). *Autophagy regulates myelin compaction in the final stages of CNS myelination*. Research!Louisville. Louisville, KY 2016.

Forston MD, Bankston AN, Howard RM, Whittemore SR. (2016). *Autophagy regulates actin dynamics during oligodendrocyte differentiation and myelination.* Neuroscience Day, University of Louisville. Louisville, KY 2016.

PROFESSIONAL ASSOCIATIONS

Society for Neuroscience Member 2015-present

TEACHING AND OUTREACH

School of Medicine Teaching Assistant 2017, 2022
Taught medical and first year graduate students' neuroanatomy. (2017).
Guest lecturer for Synaptic Organization of the Brain – Synaptic transmission. (2022).

Mentor undergrad, grad and medical students in research 2015-present

Trained students on individualized research projects and data presentation.

Brain Days **2017-2018, 2022-2023**
Taught elementary-high school students broad topics in neuroscience

KY Science and Engineering Fair **2022**
Judge for Elementary school student science projects

Louisville Regional Science and Engineering Fair **2021**
Judge for Elementary and Middle school student science projects